THE UNIVERSITY OF MICHIGAN

COLLEGE OF ENGINEERING
Department of Electrical Engineering
Space Physics Research Laboratory

Scientific Report JS-3

THE DUMBBELL ELECTROSTATIC IONOSPHERE PROBE: IONOSPHERE DATA

L. H. Brace

ORA Projects 02816-1, 03484, and 03599

under contract with:

NATIONAL AERONAUTICS AND SPACE ADMINISTRATION
CONTRACT NO. NASw-139
WASHINGTON, D.C.

UNITED STATES AIR FORCE
AIR FORCE SYSTEMS COMMAND
AIR FORCE CAMBRIDGE RESEARCH LABORATORIES
OFFICE OF AEROSPACE RESEARCH
GEOPHYSICS RESEARCH DIRECTORATE
CONTRACT NO. AF 19(604)-6124
BEDFORD, MASSACHUSETTS

DEPARTMENT OF THE ARMY
BALLISTIC RESEARCH LABORATORY
CONTRACT NO. DA-20-018-509-ORD-103
PROJECT NO. DA-5B03-06-011 ORD(TB3-0538)
ABERDEEN PROVING GROUND, MARYLAND

administered through:

OFFICE OF RESEARCH ADMINISTRATION ANN ARBOR

September 1962

engn

UMR0580

PREFACE

The Dumbbell probe is a rocket-borne symmetrical electrostatic probe which is ejected from the vehicle for the direct measurement of the ionospheric temperature and density in the approximate altitude range of 100 to 1000 kilometers. The theory and implementation of the technique have been described extensively in various University of Michigan scientific reports[5,6,7,13] and the results of early measurements, many of these preliminary, have been outlined in the literature.[4,19] The primary purpose of this report is to provide a more extensive discussion of the data reduction procedures and present the final data for the five most recent flights which were carried out between March 1960 and December 1961, primarily with the support of the National Aeronautics and Space Administration. Earlier development and implementation of the technique during the IGY were undertaken with the support of the U.S. Army Ordnance Ballistic Research Laboratories and Air Force Cambridge Research Laboratories.

TABLE OF CONTENTS

TABLE OF CONTENTS (Concluded)

LIST OF ILLUSTRATIONS

LIST OF ILLUSTRATIONS (Continued)

LIST OF ILLUSTRATIONS (Continued)

LIST OF ILLUSTRATIONS (Continued)

LIST OF ILLUSTRATIONS (Concluded)

LIST OF SYMBOLS

a	radius of positive ion sheath
r	general radius, or radius of Dumbbell hemisphere = 7.64 cm
a/r	ratio of sheath radius to probe radius
c_e	electron characteristic velocity
c_p	positive ion characteristic velocity (see Equation 3.3)
e	unit charge = $1.60206\ 10^{-19}$ coulombs
i_e	electron current
i_p	positive ion current
k	Boltzmann constant = $1.38044\ 10^{-23}$ joules/degree K
M	mass number
m_e	electron mass = $9.1083\ 10^{-31}$ kg.
m_p	positive ion mass = $1.660\ M\ 10^{-27}$ kg
N_e	electron number density
N_-	negative ion number density
N_p	positive ion number density
P	$\frac{8\sqrt{\pi}\,\epsilon_0 k}{9e^2}\frac{T}{Nr^2} = 7.503 \times 10^5 \frac{T}{Nr^2}$ (MKS)
T_e	electron temperature
T_p	positive ion temperature
V	across-the-sheath potential
W	probe velocity
δV	potential difference applied between hemispheres
θ	orientation of hemisphere (Figure 9)
λ	ratio of probe velocity to characteristic velocity, W/c
Λ	velocity factor of hemisphere current equations.

ABSTRACT

The Dumbbell probe theory is reviewed briefly, and several predicted volt-ampere characteristics are presented. Experimental characteristics, recorded in flight, are found to agree well with those predicted by the theory. The methods by which the theory is used in the reduction of electron temperature and positive ion density from volt-ampere characteristics are discussed. The ionosphere data from four day-time flights and one nighttime flight to over 300 kilometers are presented and discussed. It is concluded that the electron temperature in the quiet mid-latitude ionosphere is generally higher than currently accepted gas temperatures in the lower F-region, but that thermal equilibrium is approached in the upper F-region and in the E-region. The electron temperature appears to be directly related to the latitude and the level of solar activity, although it is difficult to separate these effects. "Spread F" in the auroral zone is associated with strong fine structure in the temperature and density profiles. Magnetic storm activity at lower latitude is accompanied by high electron temperature throughout the ionosphere, especially in the E-region and upper F-region, where lower electron temperatures prevailed under quiet conditions. The good agreement between the nighttime electron temperature and the reference atmosphere nighttime gas temperatures demonstrates the validity of the Dumbbell technique for ionosphere temperature measurement, while good agreement of the Dumbbell-derived ion densities and the electron densities measured simultaneously by two-frequency beacon and ionosonde techniques demonstrates the validity of the Dumbbell charge density measurements. A comparison of day-time and nighttime temperatures indicates a 35% to 70% total diurnal variation can be expected in the quiet F-region. A comparison of the electron and positive ion density, measured simultaneously in the lower ionosphere, shows that the negative ion population in the D and lower E-regions is larger and occurs at a higher altitude than is generally predicted by theory.

1.0 INTRODUCTION

When V-2 rockets became available to scientists after World War II, several University of Michigan investigators suggested and directed the application of Langmuir probes, commonly used in gaseous conduction studies, to ionosphere research.[1-3] Each of three of these rockets carried, among many other experiments, an unsymmetrical bipolar probe. The collector geometry, dictated by practical considerations of space and compatibility with other experiments, was less than ideal; however, enough information was obtained to indicate that the technique, more carefully implemented, might prove to be a valuable tool in ionosphere research. Later, when smaller research rockets capable of reaching the ionosphere were developed, this laboratory, with the support of AFCRC, BRL, and later NASA,* renewed its ionosphere research effort.[4,5] The rather unusual concept of an ejectable Langmuir probe, containing its own current detection and telemetry system, was implemented to insure that: (a) the collector design need not be prejudiced by vehicle imposed limitations, and (b) the probe remain well away from local disturbances of the ionosphere due to outgassing from the burned-out rocket motor as well as surface contaminants.

Over the past several years, two different probe configurations have been developed: one, an extremely unsymmetrical bipolar probe to be discussed elsewhere, and the other, a dumbbell-shaped, symmetrical bipolar probe which was used in the measurements reported here.

1.1 GENERAL REMARKS CONCERNING THE DESIGN OF AN EJECTABLE BIPOLAR PROBE

The equations for the ion and electron currents to stationary collectors of planar, cylindrical, and spherical geometries have been known for many

*Air Force Cambridge Research Center, Ballistics Research Laboratory, National Aeronautics and Space Administration.

years.[2,7-9] These can be applied to predict, with fair accuracy, the volt-ampere characteristic of any one of the wide variety of bipolar probes which could be formed from various combinations of the above geometries and degrees of symmetry in the respective collector areas.

Although it is the purpose of this report to consider a particular ionosphere probe, known as the "Dumbbell," it may be useful to discuss briefly some of the factors which guide an experimenter in his choice of the collectors which will form a probe most nearly satisfying the needs and limitations which face him. These factors fall into the following three categories: theoretical considerations, the particular ionospheric parameter to be measured, and available rocket vehicles.

1.1.1 Theoretical Considerations

It was shown by Hok[2] and Boggess[7] that simple asymptotic or approximate solutions to the general current equations are valid, under typical ionospheric conditions, when the collector dimensions are made larger or smaller than certain well-defined limits which are a function of the temperature and density of the plasma and the collector radius. When the collector is made smaller than the lower limit (typically one or two millimeters), the ion current is said to be orbital-motion-limited. When the collector is made larger than the upper limit (typically several centimeters), the ion current is said to be sheath-area limited. To take advantage of these mathematically simpler expressions in the predictions of volt-ampere characteristics and in the reductions of ion density data from experimental curves, the collector dimensions may be chosen so that it operates clearly in one mode or the other. In practice, the need for instrumentation space within the probe requires that at least one collector be so large that it necessarily operates in the sheath-area limited mode, while the other collector may be dimensioned to operate in either of the limiting

modes. Thus apparently the probes most easily handled theoretically will be symmetrical, or nearly so (both collectors sheath-area-limited), or greatly unsymmetrical (one collector operating in each mode).

1.1.2 The Particular Ionospheric Parameter to be Measured

In general, the volt-ampere characteristics of either the symmetrical or the unsymmetrical form of probe do not lend themselves equally well to the determination of all the ionospheric parameters which electrostatic probes are capable of measuring. The symmetrical probe, for example, is not well suited to electron density measurements since the collectors of this type of probe operate in a voltage region where the electron current is a rapidly varying function of collector potential, a parameter which can be determined only with limited accuracy. However, the small collector of a greatly unsymmetrical probe can be forced to operate at any potential and, when driven to the plasma potential, collects just the random electron current from which the electron density is readily obtained.

The electron temperature is based upon the measurement of the electron energy distribution, any part of which is sufficient for the determination of temperature, if a Maxwellian energy distribution is known to exist. Either type of probe is suitable for this measurement; however, the symmetrical probe has access only to those electrons having energies exceeding the negative potential of the collectors, and thus can measure only the high-energy end of the distribution. If the distribution is not purely Maxwellian, there is a possibility of an incorrect temperature determination, if indeed the term "temperature" can be used to describe such a distribution. The smaller collector of an unsymmetrical probe, however, can be driven through a wide range of potential and therefore can sample the entire electron population. Theoretically, this enables one to obtain a better measurement of the thermal energy. There is, however, evidence[10,11] that a collector which is near the plasma potential introduces more disturbance to

the plasma than does the symmetrical probe which remains moderately negative. Thus the choice of probe best suited for the measurement of electron temperature is a question which requires further study.*

The positive ion density may be obtained with either the symmetrical or unsymmetrical probe, although the former appears to offer the most straightforward measurement. The ion density is based on the measurement of the collected ion current which is a function of the charged particle density, mass, and temperature as well as the "effective" area of the collector. The effective area of the collector for ions is somewhat greater than its surface area because of the positive ion sheath which surrounds it. Since the calculation of the effects of the sheath is based on several assumptions and approximations, it is expedient to select a collector which is much larger than the sheath dimensions so that the ion current dependence upon the sheath is kept small. One could, of course, use the unsymmetrical probe for ion density measurements if the ion current equations can be shown to describe the current collection with sufficient accuracy.**

1.1.3 Rocket Vehicle Considerations

Ideally, to insure sheath-area-limited operation of the large electrode over a greater range of ion densities, one would like to maximize the dimensions of at least one electrode. However, until recently the only available research rockets with adequate peak altitude capability were of small diameter. This has limited the size of the largest collector to roughly the diameter of such rockets, 6 to 8 inches. If the rocket itself acts as one collector of the bipolar probe, this problem is somewhat reduced since the surface area of the rocket is usually ade-

*A combination symmetrical and unsymmetrical probe, discussed in Section 8.72, was launched at Wallops Island, Virginia, in March, 1961, and the temperature from both types of probes are being compared.

**The modified Dumbbell probe mentioned in the previous footnote is well suited to the evaluation of the measurement of ion density by the two types of probes.

quate. However, several other problems arise when the rocket is made part of a probe system aside from the possible contaminating effect of the vehicle. Probably the most important of these problems is the changing equilibrium potential of the rocket as it changes orientation (tumbles and spins) in free fall. Since the rocket acts as a reference element for application of a potential to the smaller collector, its changing potential enters as an unknown variable in the volt-ampere curves of the probe system. The error due to this can be minimized, however, by selecting a sweep voltage rate which is fast compared to the changes in rocket orientation.

1.2 SELECTION OF THE DUMBBELL FORM OF PROBE

The selection of the Dumbbell configuration was made on the basis of several of the design considerations outlined in the previous section. Theoretical considerations indicated that a symmetrical probe could be expected to introduce less disturbance in the surrounding plasma, since such a probe causes less electron depletion of the plasma than does an unsymmetrical probe. To provide adequate instrumentation space within the electrodes of the ejected probe, both collectors of the symmetrical pair were necessarily sheath-area-limited.

Collectors having spherical geometry were chosen over cylindrical or planar collectors primarily because of the effectiveness with which spherical collectors can be guarded to reduce the electrostatic fringe effects. In general, guard systems for cylindrical and planar collectors are larger, more elaborate, and less effective.

The availability of the 6-in. diameter Nike-Cajun combination and 8-in. Aerobee 300 or "Sparrobee" indicated that a probe instrument having 6-in. electrodes would be the largest which could be employed with the then existing high-altitude vehicles. This seemingly small size presented no problem, however, since calculations showed that a hemisphere of this size would be large enough

to operate within the sheath-area-limited mode in a plasma having electron and ion densities as low as 10^4/cc. This would make the results valid to well over 1000 km at which altitude the electron density is still greater than this lower limit. Although the separation between the Dumbbell hemispherical collectors was determined by the requirement that the entire probe act as a half-wave dipole antenna at the telemetry frequency, a certain minimum spacing was required to prevent the sheath of one end from overlapping that of the other. Calculations show that the sheaths do not begin to overlap until the density falls below 10^4/cc, again well over 1000 km.

Thus the Dumbbell, a double-sphere, sheath-area-limited, symmetrical probe, took form as a first attempt at an electrostatic ionosphere probe which would (a) introduce a minimum of disturbance to the surrounding plasma, (b) produce volt-ampere curves most easily interpretable, and (c) be small enough to carried to great altitudes in the then available vehicles.

2.0 THE DUMBBELL PROBE INSTRUMENT

Figures 1 and 2 are photographs of an assembled and partially disassembled Dumbbell probe, and Figure 3 is a functional block diagram of the system. Later versions of the Dumbbell were modified by the addition of a small cylindrical probe on the central nylon insulator to form an unsymmetrical probe as a second mode of operation which is discussed in Section 8.7.2. The external structure consists of two stainless-steel hemispherical collectors and two somewhat funnel-shaped guard electrodes which are insulated from the collectors and from each other.

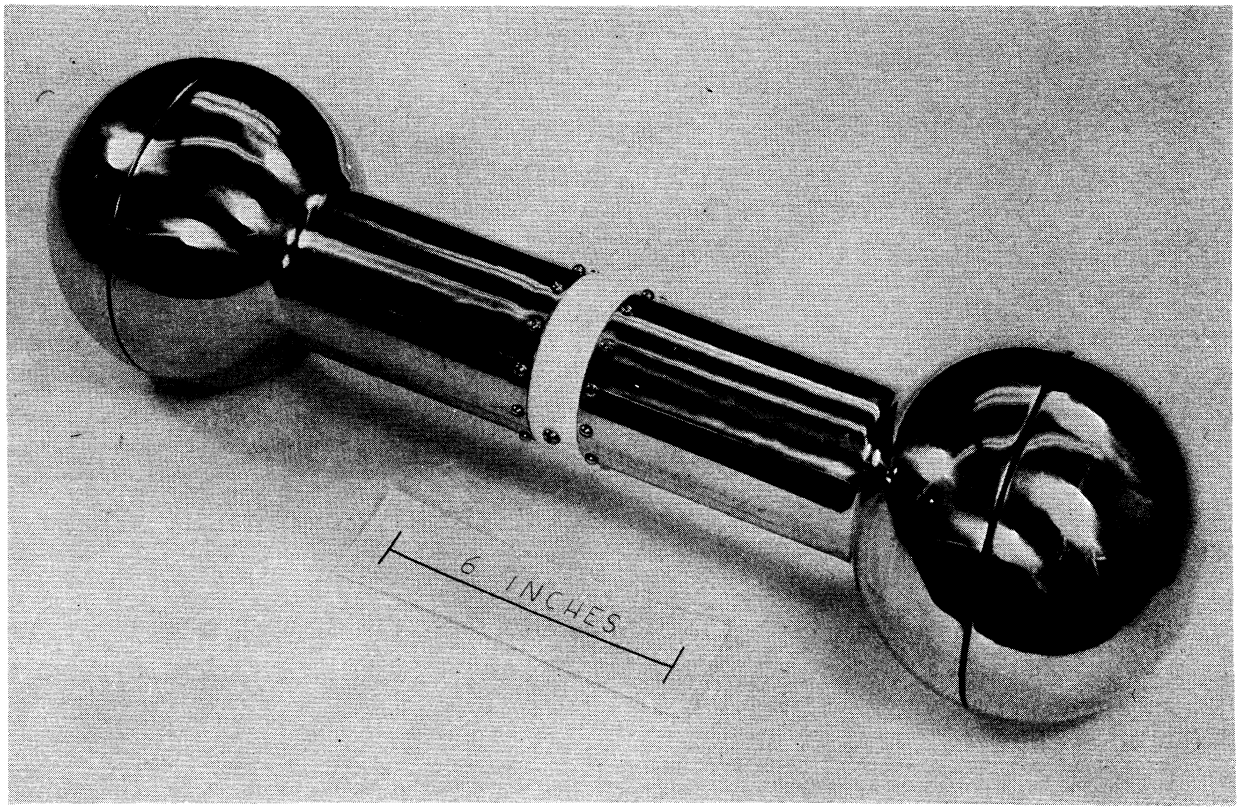

Figure 1. The Dumbbell instrument.

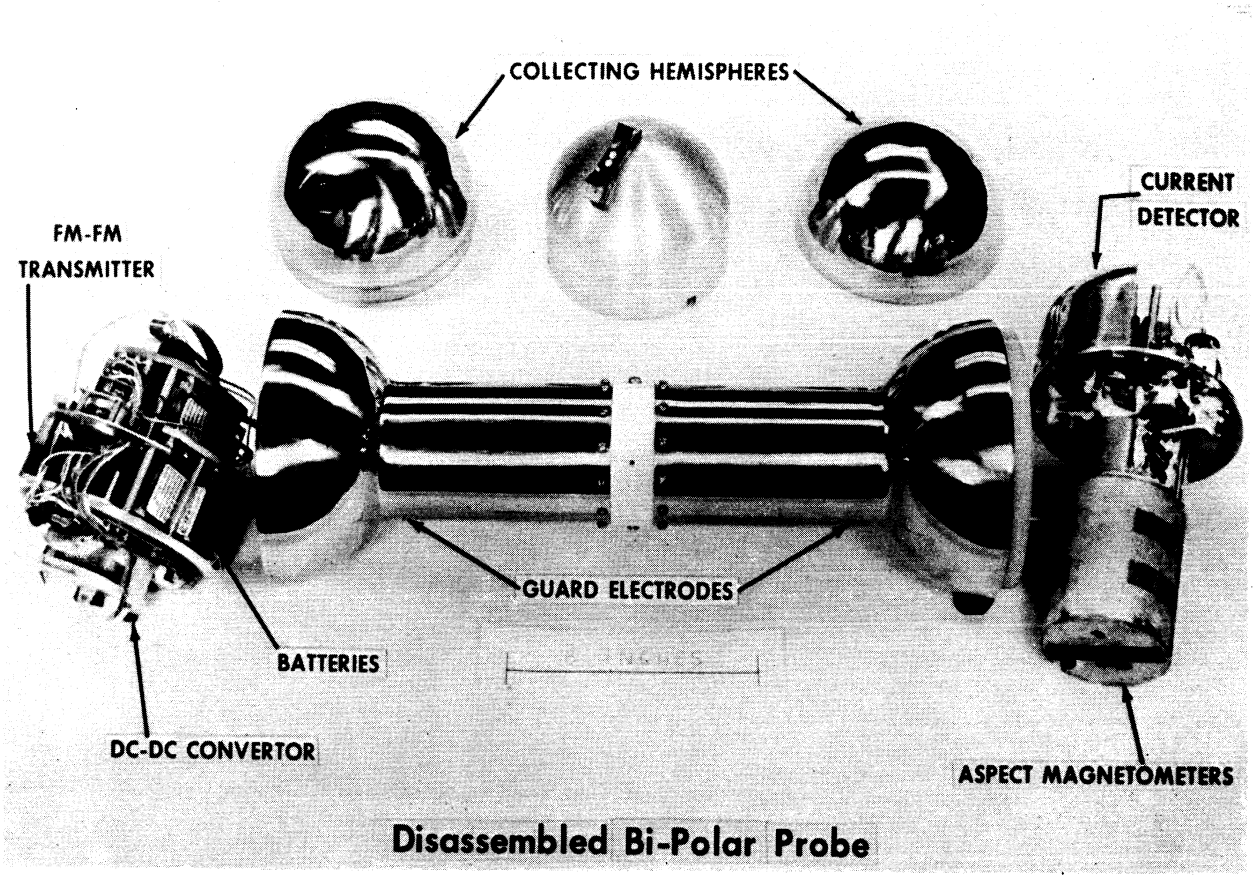

Figure 2. Partially disassembled Dumbbell.

Two identical, sawtooth voltages (δV), are applied between the hemispheres and between the guard electrodes. Two current detectors are connected in series with the hemispheres and the associated δV generator and, since this system is insulated from the "funnel" circuit, measure only the net current flowing to the hemispheres from the plasma. The detectors have 1-μa and 4-μa full-scale sensitivities, respectively, which together enable adequate resolution in the measurement of probe currents generally encountered throughout the various regions of the ionosphere. In-flight calibration of the current measurement system is accomplished by substitution of a known resistance for the "ionosphere" periodically during flight.

Also contained within the Dumbbell is an FM-FM telemetry system consisting

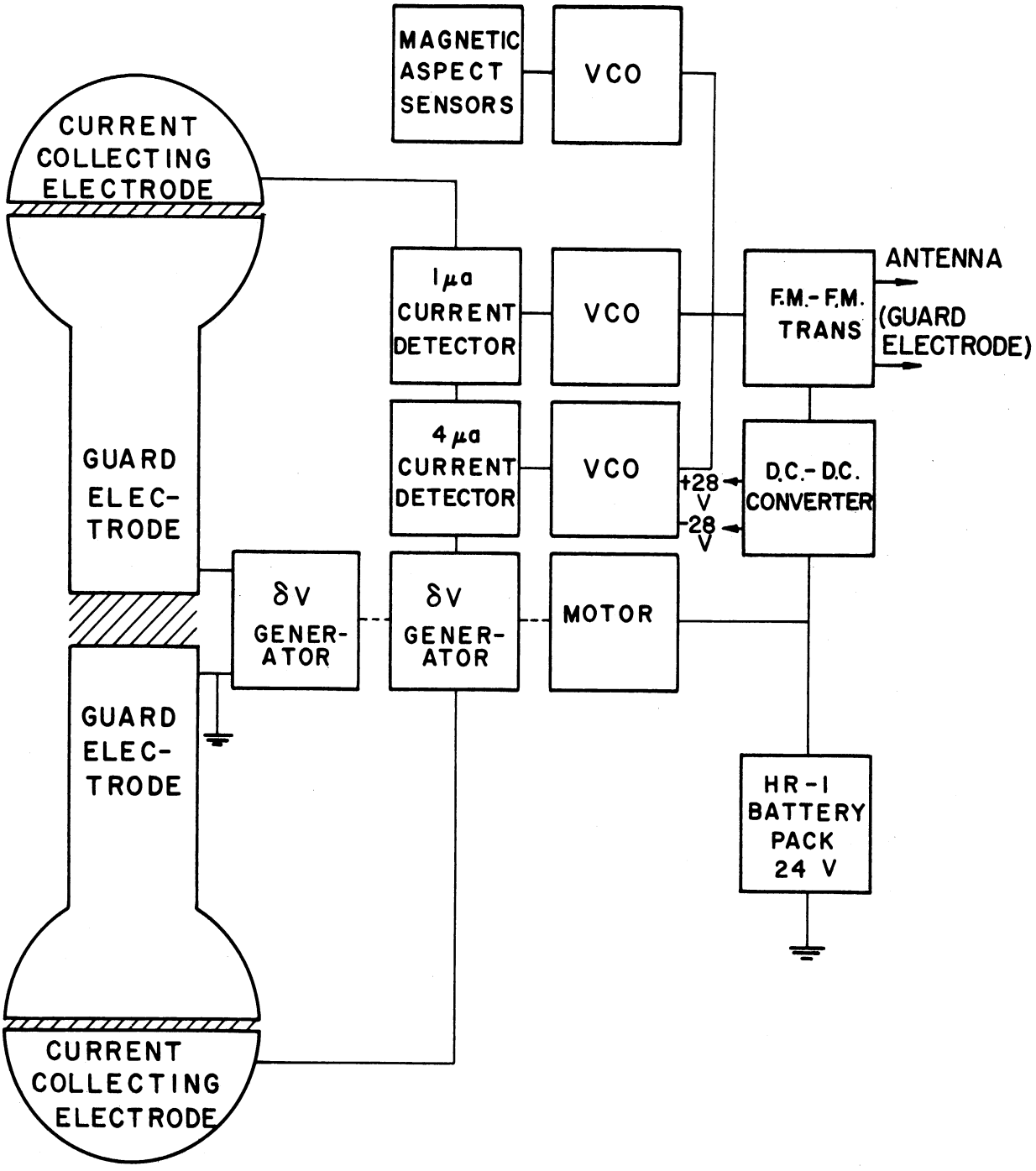

Figure 3. Functional block diagram showing bipolar probe system.

of a two-watt Bendix TXV-13 transmitter and three voltage-controlled oscillators, providing three information channels: one for each current detector and a third, time-shared by magnetic aspect sensors and other auxiliary circuits used to convey various operational information. Completing the telemetry system is the antenna which consists of the entire external surface of the Dumbbell acting as a half-wave dipole at 220 mc.

The current measuring and telemetry systems have a common power supply, employing a d-c to d-c converter operating from a 24-v pack of HR-1 Silver-Cadmium cells. The instrument and its electronic components are discussed in more detail in other reports.[5,7,12]

In use, the instrument is carried by a suitable rocket to the lower edge of the ionosphere (approximately 75 km) where a mechanical timer initiates ejection from the rocket by spring action as depicted in an artist's conception reproduced as Figure 4. The rocket and instrument, with increasing separation, follow an elliptical path in free fall to a peak altitude of several hundred kilometers (depending upon the vehicle); their position and velocity is observed by a DOVAP or a RADAR system or both. Throughout the flight, volt-ampere curves of the Dumbbell, immersed in the ionosphere, are continuously measured and transmitted to one or more ground stations where they are recorded. Each curve is later available for interpretation in terms of the electron temperature and positive ion density of the plasma which surrounded the probe at the time of recording.

Figures 5 and 6 are photographs of the nose cone which encloses and protects the Dumbbell from the aerodynamic forces encountered in passage through the lower atmosphere.

Figure 4. Artist's conception of the ejection of the dumbbell into the ionosphere.

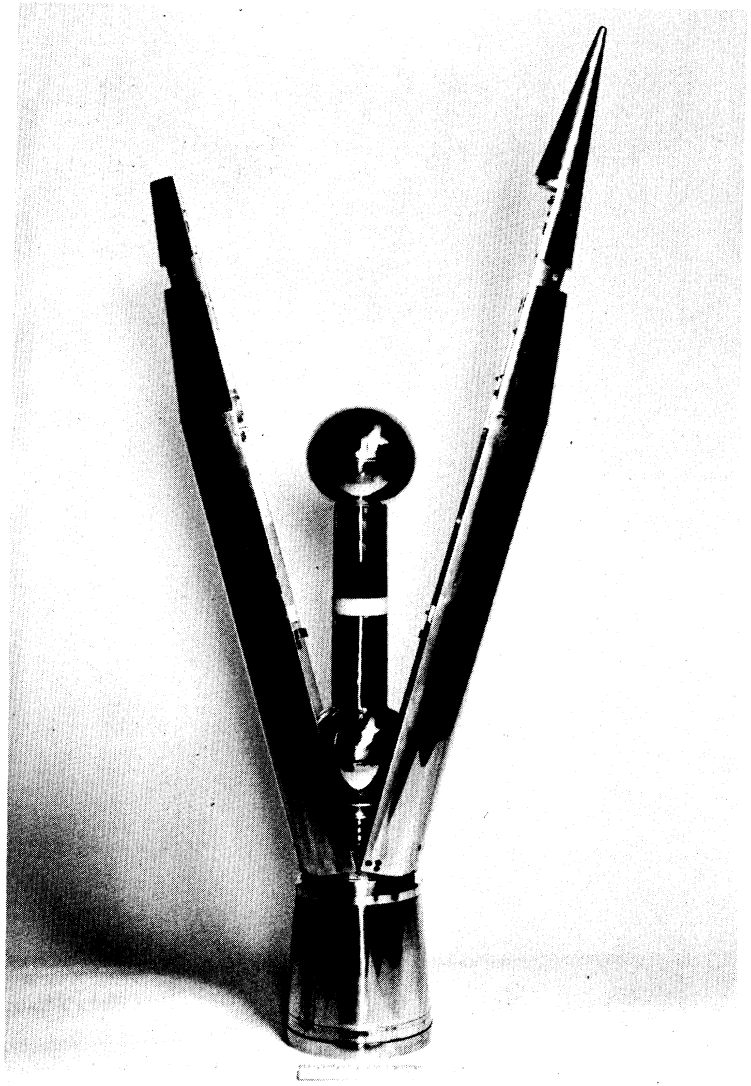

Figure 5. Open nose cone with Dumbbell in place.

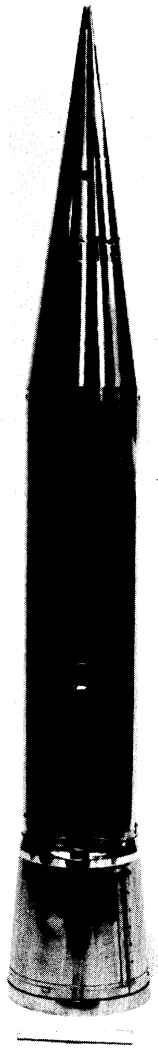

Figure 6. Closed nose cone.

3.0 REVIEW OF THE DUMBBELL PROBE THEORY

3.1 THE HEMISPHERE CURRENT EQUATION

As shown in an earlier theoretical report,[13] the net current to a Dumbbell hemisphere is given by the following equation which represents the sum of the ion and electron currents.

$$i = \frac{N_p e c_p}{2\sqrt{\pi}} \, 2\pi r^2 \left\{ \Lambda + 2\sqrt{P\Lambda} \left(\frac{eV}{kT_p} \right)^{3/4} \frac{N_e c_e}{N_p c_p} \exp \left(- \frac{eV}{kT_e} \right) \right\} \qquad (3.1)$$

where

N_p = positive ion density

N_e = electron density

e = electronic charge = 1.602×10^{-19} coulombs

$C_p = \sqrt{\frac{2kT_p}{m_p}}$ most probable ion velocity

$C_e = \sqrt{\frac{2kT_e}{m_e}}$ most probable electron velocity

k = Boltzmann constant = 1.38×10^{-23} joules/°K

T_p = ion temperature

T_e = electron temperature

m_p = ion mass

m_e = electron mass = 9.11×10^{-31} kg.

r = radius of the hemisphere = 7.64 cm.

$P = 7.51 \times 10^5 \frac{T_p}{N_p r^2}$ (mks. units)

V = voltage of the probe with respect to the plasma

$\Lambda = \sqrt{\frac{\pi}{2}} (\lambda + 1/2) \operatorname{erf} \lambda + 1/2 \exp(-\lambda^2) + \frac{\sqrt{\pi}}{2} \lambda \cos\theta$

a factor accounting for the velocity effect on the ion current (see reference 13)

$\lambda = \frac{|\bar{W}|}{C_p}$ ratio of probe to most probable ion velocity

$\bar{W}$ = rocket velocity

θ = angle between the axis of the hemisphere and $\bar{W}$

When volume neutrality ($N_e = N_p$) and thermal equilibrium ($T_e = T_p = T_g$) are assumed to exist in the plasma, (3.1) reduces to

$$i = \sqrt{\frac{kT}{2\pi m_p}}\, N\, e\, 2\pi r^2 \left\{ \Lambda + 2\sqrt{P\Lambda}\left(\frac{eV}{kT}\right)^{3/4} - \sqrt{\frac{m_p}{m_e}} \exp\left(-\frac{eV}{kT}\right) \right\} \quad (3.2)$$

where the first two terms in the brackets represent the ion current component to the hemisphere and the last term, the electron current. Figure 7 is a graph of this current characteristic for a 3-inch radius hemisphere (Dumbbell) at various orientations and for a relative velocity ratio, $\lambda = 1$, under conditions normally found in the daytime F_1 region. It is apparent that the ion current is a weak function of hemisphere orientation for angles of less than 45°, a fact which is important in the reduction of ion density from experimental curves.

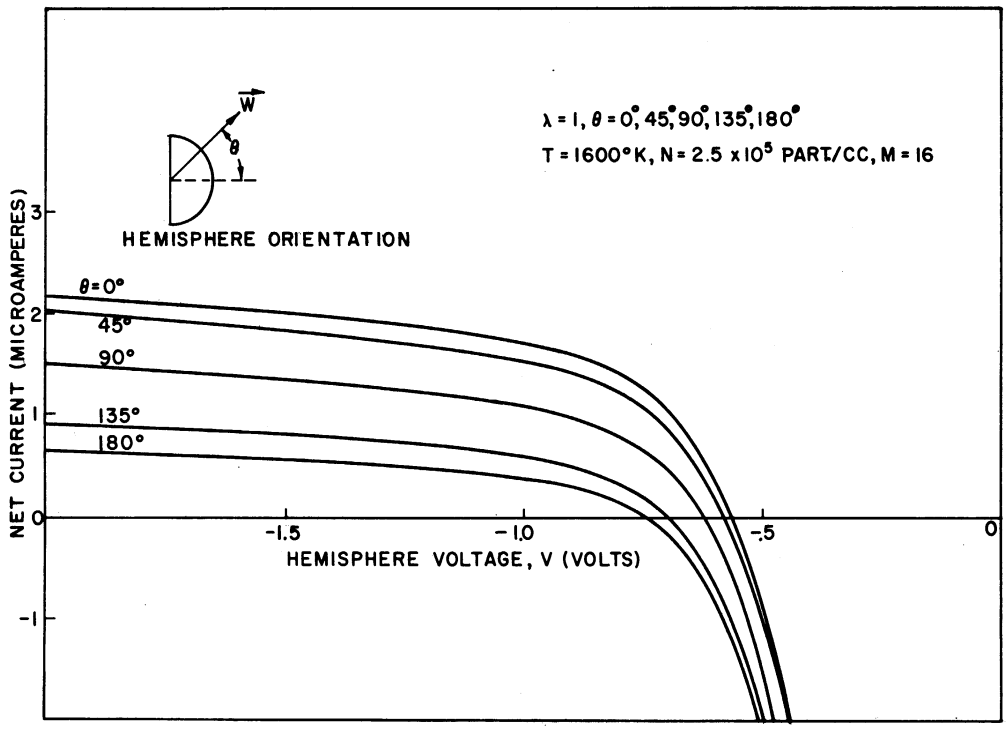

Figure 7. Single-hemisphere current curves for a fixed velocity and selected orientations.

3.2 THE VOLT-AMPERE CHARACTERISTICS

The Dumbbell collector system consists of two hemispheres, each of which has the current characteristic described by (3.1)or (3.2). Since the net current to the entire probe must be zero, the current to one hemisphere is equal and opposite in sign to the current to the other, over the entire range of difference voltage, δV, which may be applied between them. Using this fact, it is convenient to plot the net current to the individual hemispheres as shown in Figure 8, where one characteristic is inverted and superposed upon the other. Figure 8 shows the superposed currents when one hemisphere is oriented at $\theta = 45°$ while the other is at $\theta = 135°$ as shown in Figure 9.

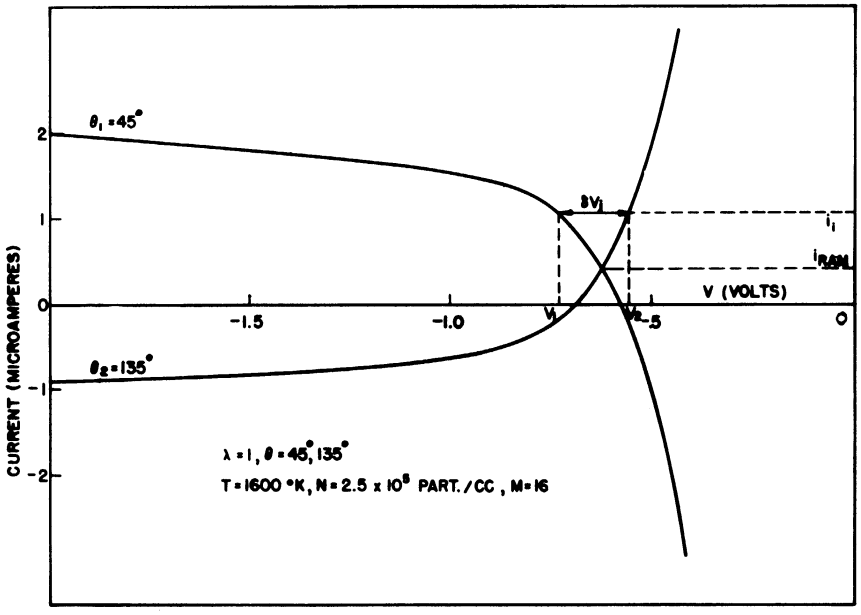

Figure 8. Superposed current characteristics of two oppositely oriented hemispheres.

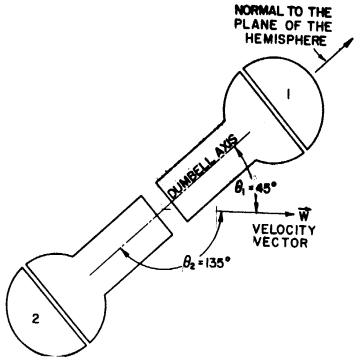

Figure 9. A particular Dumbbell orientation.

Due to the motion of the probe through the plasma the ion current to the leading hemisphere, 1, exceeds that to the trailing hemisphere, 2, so that when the two hemispheres are shorted directly together with no voltage applied between them, a net current, i_{ram}, results. When a particular difference voltage, δV_i, is applied, the hemisphere potentials, V_1 and V_2 adjust to cause a net current i_i (a net positive current to 1 and an equal negative current to 2). The volt-ampere characteristic of the pair of hemispheres, at this particular relative velocity and orientation, obtained graphically by plotting δV versus i from Figure 8, is shown in Figure 10. The right side of the graph is dominated by the current characteristic of hemisphere 1 because the applied δV occurs mostly as a change in potential at this collector which is being driven negative. The ready

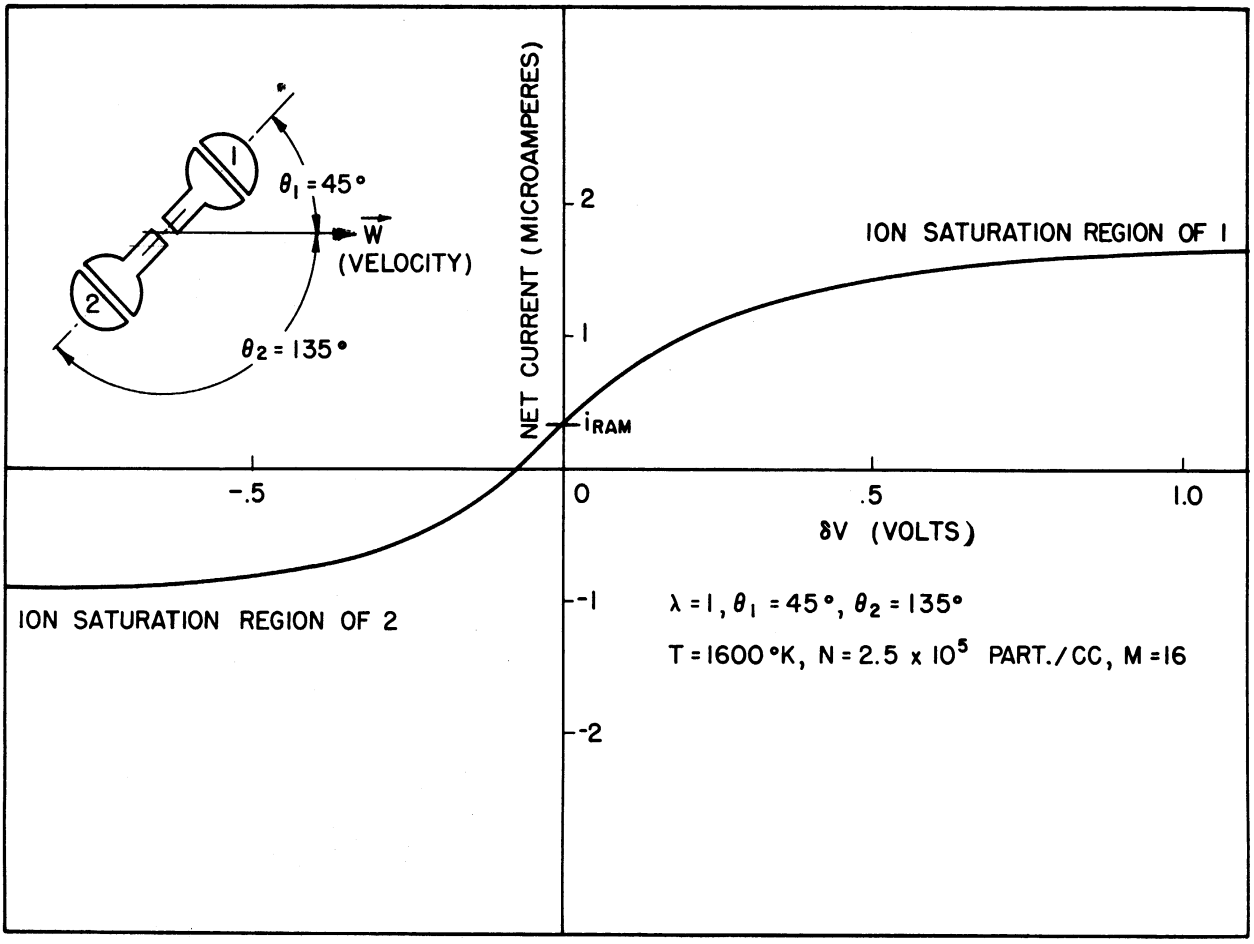

Figure 10. Volt-ampere characteristics of Dumbbell having orientation shown in Figure 9.

availability of electrons prevents the positive-going-hemisphere from accepting much of the δV. As shown in Figure 8, this is particularly true at higher values of applied δV as the negative-going-hemisphere approaches the ion saturation region where electrons are completely retarded. Here, the negative-going-hemisphere accepts nearly all the further increase in δV.

Figures 11-14 illustrate the effect of various Dumbbell velocities and orientations upon the volt-ampere characteristics, under typical ionosphere conditions. Figure 11 shows the predicted volt-ampere curves for selected velocity ratios λ when the Dumbbell is oriented so that one hemisphere points forward into the trajectory, $\theta_1 = 0°$, and the other hemisphere points backward along the trajectory, $\theta_2 = 180°$. The right-hand linear portion of each curve represents the ion saturation region of the leading hemisphere, while the left-hand linear portion represents the same region for the trailing hemisphere. Note that the

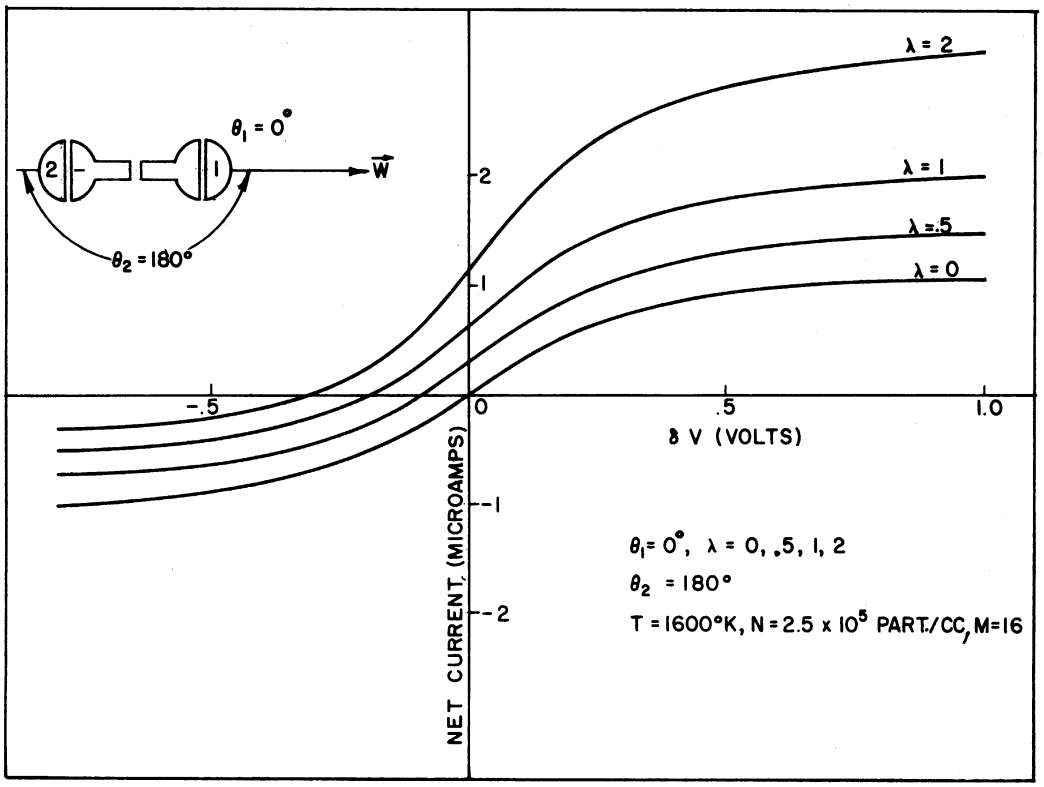

Figure 11. Dumbbell volt-ampere characteristics for θ = 0° and selected velocity ratios.

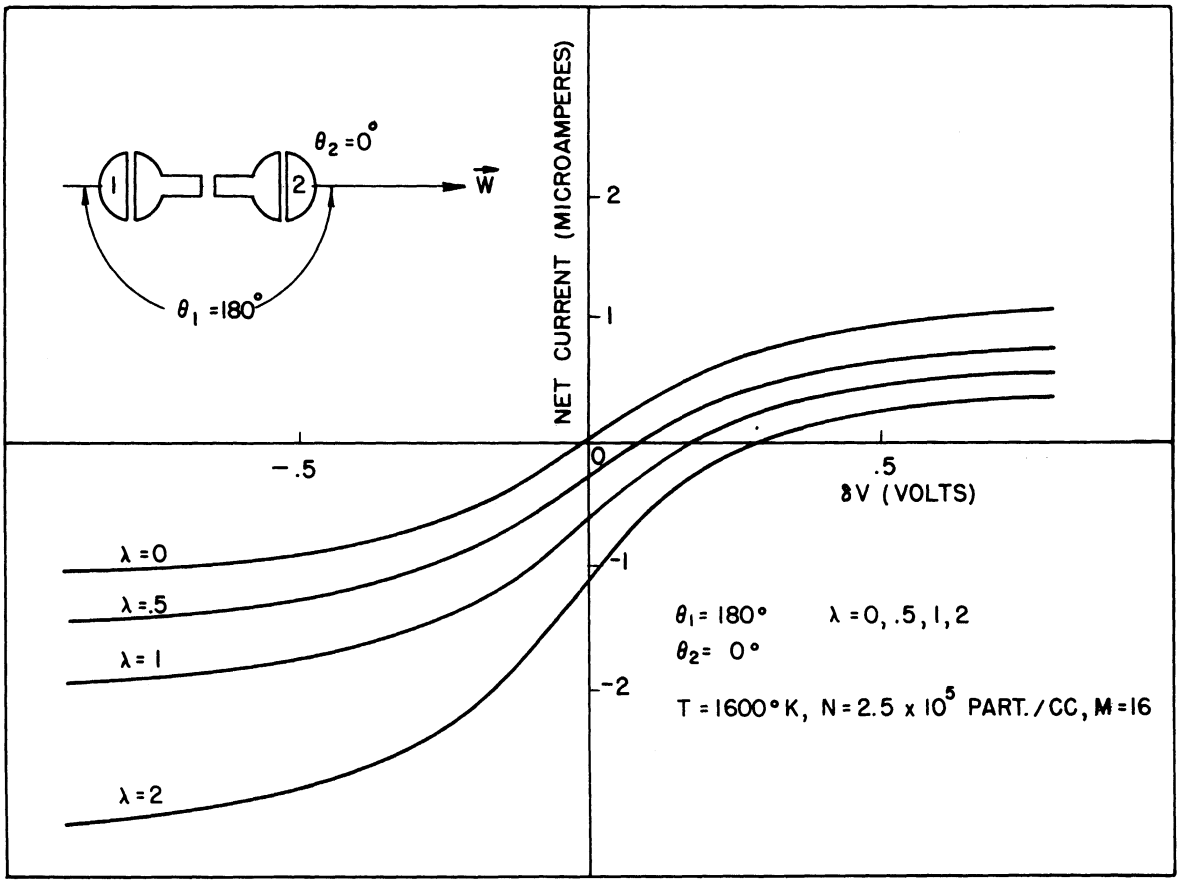

Figure 12. Dumbbell volt-ampere characteristics for θ = 180° and selected velocity ratios.

curve for λ = 0 represents the stationary probe characteristic and the other curves show the distortion due to various probe velocities. Note further that the leading hemisphere sweeps out more current as the velocity is increased and the trailing hemisphere, leaving the lower velocity ions behind, collects less current. At zero δV, for this orientation, there is a bias current which varies with velocity.

Figure 12 shows the Dumbbell characteristics at the opposite orientation, after the probe has tumbled (rotated) 180°. It is entirely analogous to the previous case except that the leading and trailing hemispheres have switched positions.

Figure 13 shows the characteristics when both hemispheres are perpendicular to the probe velocity, $\theta_1 = \theta_2 = 90°$. As one would expect, the characteristics are symmetrical, and somewhat less affected by velocity than in other orientations. Note that at zero δV, no bias current exists at any velocity since the ion currents swept out by each hemisphere are identical and therefore cancel.

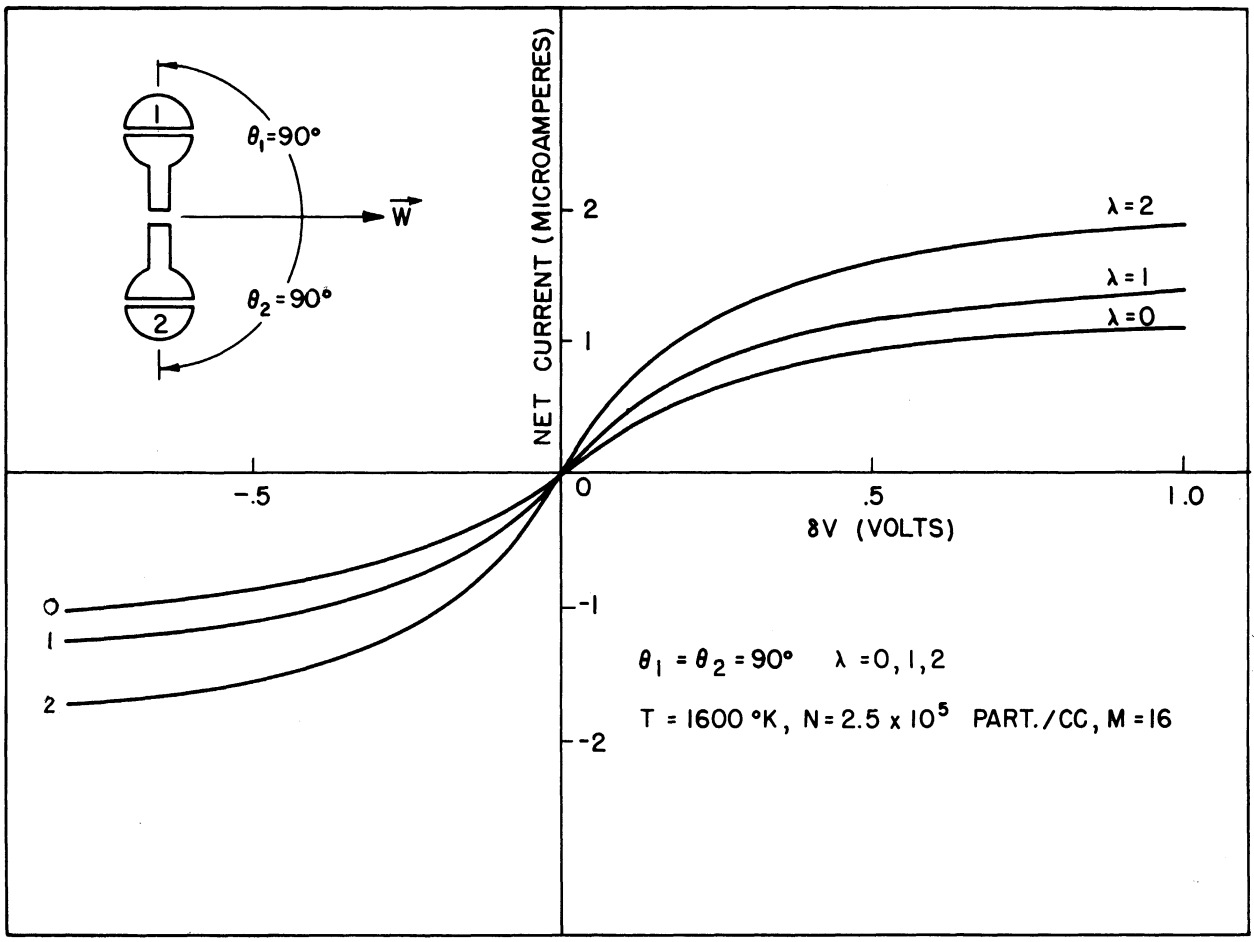

Figure 13. Dumbbell volt-ampere characteristics for $\theta = 90°$ and selected velocity ratios.

Figure 14 shows Dumbbell characteristics at an intermediate orientation in which the trailing hemisphere exhibits a decreasing ion current at lower velocities, and then increases at higher velocities as its small forward-projected area sweeps out greater ion current than is left behind. Similar curves can be drawn for other orientations and velocities, but those shown illustrate the essential features of the Dumbbell characteristics.

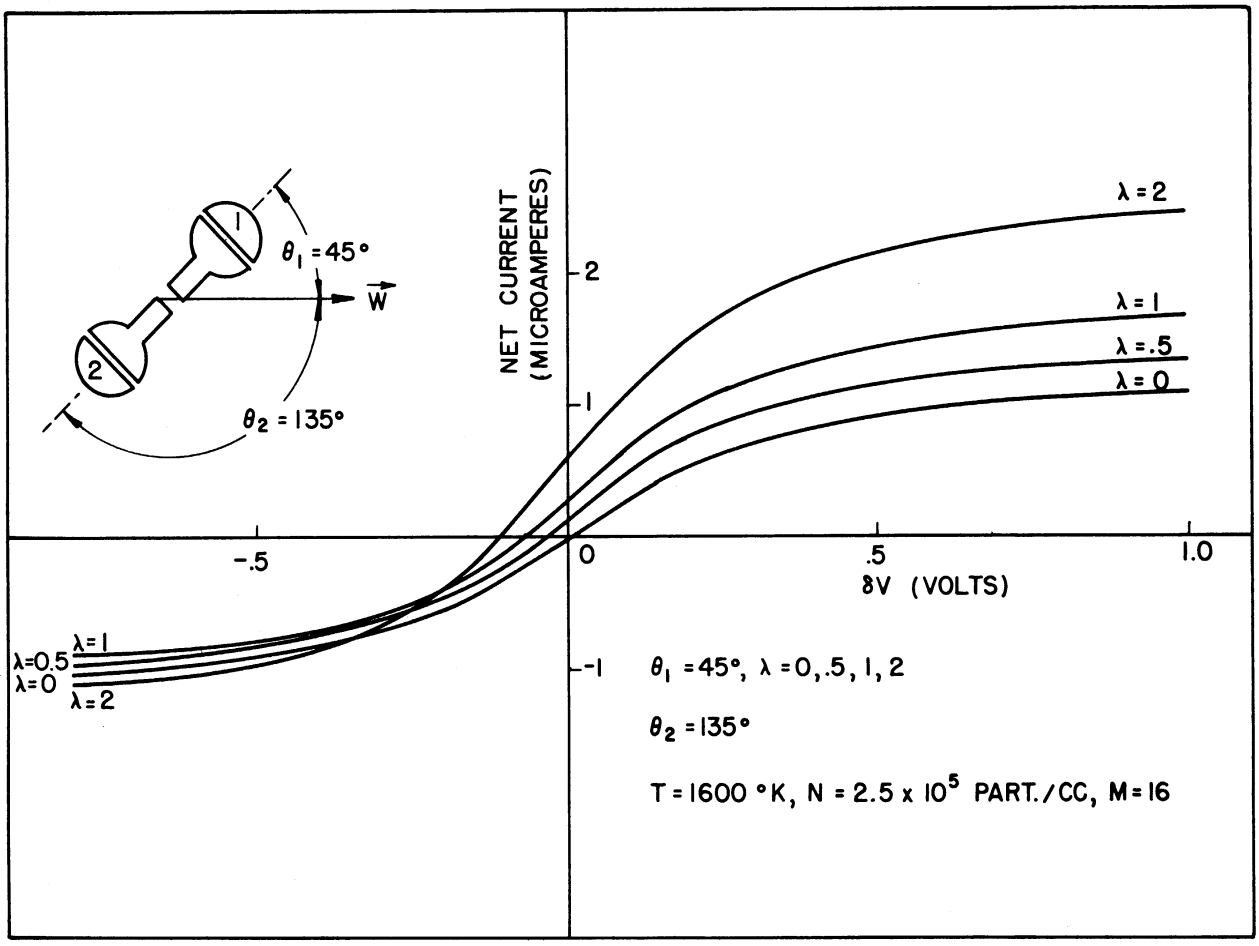

Figure 14. Dumbbell volt-ampere characteristics for $\theta = 45°$ and selected velocity ratios.

4.0 THEORY OF THE ELECTRON TEMPERATURE REDUCTION

The determination of electron current from a predicted volt-ampere characteristic, such as shown in Figure 15, is carried out as follows. Since the positive ion saturation region contains no electron current component (all electrons are retarded), it defines the positive current characteristic of the negative-going-hemisphere. As the applied voltage is reduced, some of the higher-energy electrons overcome the retarding potential and electron current begins to flow, rapidly decreasing the net positive current. The electron current can be separated from the net current by extrapolating the ion current characteristic, as shown in Figure 15, and subtracting the net current from the extrapolated ion current. The extrapolation is straight-forward since the ion current characteristic of a hemisphere is nearly linear with voltage and can be done graphically with a straight edge, or by machine with least-squares fitting.

An important feature of this method of obtaining the electron current is that it does not assume that the net positive current is composed only of ion current. It assumes only that the positive current characteristic does not exhibit abrupt changes in character over the relatively small region which is approximated by the extrapolation. Other positive components such as photoemission due to solar radiation and secondary emission due to high-energy particles are independent of the hemisphere potential and thus will not affect the electron current determination. This method has the additional feature that the velocity-induced distortion of the current characteristics, in the ion-saturated region, need not be calculated but is actually measured. Thus the extrapolation represents the net positive current including the effects of velocity which will not be carried over to the resulting electron current characteristic.

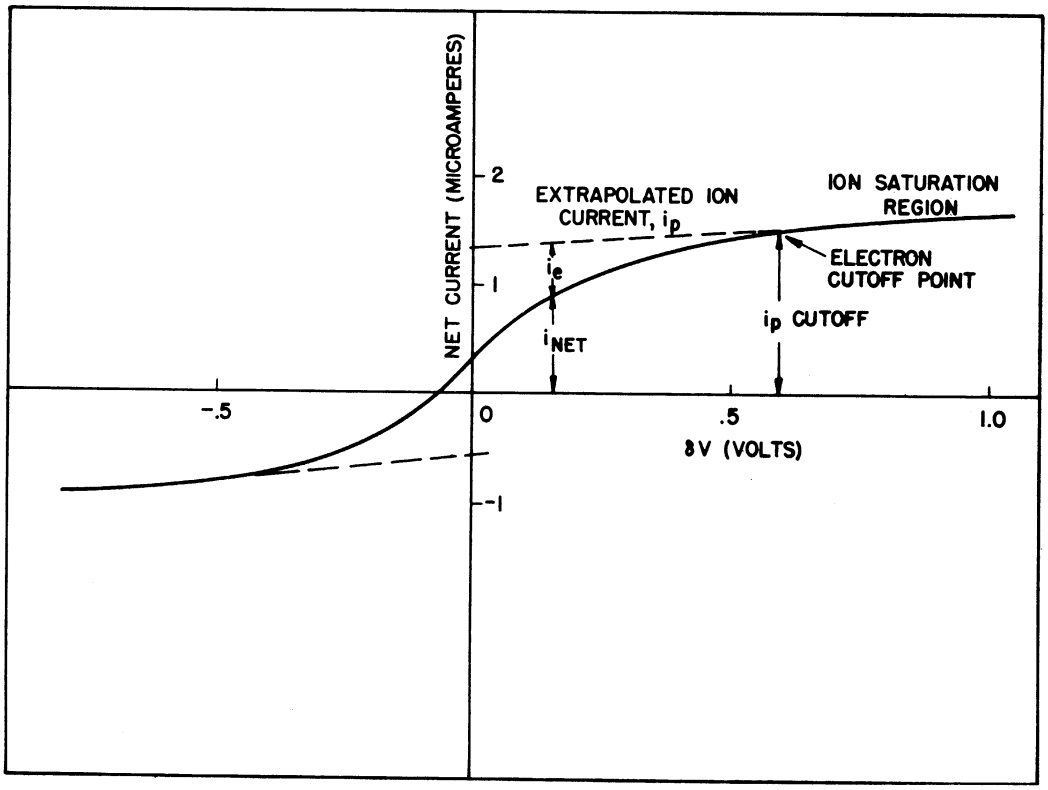

Figure 15. Dumbbell volt-ampere characteristics showing pertinent factors in the reduction of ionospheric parameters.

From the above discussion it can be seen that the electron current characteristic, i_e as a function of δV, can be obtained readily from a volt-ampere characteristic of the Dumbbell.

The relationship between i_e and V is given by

$$i_e = K \exp\left(-\frac{eV}{kT_e}\right) \tag{4.1}$$

where

$$K = \frac{Nec}{2\sqrt{\pi}}\, 2\pi r^2$$

and, taking the natural log, and then the derivative, one obtains

$$\frac{d\ \ell n\ i_e}{dV} = -\frac{e}{kT_e} \quad . \tag{4.2}$$

If one plots the natural log of i_e versus V on linear graph paper, the result is a straight line of slope e/kT_e, and the electron temperature is given by

$$T_e = -\frac{e}{k}\frac{dV}{d\ \ell n\ i_e} \qquad (4.3)$$

Thus, the task of finding the electron temperature reduces to that of finding the true change in potential, dV, of the negative-going-hemisphere when the applied δV is known. As discussed in Section 3.0, most of the applied voltage, δV, appears as a change in voltage, dV, at the negative-going-hemisphere; so that, to a close approximation

$$dV \approx d\delta V \ . \qquad (4.4)$$

However, some change in potential <u>does</u> occur at the positive-going-hemisphere. Theoretical studies using curves such as shown in Figure 8 show that this approximation leads to electron temperature values which are about 10% higher than the true values. That is, in the region of the curve from which the electron temperature is obtained, approximately 90% of the change in δV occurs as a change in potential, dV, of the negative-going-hemisphere, so that, in (4.3), the value of dv can be replaced by 0.9 $d\delta V$.

5.0 THEORY OF THE POSITIVE ION DENSITY REDUCTION

The ambient positive ion density is derived from the Dumbbell current characteristics, such as illustrated in Figure 15, by means of a theory[13] which accounts for the most significant known factors which affect the ion current collection. As discussed in Section 3.0, the electrons are completely retarded when a particular hemisphere is force sufficiently negative. Only positive ion current remains. This current is primarily a function of the ambient ion density, N_p, and the probe voltage, V; however, since the ion temperature T_p and mass m_p affect the most probable ion velocity, these are also factors in the current equations. In addition to this, the translational motion of the probe causes the hemisphere to sweep out additional ions which would not otherwise arrive at the collector surface as a result of their own random motion or the accelerating potential. All of these factors are included in the first two terms of equation (3.2) of Section 3.0 which was derived in the earlier theoretical study.[13] The ion current alone is rewritten,

$$i_p = \sqrt{\frac{kT}{2\pi m_p}}\, N_p\, e\, 2\pi r^2 \left\{ \Lambda + 2\sqrt{P\Lambda}\left(\frac{eV}{kT}\right)^{3/4} \right\} \qquad (5.1)$$

where, as given in Section 3.0,

$$\Lambda = \sqrt{\frac{\pi}{2}}\,(\lambda + 1/2\lambda)\,\mathrm{erf}\,\lambda + 1/2\,\exp(-\lambda^2) + \sqrt{\frac{\pi}{2}}\,\lambda\,\mathrm{Cos}\,\theta\,,$$

a term which accounts for the hemisphere motion.

$$P = 7.51 \times 10^5 \frac{T}{N_p r^2} \quad \text{(mks units)}$$

V = probe potential wrt. the plasma.

Equation (5.1) lends itself well to a machine solution for N_p when the other variables, i_p, V, θ, λ, T, m_p are ascertained. Taken in order, i_p is the ion current measured at some δV in the ion saturation region of the hemisphere

current characteristic. The point of measurement is chosen such that the probe voltage, V, can be determined most accurately, given the applied δV and the probe theory. One such point, the so-called electron cutoff point illustrated in Figure 15, has been used to obtain the density data reported here. By this method, equation 4.1 is solved (using the measured electron temperature) for the potential of the hemisphere at the easily recognized point where the electron current approaches its minimum resolvable value. An advantage of this means of selecting the point of measurement is that the resulting probe potential, V cutoff, and the measured current, i_p cutoff, are ionosphere-related rather than instrument-related in that the applied δV and the manner in which it divides between the pair of hemispheres need not be known.

A second point of ion current measurement, which has been used extensively to check the validity of the electron cutoff method, is to use the ion current at the point of maximum applied δV (approx. 3 volts), a point which is far into the ion saturation region and well off the volt-ampere characteristic shown in Figure 15. An advantage of using this point in the density reduction is that the relatively high and accurately known δV represents nearly the entire potential of the hemisphere with respect to the plasma. The small potential of the opposite hemisphere (approx. 1/2 volt), which must be added to obtain the hemisphere potential, V, need not be known extremely well to obtain an accurate value.

θ and λ are known from aspect and trajectory data, however, λ depends partly on the temperature, T, which is measured directly as described in Section 4. The ion mass, m_p, is assumed on the basis of a series of rocket-borne measurements at Ft. Churchill, Manitoba, and Wallops Island, Va., using Bennett rf mass spectrometers.[14,15] The resulting m_p profiles which were used in our reductions of ion density are shown in Figures 16 and 17.

A question arises here concerning the use of the electron temperature, T_e, in solving (5.1) for N_p, since the data presented in later sections strongly

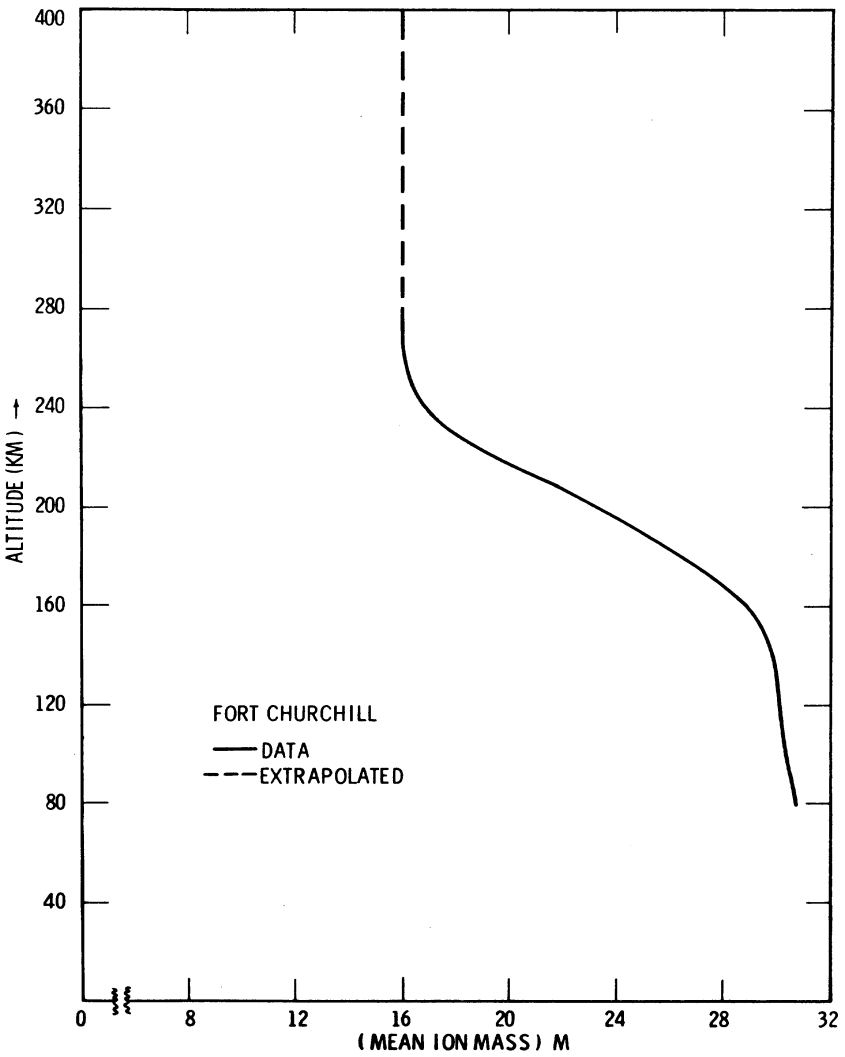

Figure 16. Mean ion mass profile used in ion density reduction from Ft. Churchill data.

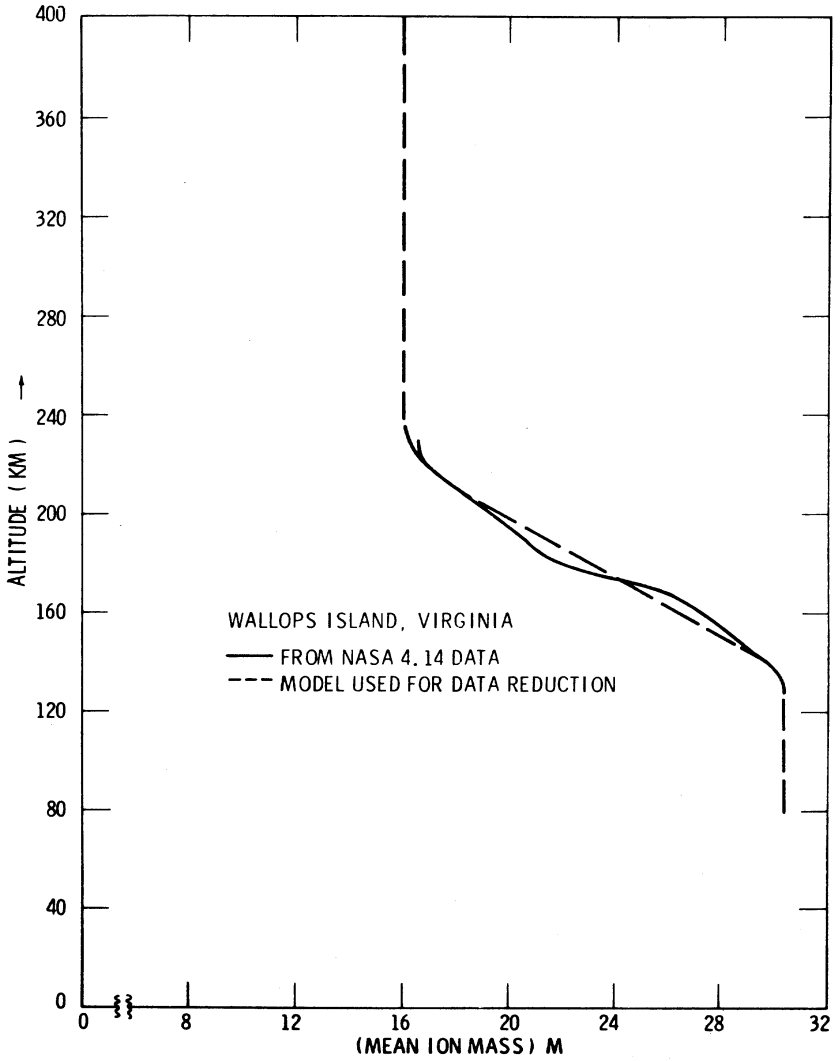

Figure 17. Mean ion mass profile used in ion density reduction from Wallops Island data.

suggests that T_e may, in some regions, be somewhat higher than T_p. It has been shown, however, that the electron temperature rather than the ion temperature is more important in the collection of ion current.[16] For this reason, and because it is a directly measureable quantity, T_e is used in solving (5.1) for the positive ion density.

The need to assume the mean ion mass, m_p, represents possibly the greatest potential source of error in the Dumbbell measurements of ion density. The ion mass spectrometer results at Ft. Churchill and Wallops Island, though quite consistent among themselves, do not sufficiently define the diurnal, seasonal, latitudinal, and solar cycle variations to permit their unqualified use in interpreting all total ion density measurements at these and other launch sites. Indeed, the different degrees of agreement between ionosonde and/or two-frequency beacon values of N_e and Dumbbell-derived values of N_p, measured on the flights to be discussed here, tends to emphasize this. This will be discussed at greater length in Section 9.3.

6.0 EXPERIMENTAL VOLT-AMPERE CHARACTERISTICS OF THE DUMBBELL

6.1 THE CURRENT DETECTOR CHARACTERISTICS

The accurate measurement of volt-ampere characteristics such as shown in Figures 10 through 14 is a challenging engineering task for several reasons: (1) The currents which must be resolved are both positive and negative; (2) the magnitude of current varies from a few tenths of a microampere in the lower E region to several microamperes in the F region of the ionosphere; (3) the response time of the current measurement system must be on the order of a few milliseconds to permit a nearly instantaneous sweep voltage; (4) the physical dimensions of each detector is severely limited by the available space (on the order of one cubic inch per detector); and (5) the environmental stresses placed on the detectors are severe.

An all solid state detector which met these requirements was designed utilizing a ring bridge type modulator, a suitable amplifier and a demodulator. Its design and physical configuration are documented in other reports.[5,12] Our purpose here is to discuss the electrical characteristics of the detector as they bear upon the appearance of the data when displayed on a paper telemetry record. The volt-ampere curves are modified by the detector in two ways:

1. The current characteristic is rectified so that currents of both polarity produce a positive output from the detector.

2. The lower 10% of the current range is somewhat nonlinear since the chopper type modulator has a small null output with zero input current. These effects are illustrated by Figure 18a, b, c which show the applied 8V, a zero velocity Dumbbell current characteristic and the detector output which results, respectively. Figure 19, for further illustration, shows the detector output waveform to be expected for the predicted curves of Figure 14.

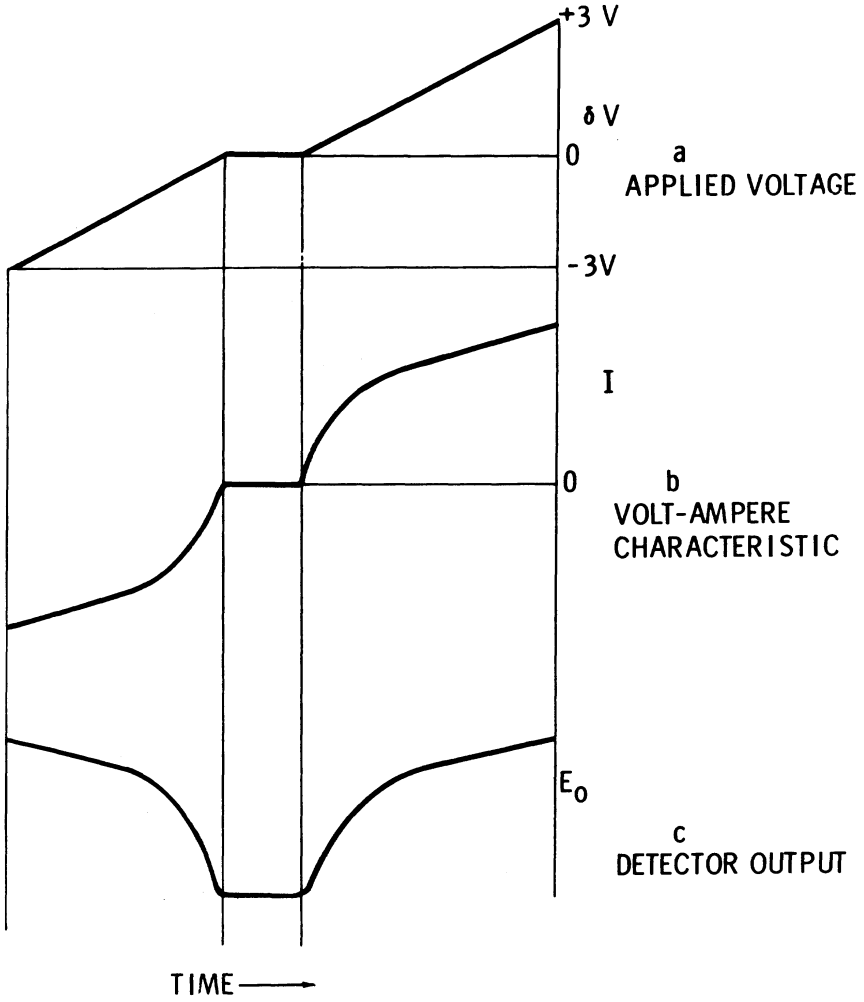

Figure 18. (a) Applied δV; (b) predicted volt-ampere characteristic; (c) current detector output resulting from (b).

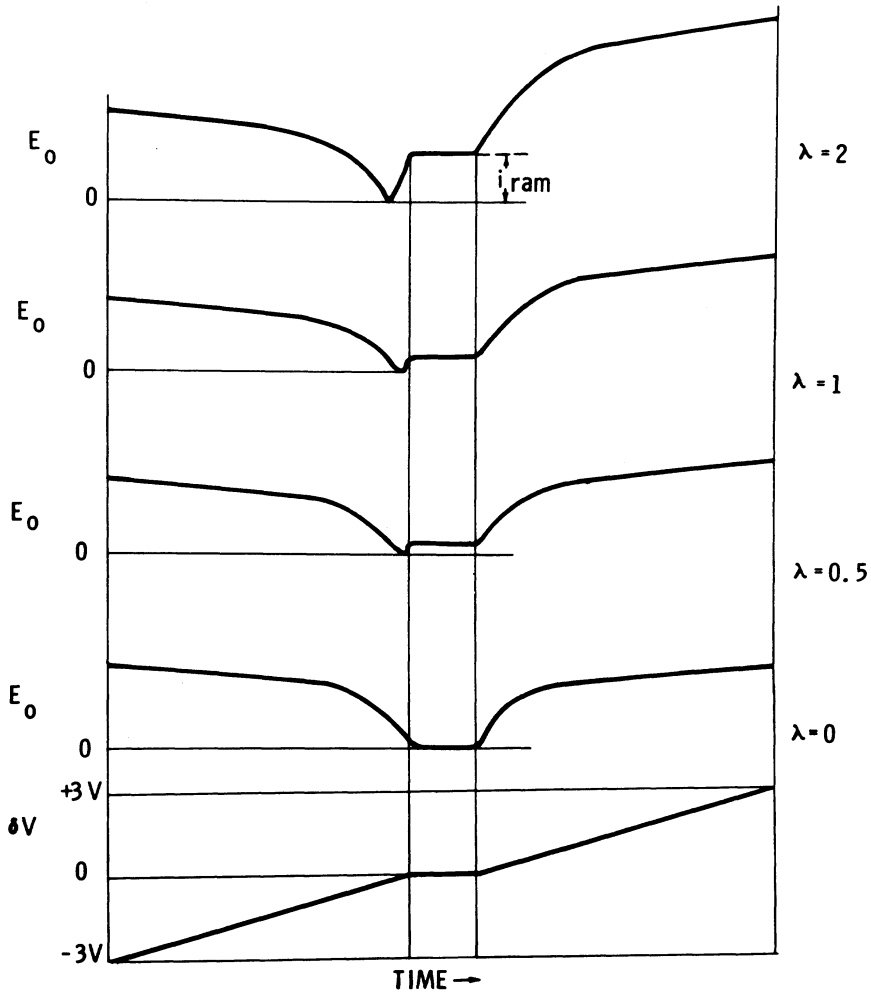

Figure 19. Detector output for the theoretical characteristics of Figure 14.

6.2 EXPERIMENTAL CHARACTERISTICS

Having illustrated the type of Dumbbell volt-ampere characteristics which should be expected from theoretical considerations, we now examine some of the experimental characteristics which constitute the raw data from actual flights. Figures 20 and 21 are photos of segments of the telemetry records showing V-A characteristics recorded near the apogee (F-region) of NASA 6.01 and 6.02, respectively. The 1 μa channel, designed for use primarily in the E region, is saturated, except near zero 8V; and the 4 μa channel, connected in series, shows nearly full-scale currents. The vertical grid lines occur at 0.1-second intervals. The 1 μa channel of the 6.01 record shows the expected bias current which results from a combination of the following factors: (1) the translational motion of the Dumbbell; (2) unequal photo-emission from the two hemispherical collectors at the particular orientation which existed; (3) anisotropy of the plasma; (4) slight differences in the surface conditions of the collectors, and (5) slight unbalance in the current detector response to opposite polarity currents. Factors (1) and (2) can be separated from (3) by the known orientation of the instrument with respect to the velocity vector, the Sun, and the geomagnetic field. An attempt is made to closely control (4); and (5) can be evaluated using the inflight calibration records such as shown in Figures 22 and 23 for these flights.

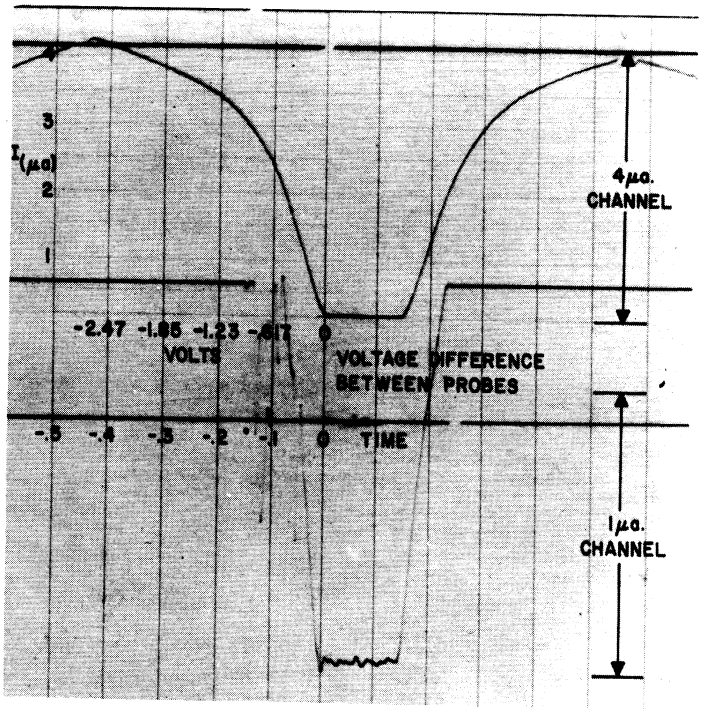

Figure 20. Typical current characteristics recorded at apogee of NASA 6.01, March 1960, Ft. Churchill.

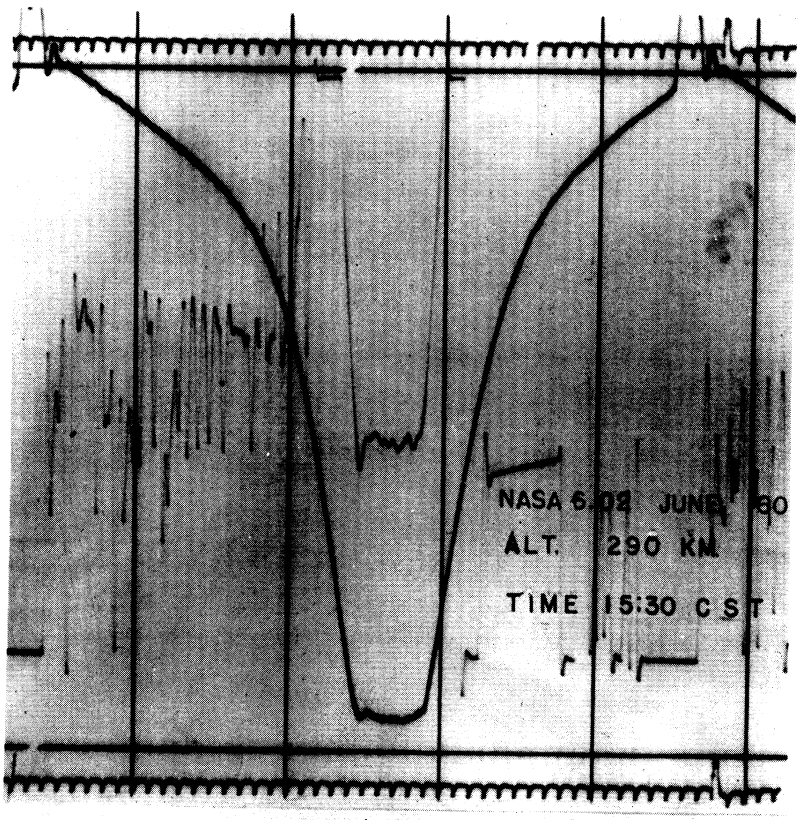

Figure 21. Typical current characteristics recorded at apogee of NASA 6.02, June 1960, Ft. Churchill.

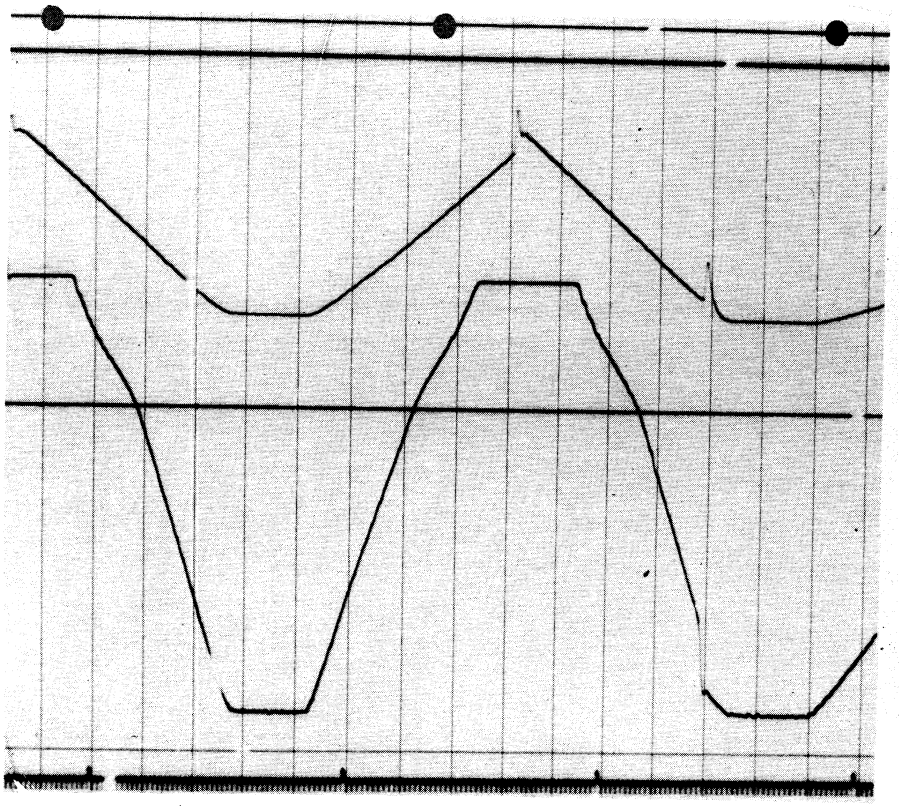

Figure 22. In-flight current calibration of NASA 6.01 current channels.

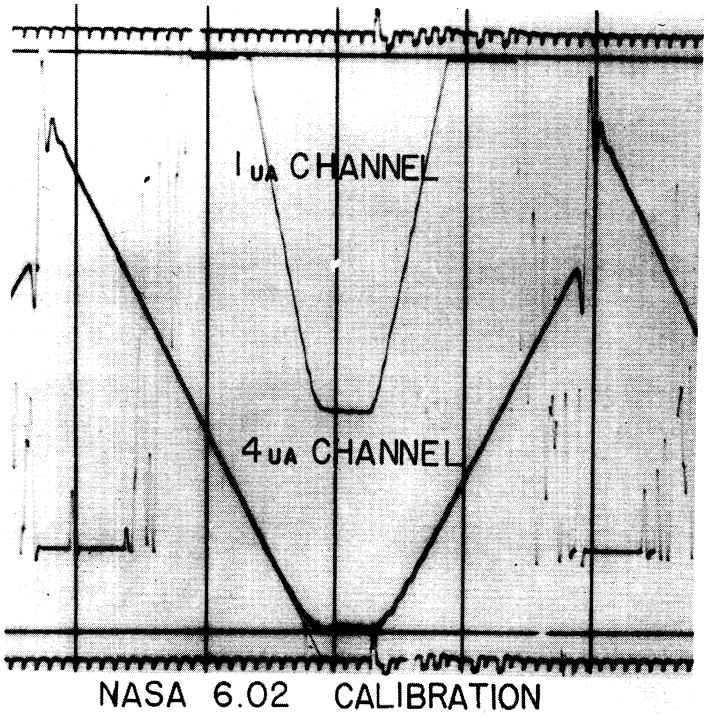

Figure 23. In-flight current calibration of NASA 6.02 current channels.

7.0 THE REDUCTION OF DATA FROM EXPERIMENTAL CHARACTERISTICS

7.1 DEMONSTRATION OF THE ELECTRON TEMPERATURE REDUCTION

Figure 24 illustrates the method of T_e reduction from a randomly chosen Dumbbell characteristic which was recorded near apogee during the June 1960 flight at Ft. Churchill, Manitoba. The telemetry record is shown approximately actual size. The ion saturation regions of the two collectors are evident at the far left and right. To obtain the electron current as a function of applied voltage, δV, the ion current region is extrapolated linearly and is then subtracted from the net (measured) current as described in Section 4.0. The natural log of the electron current is a linear function of the probe voltage as indicated by the straight line which results, and the slope of the line is related to the electron temperature by the equation

$$\frac{d(\ell n\ Ie)}{dV} = -\frac{e}{kT_e} \qquad (4.2)$$

The slope which results indicates a temperature of 2890°K at an altitude of 297 km. As the applied δV approaches zero (the time designated 0 on the record), it no longer divides as strongly in favor of the more negative hemisphere which causes the observed deviation from linearity at lower values of δV. When I_e is plotted versus the calculated dV, however, linearity is restored to the plot and the temperature obtained is in good agreement with the value shown.

7.2 DEMONSTRATION OF THE POSITIVE ION DENSITY REDUCTION

The ion density is obtained from the ion current by the method given in Section 5.0. To demonstrate the self consistency of the density reduction technique, an experimental curve was reduced to T_e and N_p. These values were then substituted into the current equations and used to generate a theoretical

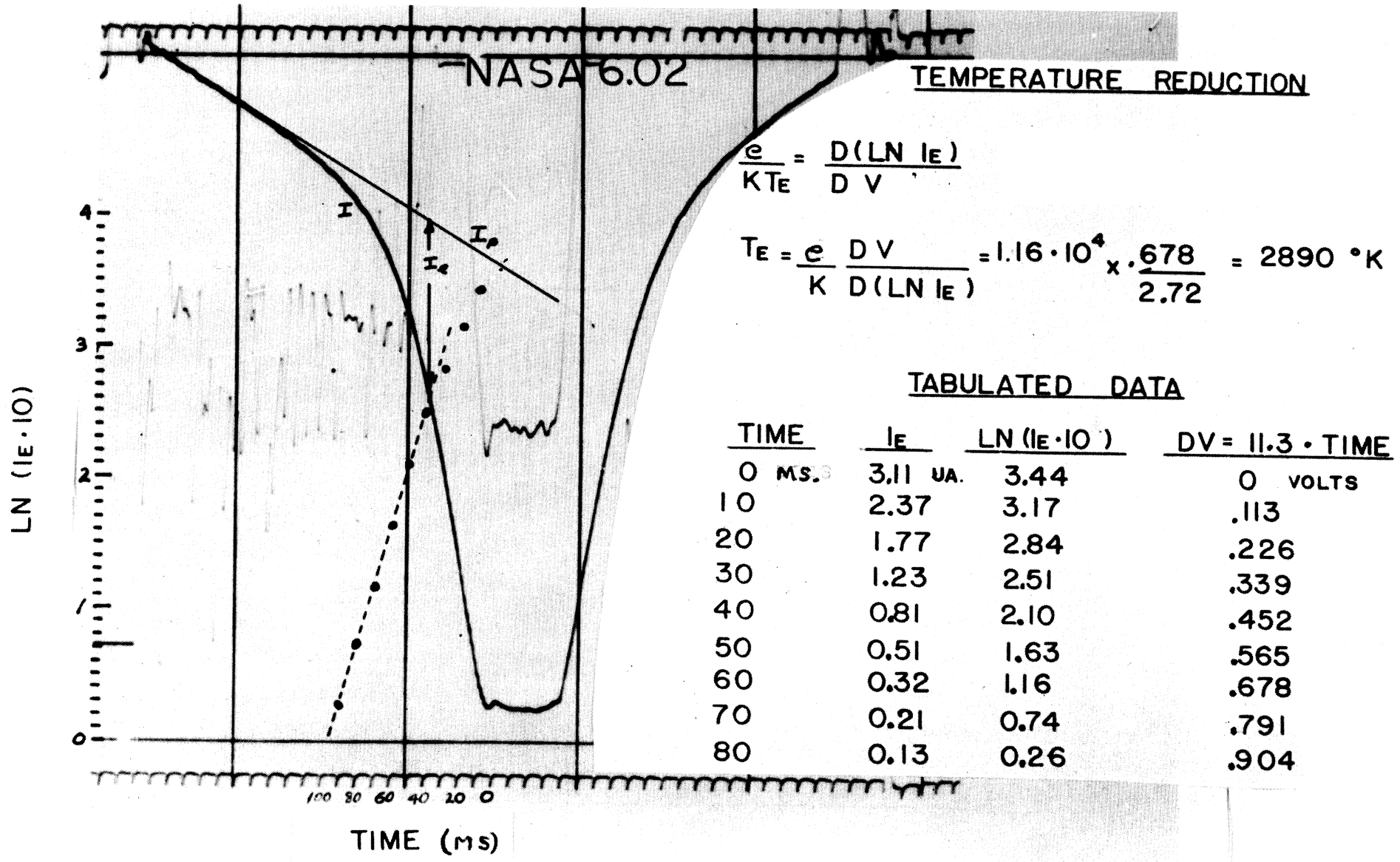

Figure 24. Illustration of the electron temperature reduction process from an experimental characteristic.

volt-ampere characteristic, which was then superposed on the telemetered experimental curve as shown in Figure 25; the curve labelled with an ion density of 7×10^5 part/cc. For comparison, a second curve corresponding to $N_p = 6 \times 10^5$ part/cc is also shown. The reduced ion density value is approximately 10% high because the effect of probe motion (not considered in this particular calculation) is not entirely negligible even at apogee where this curve was measured.

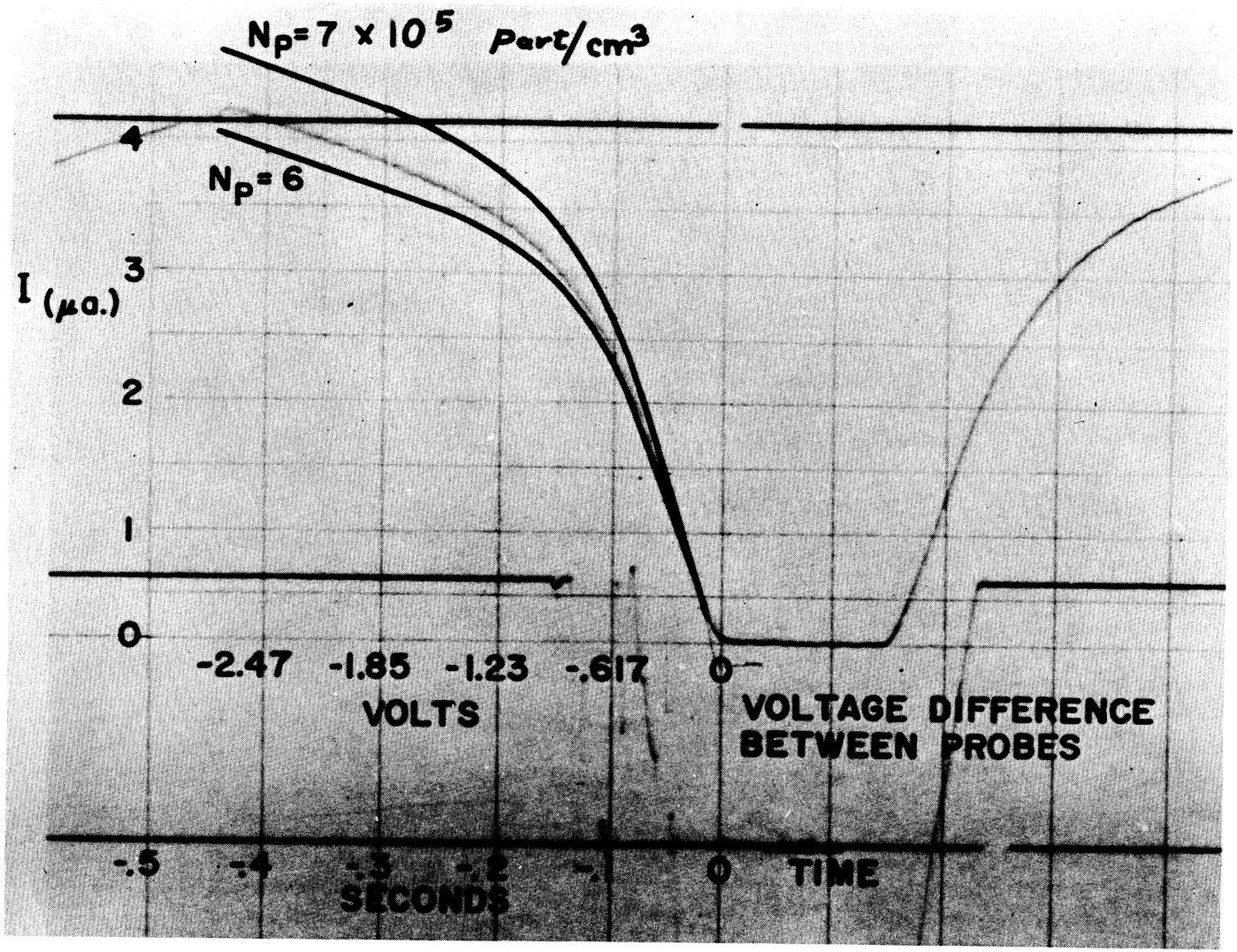

Figure 25. Demonstration of the experimental-theoretical self-consistency of the technique.

8.0 THE IONOSPHERE DATA

8.1 INTRODUCTION

In the previous sections the theory of the Dumbbell probe has been reviewed and some of the many volt-ampere characteristics which constitute the raw data have been shown. The self-consistency between theoretical and experimental characteristics is evident. The present section is devoted to a description of each flight and a presentation of the resulting ionosphere profiles of electron temperature and positive ion density, as well as a brief discussion of the data. In Section 9.0, the data from all five flights are compared and correlated with the work of other investigators to attempt to uncover some of the geophysical significance of these data.

8.2 PHILOSOPHY OF THE DATA PROCESSING

Given a sampling rate on the order of five sweeps per second and a flight time of 500 seconds, it is not difficult to see that several thousand volt-ampere characteristics are accumulated (recorded) during each flight.

Machine Data Reduction.—It soon became clear that the hand-reduction technique discussed in Section 7.0 was too time consuming to permit the analysis of all recorded curves from each flight. On the other hand, since the Dumbbell probe was new to ionosphere research, we did not feel justified in using only a random sampling of curves. Indeed, this course would bypass a prime advantage of the method; i.e., nearly instantaneous measurements at small altitude intervals which permit the detection of the fine structure known to exist in the ionosphere and not as readily detectable by other techniques. Thus a machine data reduction program was developed for use on the University of Michigan IBM 704, and later IBM 7090 computer. Each analog curve was digitized and placed on punch cards by the University of Dayton Computing Service. Extensive hand reductions,

directly from the analog records and from the digitized data, were carried out to evaluate the machine-reduced values for systematic and random error. No systematic difference between machine and hand-reduced values was observed; however, the "spread" in the machine-derived values was approximately $\pm$ 10% while the hand-derived values were normally spread less than $\pm$ 5%. These figures should be considered approximate, since curve resolution varied from flight to flight and during each flight, and later Dumbbells had improved guard action which reduced the amount of spread in consecutive data points. The data from later flights was, in general, reduced primarily by hand as curve sampling techniques were developed which permitted the ionosphere profiles to be obtained using fewer characteristics.

In the following sections, the electron temperature and ion density profiles are presented and discussed, then photographs of the telemetry records of typical up-leg and down-leg V-A characteristics are shown and are discussed in relation to the ionosphere profiles.

8.3 FLIGHT STATISTICS AND IONOSPHERE-CONDITIONS AT LAUNCH TIME

Five Dumbbell probes were launched between March 1960 and December 1961. Similarities and differences in ionosphere conditions at the time of launch and the characteristics of the instruments are summarized below:

Similarities.—

1. Physically identical Dumbbell-shaped probes were used in all flights.
2. The electrical measurements systems were identical in the first three of the probes. The fourth and fifth, NASA 6.04 and 6.05, were slightly modified to improve the guard action as discussed in Section 8.7.2.
3. All of the Dumbbells were launched on Aerobee 300 rockets, and the instruments reached peak altitudes ranging from approximately 300 to 400 kilometers.

Differences.—

1. Minor differences in the internal circuitry were adopted to test the validity of various assumptions concerning the measurements.
2. Differences in performance characteristics of the rocket and the instrument, as indicated in Table A.
3. Differences in the state of the ionosphere as indicated in Table B.

8.4 NASA 6.01—EARLY SPRING, DISTURBED AURORAL ZONE IONOSPHERE

Figure 26 shows NASA 6.01 (an Aerobee 300) leaving the Ft. Churchill tower in mid-afternoon on March 16, 1960. An ionogram showing the "spread F" condition which existed at the time of launch is shown in Figure 27. The clamshell nose cone opened on schedule at 97 kilometers, ejecting the Dumbbell into the atmosphere just below the E region. Measurements were made continuously at the rate of two per second as the instrument tumbled, in free fall, up to a peak of 332 kilometers and then back through the ionosphere, passing out of the E region over a point on the Earth some 99 kilometers from the launcher at an azimuth of 62°, about nine minutes after launching. The horizontal velocity was approximately 200 m/sec. Ground receiving stations recorded the output of the three telemetry channels; one for each of two current detectors in the Dumbbell and a third which is time-shared by aspect magnetometers and special tests. Other data recorded included the AGC output from a receiver operating from a helix antenna (used with the aspect magnetometers in determining Dumbbell orientation and range timing).

8.4.1 The Ionosphere Profiles

The Ion Density.—The electron temperature and ion density profiles are shown in Figure 28. It is apparent from the density profiles that the Dumbbell had not quite reached the F_2 maximum at its apogee of 332 kilometers. Proceeding down the density profile, the up-leg and down-leg curves show strong similarity in

TABLE A

DESIGN AND PERFORMANCE CHARACTERISTICS OF THE DUMBBELL PROBES

Characteristics	NASA 6.01	NASA 6.02	NASA 6.03	NASA 6.04	NASA 6.05
Current sensitivity, μa	1 and 4	1 and 4	1 and 4	2.25 and 5	1 and 4
Measurement programming	Continuous with timer initiated calibration and special tests.	Continuous with stepping Ledex calibration and special tests.	Same as 6.01	Same as 6.02	Same as 6.02
8V sweep rate, cps	1	2.5	3.1	2.5	2.5
Special tests (in flight)	1. Measurement of the collector-to-guard voltage to evaluate guard action. 2. Alternate application of both high and low 8V to observe possible overlapping of sheaths and to investigate ion saturation regions.	Periodic shorting of a hemisphere and guard to improve guard action at opposite hemisphere.	None	1. Continuous shorting of one hemisphere and guard to improve guard action at opposite hemisphere. 2. Measurements of V-A curves of auxiliary small cylinder collector. 3. Periodically reduced rf power to observe the effect, if any.	Same as 6.04
Tumble period, seconds	2	4	20	9	5
Probe ejection altitude, km	97	82	98	86	83
Peak altitude, km	332	297	420	359	365
Instrument performance	Excellent	Excellent	Good (somewhat low rf signal but essentially complete data recovery)	Excellent	Excellent
Data recovery from Dumbbell, %	100	100	100	100	100
Other potential simultaneous measurements	N_e from DOVAP N_e from Ionosonde	Same as 6.01	N_e from both Ionosonde and Two-Frequency Beacon.	Same as 6.03	N_e from Ionosonde
Data recovery from other measurements	None	N_e from Ionosonde	N_e from both Ionosonde and Two-Frequency Beacon.	Same as 6.03	N_e from Ionosonde

TABLE B

EFFECTS CONTRIBUTING TO THE STATE OF THE IONOSPHERE

Effect	NASA 6.01	NASA 6.02	NASA 6.03	NASA 6.04	NASA 6.05
Latitude	Auroral Zone, 59° North Ft. Churchill	Auroral Zone, 59° North Ft. Churchill	Mid-latitude, 38° North Wallops Island	Mid-latitude, 38° North Wallops Island	Mid-latitude, 38° North Wallops Island
Seasonal	Early spring, 16 March 1960	Early summer, 15 June 1960	Mid-summer, 3 August 1960	Early spring, 26 March 1961	Early winter, 21 Dec 1961
Diurnal	Mid-afternoon, 3:26 p.m.	Late afternoon, 4:56 p.m.	Late morning, 11:26 a.m.	Noon, 11:56 a.m.	Midnight, 11:25 p.m.
Other	Strong spread F	Fairly quiet for auroral zone	"S" condition— third day of a magnetic storm	Quiet	Quiet

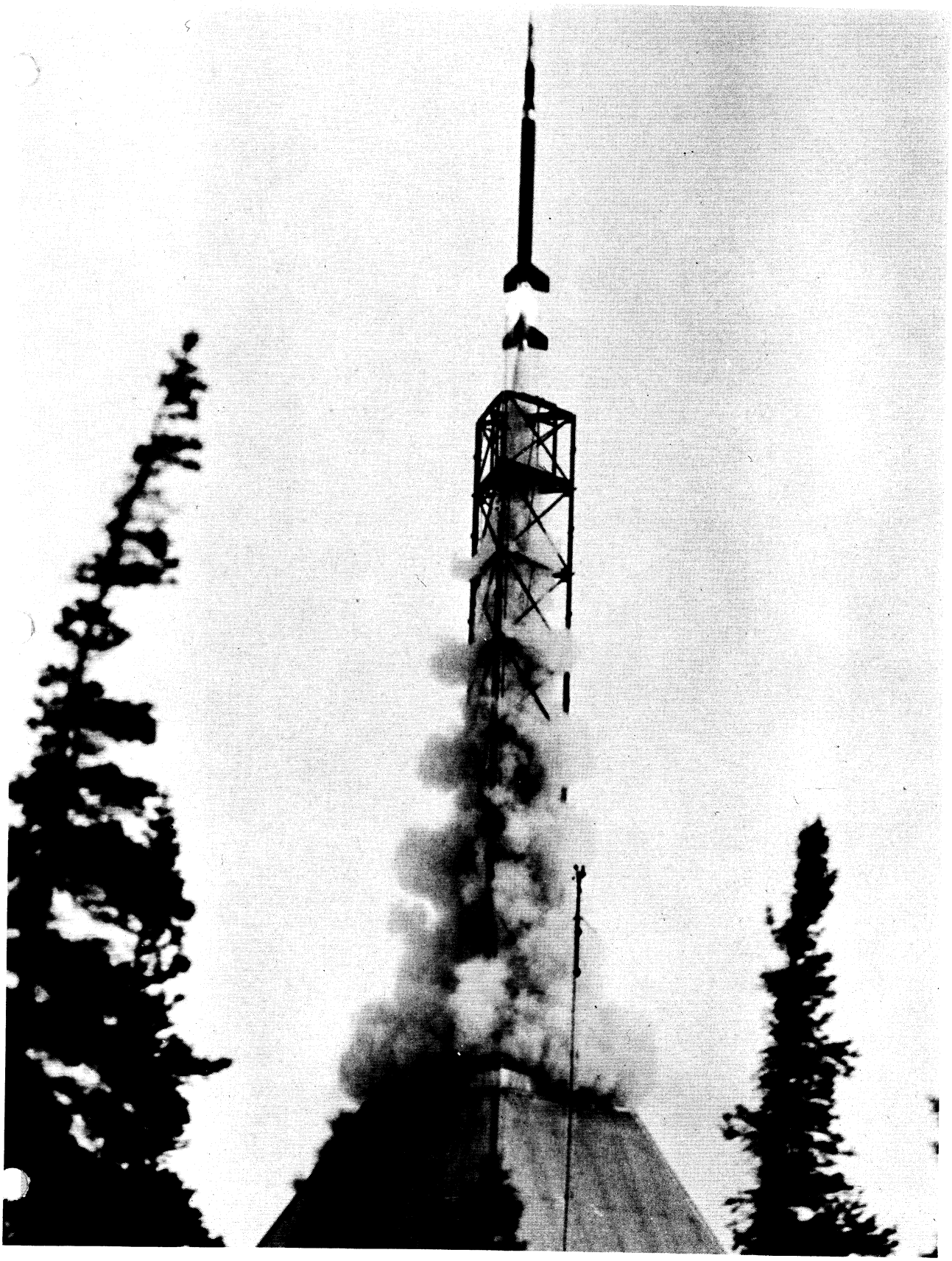

Figure 26. NASA 6.01 launching at Ft. Churchill in March 1960.

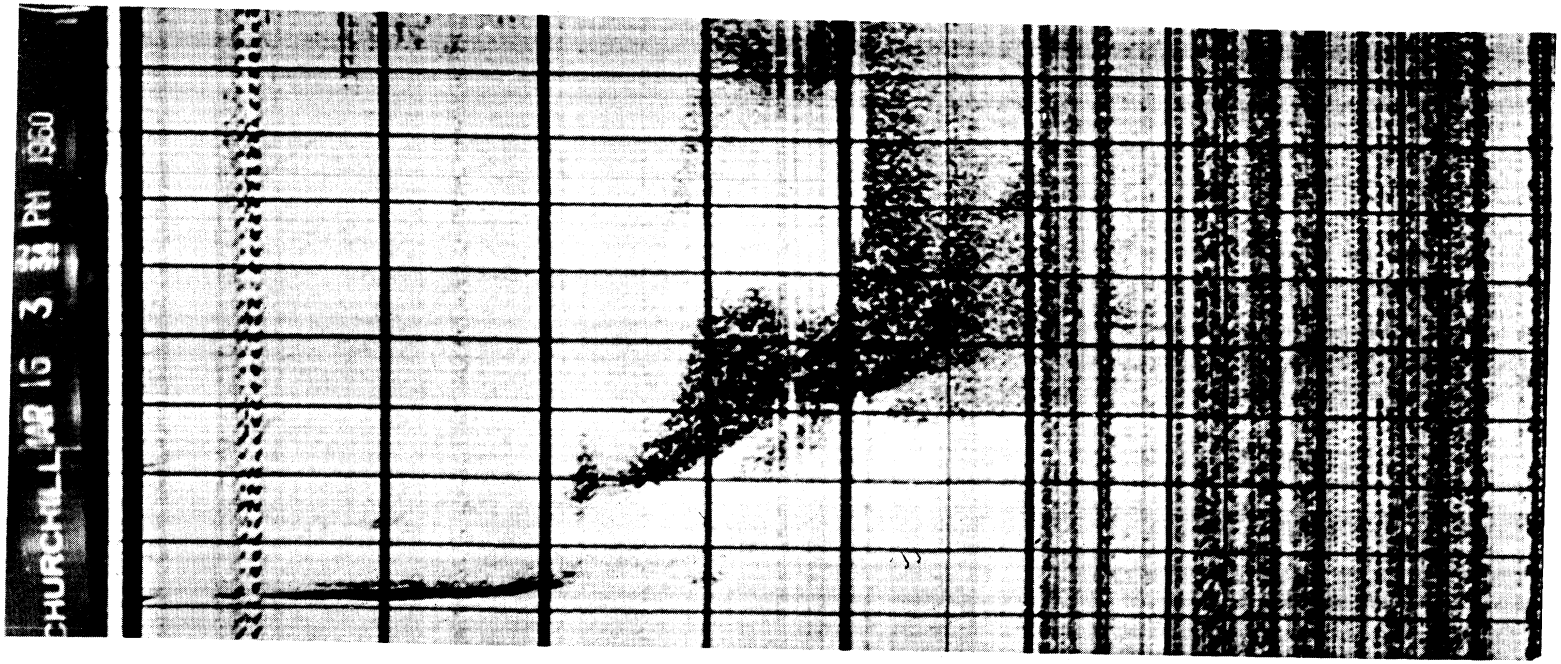

Figure 27. Ionogram recorded at Ft. Churchill during NASA 6.01 flight showing "spread F" condition.

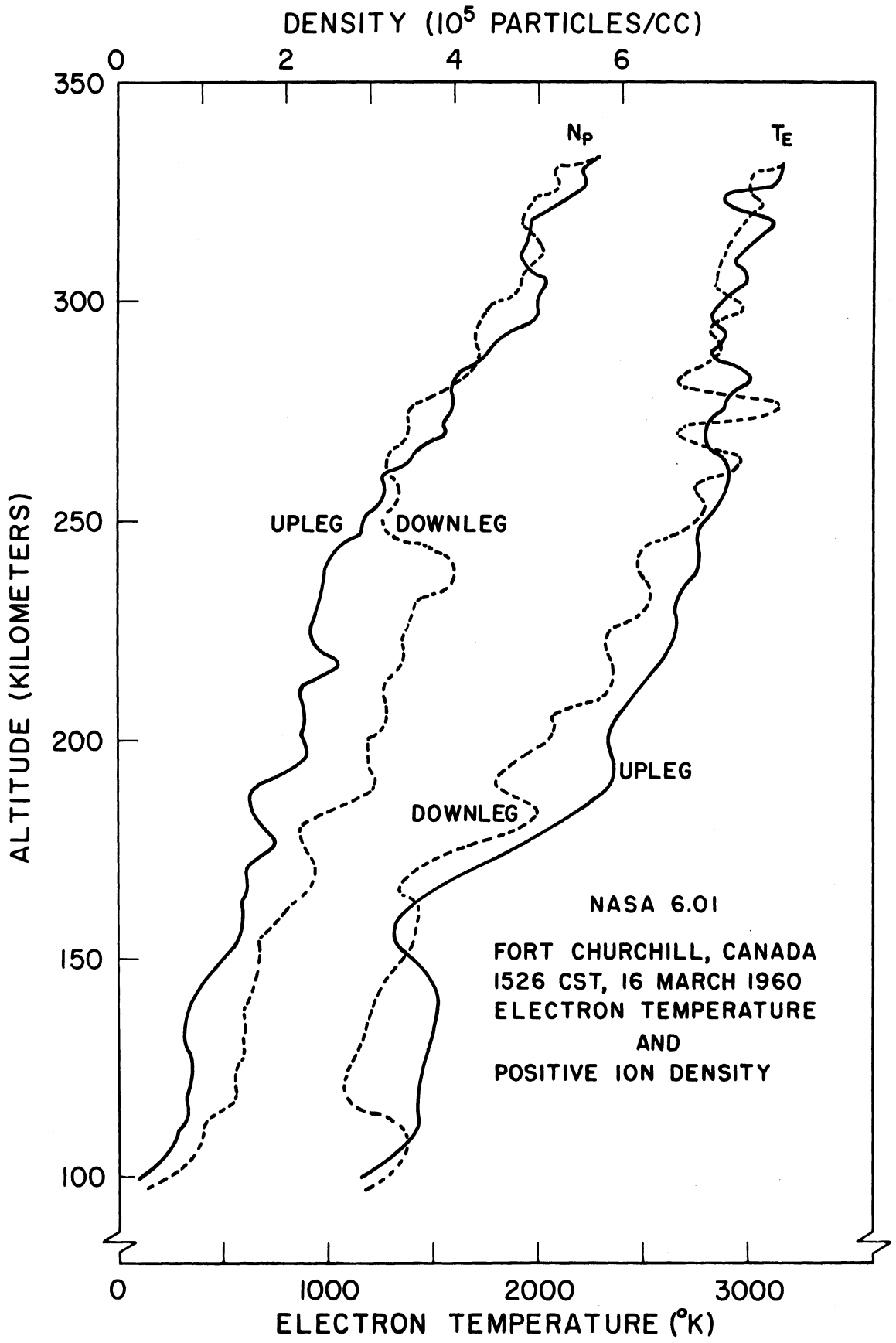

Figure 28. T_e and N_p profile from NASA 6.01.

the shape of the fine structure but not necessarily in its altitude. For example, just below apogee a small S-shaped curve in the up-leg profile at 327 kilometers finds a strong resemblence in the down-leg profile at the same altitude, while a similar density variation between 270 and 280 kilometers, although apparent in both curves, differs in altitude by as much as 10 kilometers. The S-shaped curve near 180 kilometers shows a similar altitude shift of the fine structure. At first consideration one might attempt to attribute this shift to an error in the trajectory, but this would normally cause an increasing shift in the fine structure at lower altitudes on the down-leg, a condition not evident as the structures of the up and down profiles come back nearly into phase at 100 kilometers.

A marked ionosphere irrgularity is visible below 250 km on the down-leg density profile where the ion density increases by some 25% and remains higher than the up-leg profile throughout the remainder of the flight. This is probably caused by the horizontal motion of the Dumbbell which permits horizontal as well as vertical gradients to appear in the flight profiles.

The Electron Temperature.—The most striking feature of the T_e profile is the rather high electron temperature which, except near 160 to 170 kilometers, is considerably higher than present accepted gas temperatures.

The strong positive temperature gradient between 160 and 190 kilometers apparently identifies the region of maximum energy input to the ionosphere where the electron production rate is greatest. At the bottom of the E-region the electron temperature appeared to have another strong positive gradient, but the ion density (thus the measured ion current) below 100 kilometers was too low to permit accurate temperature reductions. This was not true in later flights at Wallops Island as will be seen in the profiles of NASA 6.03 and 6.04 when temperatures as low as a few hundred degrees were resolved.

Fine Structure.—Fine structure is observed in the up-leg and down-leg profiles of both electron temperature and ion density, although there is no obvious correlation between the T_e and N_p details. Since fine structure of this magnitude was not found in later flights, it may have been related to the existence of the "spread F" condition.

Further discussion of the data from this flight, and its possible geophysical significance, is reserved for Section 9.0 where the results of all of the five flights will be considered and compared. The following section is devoted to photographs of telemetry records displaying typical volt-ampere characteristics which comprise the raw data from this flight.

8.4.2 The Raw Data

Ejection and Apogee Telemetry Records.—The upper half of Figure 29 shows a four-second segment of the telemetry record of the current channels beginning just before Dumbbell ejection, which is recognized by the commencement of rf signal. Ejection occurred during an inflight current calibration period which is followed, here, by several volt-ampere characteristics measured in the lower E-region (100 kilometers). The upper and lower traces on each record represent the outputs of the series-connected 4 μa and 1 μa current detectors, respectively.* The current calibration on the scale shown here is approximately 5 μa per inch of vertical deflection for the 4 μa channel and 1.3 μa/inch for the 1 μa channel. The horizontal scale represents time (or the applied 8V, which is a function of time as shown in Figure 18). The voltage sweep rate, dV/dt, was 6.3 volts/second. The vertical grid lines occur at 0.1-second intervals, with time increasing to the right in all cases. The vertical and horizontal scales are the same throughout this series of photos for NASA 6.01. The occasional dropout of signal occurs when a null of the rf field dipole pattern is directed toward the ground station

*The "noise" of the up-leg 1 μa channel is thought to be instrumental.

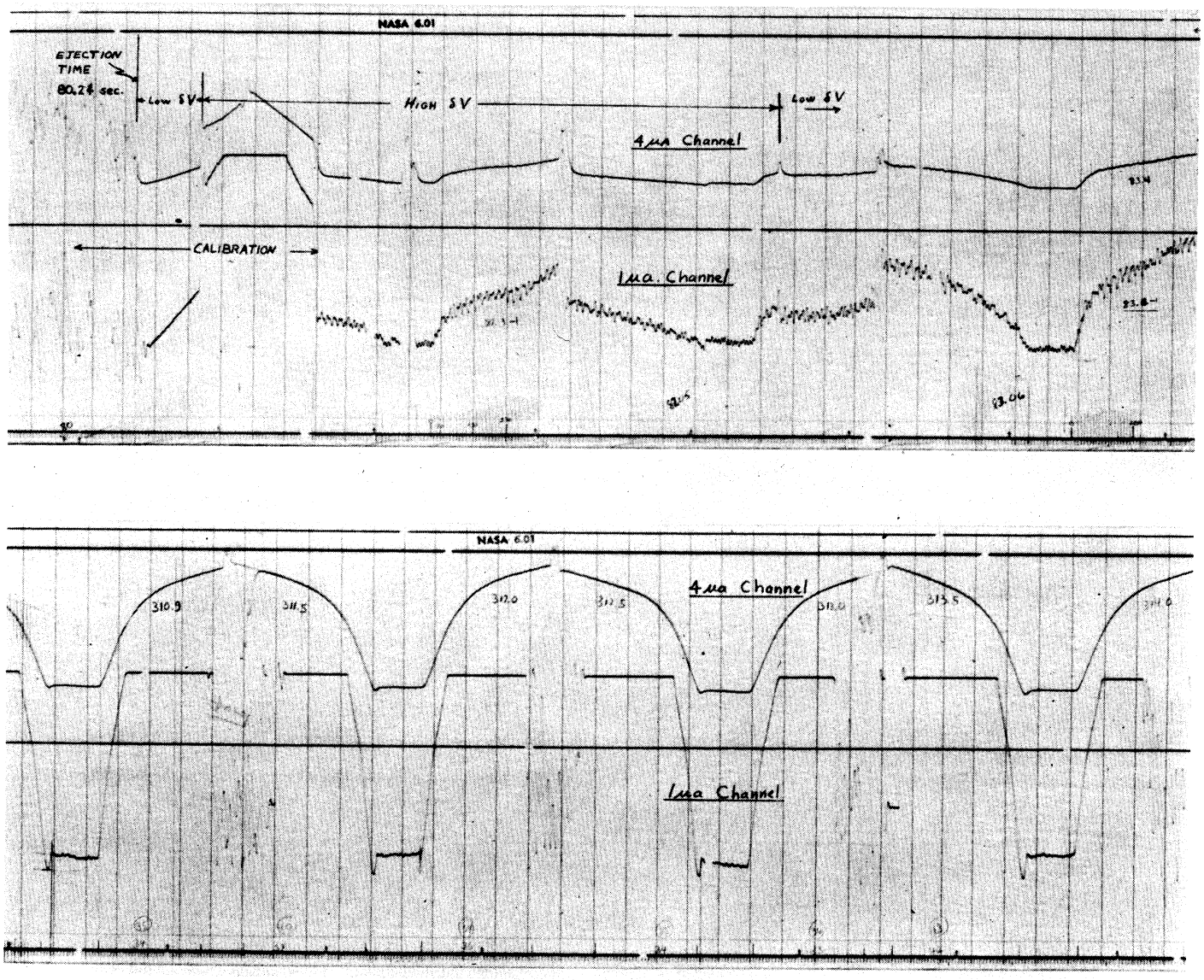

Figure 29. Segments of NASA 6.01 telemetry record near the time of Dumbbell ejection (97 km) and at apogee (330 km), respectively.

at approximately two-second intervals corresponding to the tumble period.

For contrast, the lower half of Figure 29 shows several volt-ampere characteristics recorded near apogee (330 km), which was apparently somewhat below the altitude of the F_2 maximum. Here, the ion saturation region of the Dumbbell characteristics reached currents of just over 4 μa, thus saturating the 1 μa channel whose output represents an approximately four-fold amplification of the 4 μa channel. Zero current for each channel is the lowest point on the trace.*

The effect of probe motion upon the shape of the characteristics is evident in the upper telemetry record which was recorded when the probe velocity was two to three times the average ion velocity. However, in the apogee curves, the velocity effect is barely visible and is detected primarily as a small bias current at zero δV and a slight unsymmetry in the magnitude of current in the ion saturation regions of the opposing hemispheres.

E-Region Records.—Figure 30 shows the Dumbbell volt-ampere characteristics recorded at approximately 112 kilometers as the probe passed through the E-region on the up-leg (upper record) and on the down-leg (lower record). The up-leg curves were recorded about 5 seconds after ejection; and, as can be seen by comparison with the previous figure, the ion current has approximately doubled between 97 and 112 kilometers. This is reflected directly in the N_p profile. The down-leg curves are strikingly similar to those recorded on ascent but their average amplitude is slightly higher, which produces the higher value of N_p in

*Zero current does not necessarily correspond to zero δV (except during calibration as shown in Figures 22 and 23) because bias currents may exist due to (1) the probe motion, (2) unequal photoemission from the pair of hemispheres, and (3) slight unbalance in the current detector (causing an apparent bias current). The first factor is to be expected and is always detectable even at apogee where only the horizontal velocity remains. The solar-induced photoemission has not been detected since, in the altitude range of these measurements, it is small enough to be entirely masked by the normal ionosphere currents. The third factor would be apparent in the calibration curves and has not been significant in any of the flights.

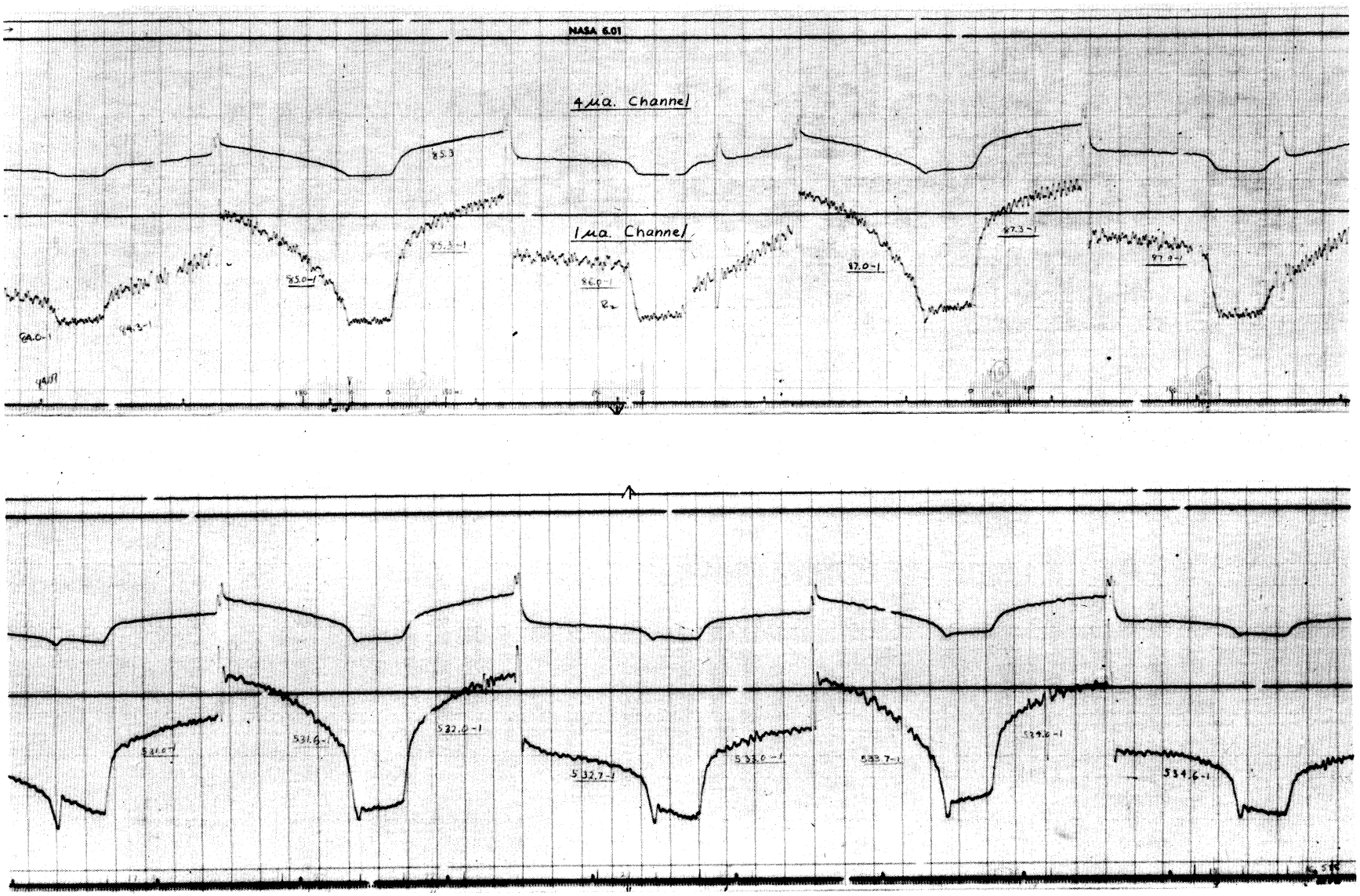

Figure 30. Segments of NASA 6.01 E-region telemetry records on the up-leg (above) and down-leg (below), respectively.

the down-leg E-region profile.

The ram current variation, which is a function of Dumbbell orientation, can be readily observed in the zero δV segments of the 1 μa channel on which they appear to follow a sinusoidal variation having a period coincident with the Dumbbell tumble period.

It can be seen that ion saturation, in these E-region curves, is reached with an applied δV of only about 0.7 volts while the F-region curves (apogee) required almost 3 times this value, which is the approximate ratio of F region to E region electron temperature as deduced from the records by the log plot technique of Section 4.0.

F_1- Region Records.—Figure 31 shows a section of the up-leg and down-leg records in the F_1-region (200 kilometers). The notably higher current on the down-leg record leads to the higher N_p shown for the down-leg F_1 region in Figure 28. The F_1-region characteristics are decidedly less sharply curved, and ion saturation occurs at about twice the value of δV required in the E-region; both of which are indications of the higher-temperatures in the F_1-region. The beginning of an inflight current calibration is visible at the right of the down-leg record shown.

As indicated in Section 2.0 the use of two series-connected current detectors provides adequate resolution in the current measurement in both the E-region and the F_2-region. In some range of altitudes, often the F_1-region, the ion density is such that both detectors are capable of high resolution measurement. In these regions of overlap, such as shown in Figure 32, the electron temperatures and ion densities obtained from both channels are carefully compared to detect any systematic error due to inaccurate calibration or nonlinear characteristics of the detectors.

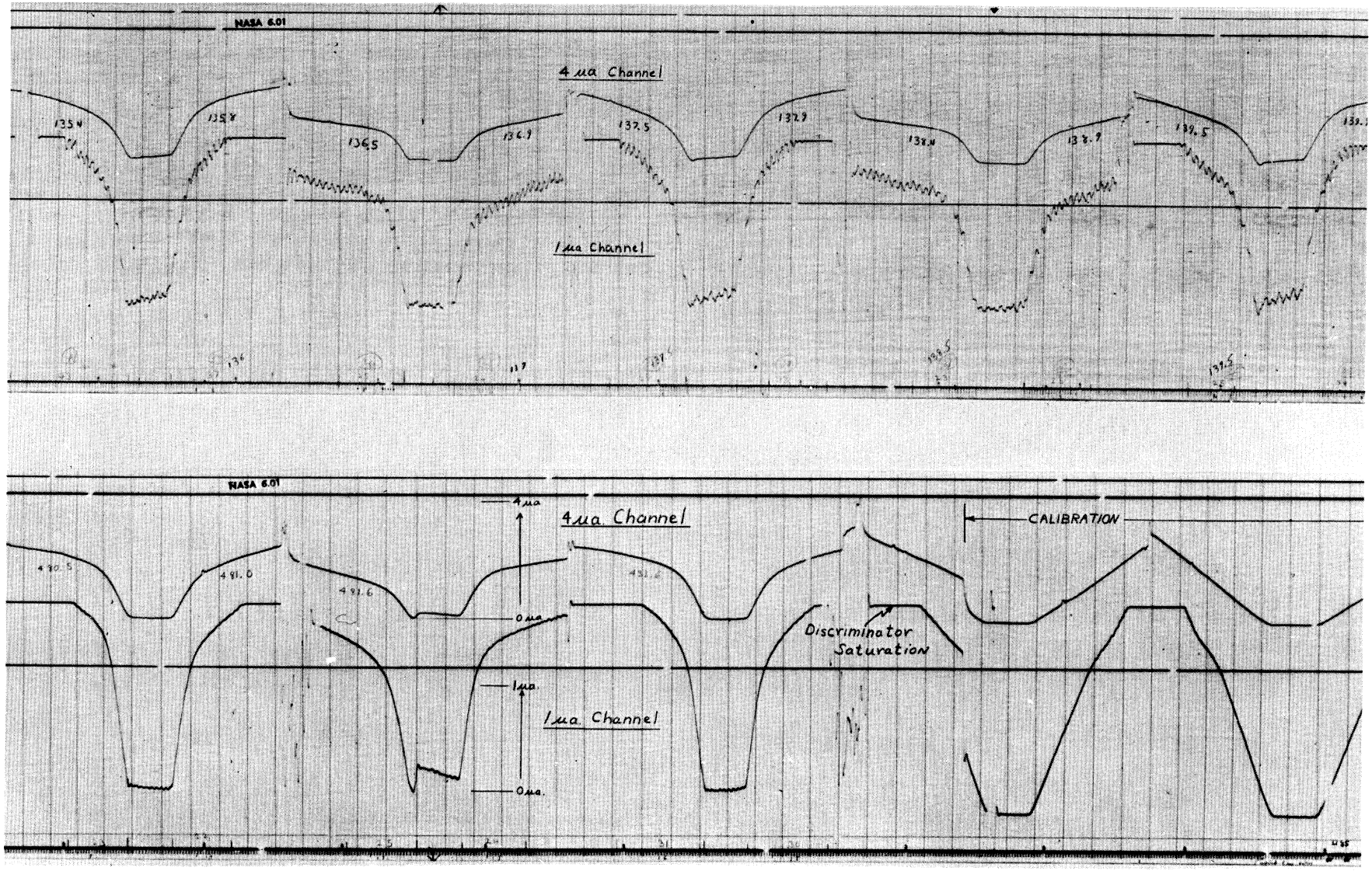

Figure 31. Segments of NASA 6.01 F_1- region telemetry record on the up-leg and down-leg, respectively.

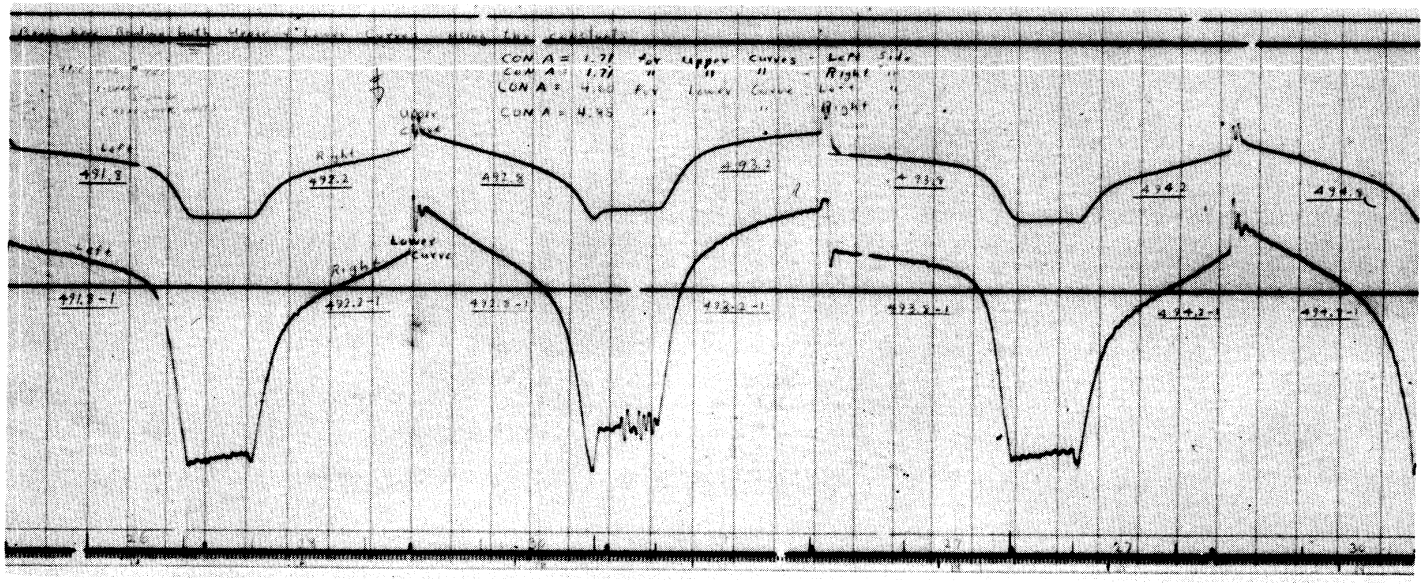

Figure 32. 1 μa and 4 μa channels in the region of overlapping use (NASA 6.01—180 km, down-leg).

8.5 NASA 6.02—EARLY SUMMER, QUIET AURORAL ZONE IONOSPHERE

About three months after the launching of NASA 6.01 a second Aerobee 300 was launched at Ft. Churchill on the afternoon of June 15, 1960. The ionosphere appeared fairly quiet, as shown on the ionosonde record, Figure 33, where the classic E, F_1 and F_2-regions are apparent. Ejection of the Dumbbell occurred just below the E-region, at 82 kilometers, and measurements were made at the rate of 5 per second as it tumbled nearly in the plane of the trajectory. The instrument traveled to a peak of 297 kilometers and returned to Earth, passing out of the E-region approximately 175 kilometers from the launcher at an azimuth of 42°, and moving with a horizontal velocity of about 380 meters per second.

8.5.1 The Ionosphere Profiles

The T_e and N_p profiles as well as an N_e profile obtained from the ionosonde record are shown in Figure 34. The Dumbbell apogee was approximately 50 kilometers below the F_2 maximum given by the ionosonde.

Both the N_p and T_e profiles show considerably less of the fine structure than was evident in the "spread F" ionosphere of NASA 6.01. This may be due primarily to the quieter ionosphere conditions, but is partly caused by the smoothing of the machine-reduced data. As pointed out earlier, smoothing of the data provides a more accurate mean temperature but attenuates the fine structure. To illustrate this, a series of several hundred consecutive up-leg curves, recorded from 170 to 235 kilometers were reduced by hand. The resulting profile, Figure 35, shows a better defined temperature fine structure. For instance the well defined temperature minimum at 195 km is only suggested in the machine-reduced values of Figure 34. The temperature values in Figure 34 are "raw", i.e., not corrected for the voltage drop within the current measurement circuit and thus are 10% higher than the actual temperature values.

The Electron Temperature.—With the exception of fine structure, the general

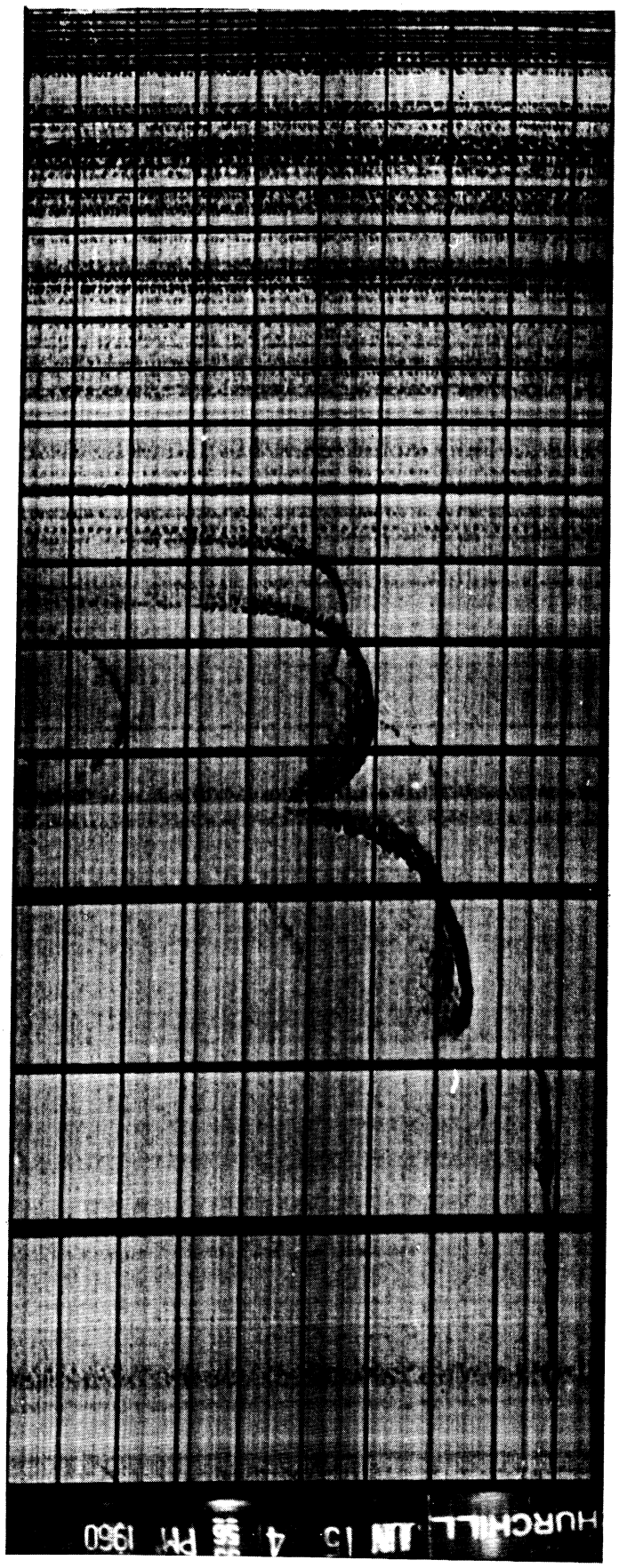

Figure 33. Ionogram recorded at Ft. Churchill during NASA 6.02 flight.

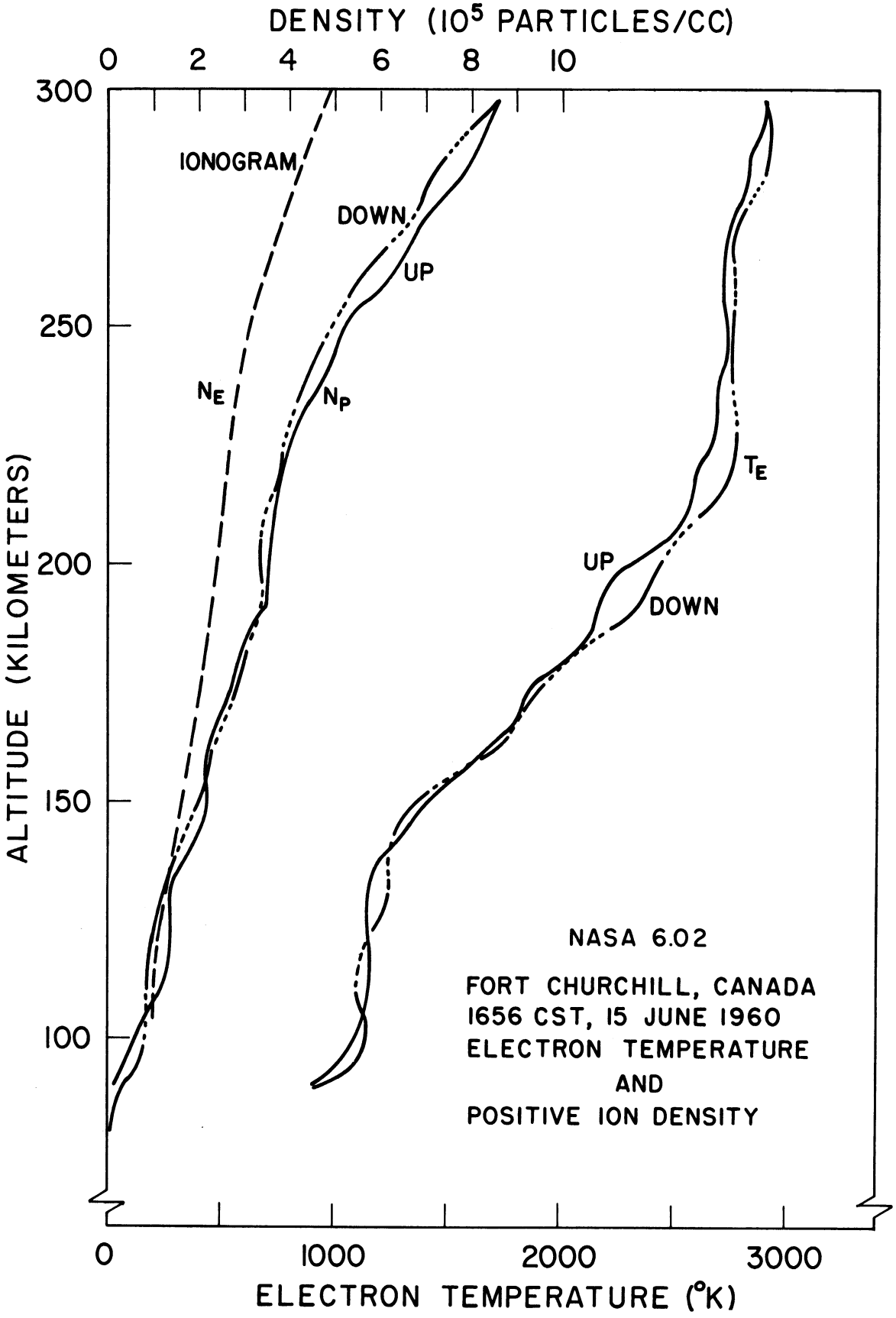

Figure 34. T_e and N_p profile from NASA 6.02—ionogram-derived N_e is also shown.

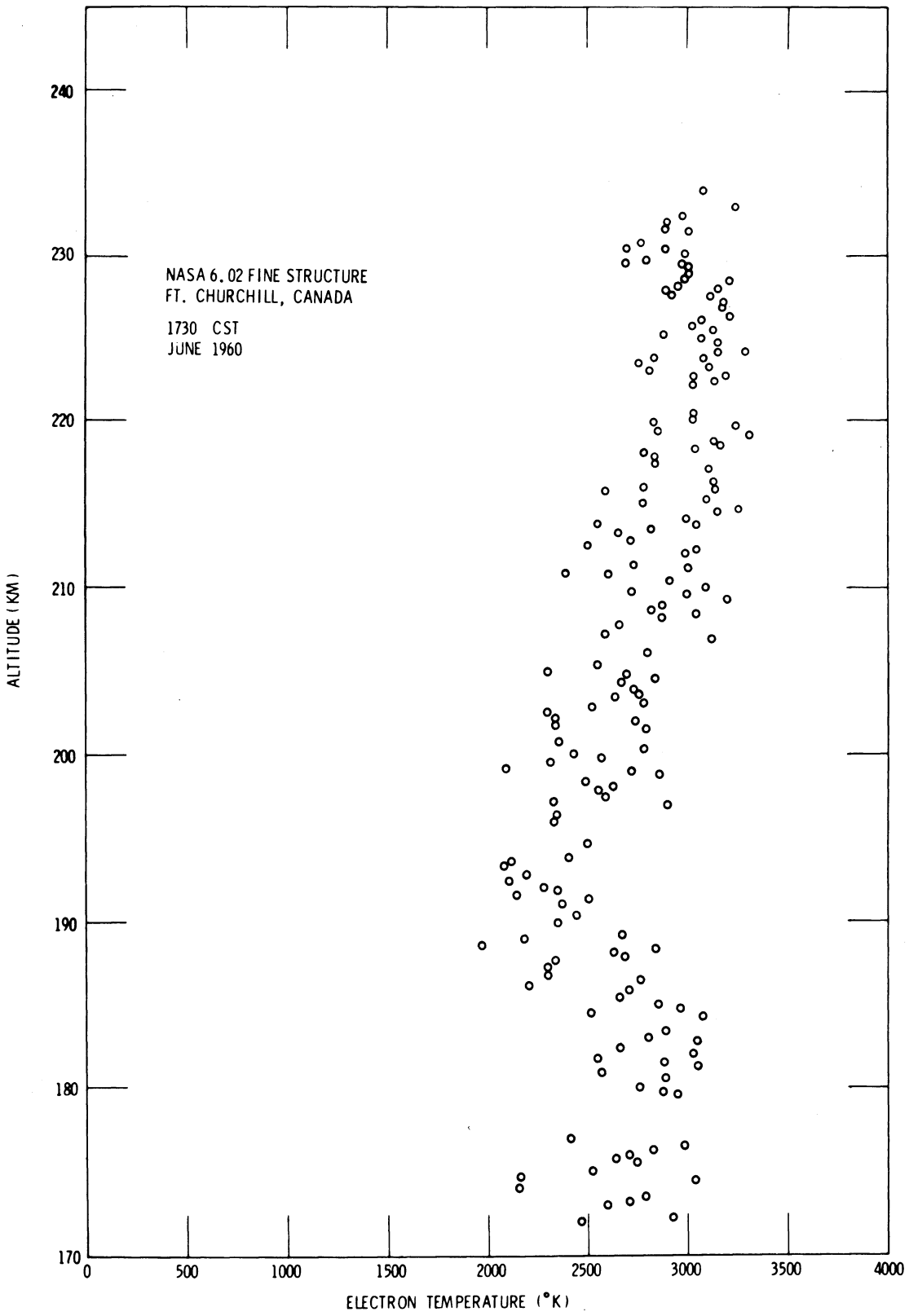

Figure 35. Fine structure in the electron temperature found by hand reduction of consecutive up-leg curves of NASA 6.02.

features of the electron temperature profile are very similar to those found in the early spring ionosphere; namely, an E-region which is isothermal at approximately 1000°K, followed by a steep positive temperature gradient in the F_1-region, and finally an F_2-region which is isothermal at approximately 2800°K. Based on the measurements of these two flights, these appear to be general features of the auroral zone ionosphere. It will be seen in Section 8.6 that a quite similar profile may be characteristic at lower latitudes when the ionosphere is experiencing the "negative phase" of a magnetic storm. At these times a considerable portion of the heat input to the atmosphere may be due to particle fluxes[23] which presumably are always a significant energy source in the auroral zone ionosphere.

The Positive Ion Density.—The ion density shows the same general profile as the ionosonde-derived electron density but, above 200 kilometers, is considerably higher in magnitude. The poor agreement is not fully explained, but may be due, in part, to (1) the existence of lighter ions (H_e^+ and H^+) at the higher altitudes over Ft. Churchill (we assume only O^+ above 240 km in the N_p reduction), (2) the inexactness of the probe theory, in the interpretation of the ion current which tends to give densities too high, (3) error in the ionosonde N_e reduction which has a tendency to give somewhat low densities. The good agreement which was found in the later flights at Wallops Island suggests that the accuracy of the probe theory cannot be a major factor here.

Further discussion of the data is reserved for Section 9.0. In the next section, segments of telemetry record showing the raw data from this flight are presented. As before, the Dumbbell characteristics recorded on both ascent and descent of the E, F_1 and F_2-regions, as well as the record at ejection, are shown.

8.5.2 The Raw Data

Ejection and Apogee Telemetry Records.—The upper part of Figure 36 shows a 1.5 second segment of telemetry, recorded near the time of ejection. At the far left, the Dumbbell is still within the nose cone; no signal is being received and random noise is recorded. At 82 kilometers the Dumbbell emerges, and the rf signal strength rises (not shown here). After a few transients, presumably related to the shock of ejection, the two current channels settle down and record only the capacitive charging currents between δV cycles. Clearly, ejection occurred before the rocket reached the sensible ionosphere. At 84 kilometers (far right) a small current begins to appear on the 1 μa channel while the current is still below the null level of the 4 μa channel which shows little change in output.

For contrast, the lower part of the figure shows the current channels as they appeared near apogee (297 kilometers). The 4 μa channel deflects somewhat over full-scale in the ion saturation region of both hemispheres, while the 1 μa channel is off-scale, except near zero δV. The background "hash" on the record results from the failure of the ground station recording system to "lock out" when the 1 μa channel was driven off-scale and should be ignored. The curves at the left show a small bias current (visible on both series-connected channels) which slowly disappears in successive curves as the Dumbbell changes orientation. Close examination shows that the left hand characteristics (those which curve to the left) have a longer ion saturation region than do the right curves. This results from the slightly unsymmetrical δV employed in this flight which applied 2.8 volts in one direction and 2.2 volts in the other. The left curves here represent primarily the current characteristic of the number 1 hemisphere (current detector end of Dumbbell) and the right curves, the number 2 hemisphere (transmitter end of the Dumbbell), as defined in Figure 9.

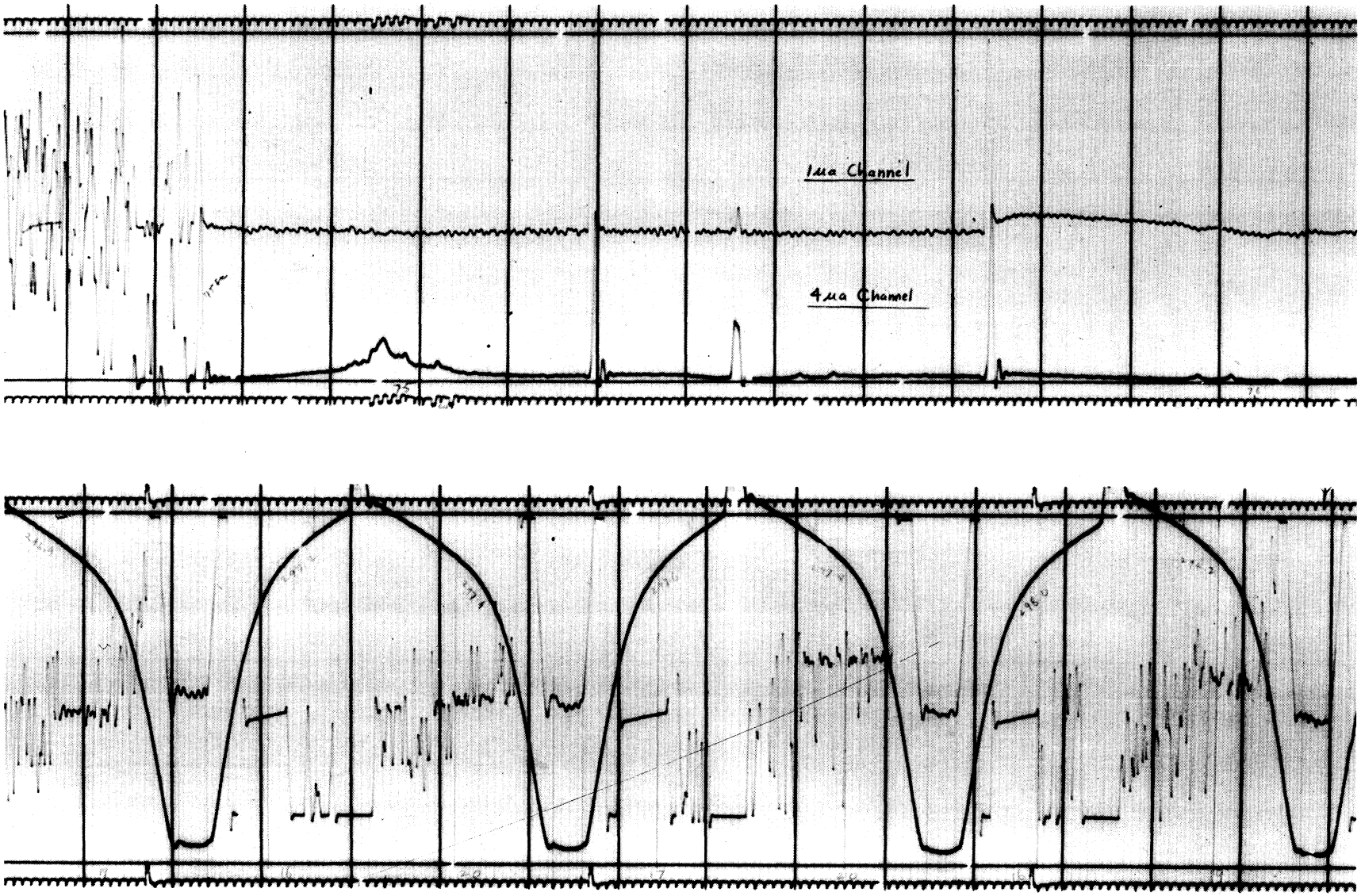

Figure 36. Segments of NASA 6.02 telemetry record at ejection (above) and apogee (below).

E-Region Curves.—Typical E-region (120 kilometers) Dumbbell characteristics are shown together in Figure 37 for the purpose of comparison. The down-leg curves (lower) are somewhat noisy due to low signal strength from a non-steerable helix antenna which was used at the ground station. On both records, the Dumbbell is seen to rotate from an orientation of full ramming of the number 1 hemisphere ($\theta_1 = 0°$, $\theta_2 = 180°$) at the left of the record shown, to full ramming of the number 2 hemisphere ($\theta_2 = 0°$, $\theta_1 = 180°$) at the right, and to the intermediate symmetrical position ($\theta_1 = \theta_2 = 90°$) in the curves displayed in the center. These orientations correspond qualitatively to the predicted V-A characteristics shown in Figures 11, 13, and 12, respectively.

F_1-Region Curves.—Typical F_1-region currents recorded on ascent and descent are shown together in Figure 38 where each segment of record again represents 1.5 seconds of flight. The up and down-leg curves, recorded at the same altitude (190 kilometers) are strikingly similar, and through the data reduction process lead to almost identical up-leg and down-leg T_e and N_p values in the F_1-region. The effects of velocity, still in evidence, are not as pronounced as in the E-region curves, but are considerably greater than in the apogee curves.

8.6 NASA 6.03—MIDSUMMER, DISTURBED, MID-LATITUDE IONOSPHERE

NASA 6.03, also an Aerobee 300, was launched at Wallops Island (39° N) about one-half hour before noon on August 3, 1960, two and one-half months after NASA 6.02 was fired at Ft. Churchill. The ionosphere was recovering from a disturbed condition due to a magnetic storm which had begun three days before. A so-called "S" conditions existed in which the electron densities in the F_1 and F_2-regions were nearly identical and the density profiles have the appearance of a suppressed F_2-region rather than an exagerated F_1. The nose cone opened at 98 kilometers, ejecting the Dumbbell into the lower E-region where the density was approximately 1.0×10^5 ions/cc, and measurements were made

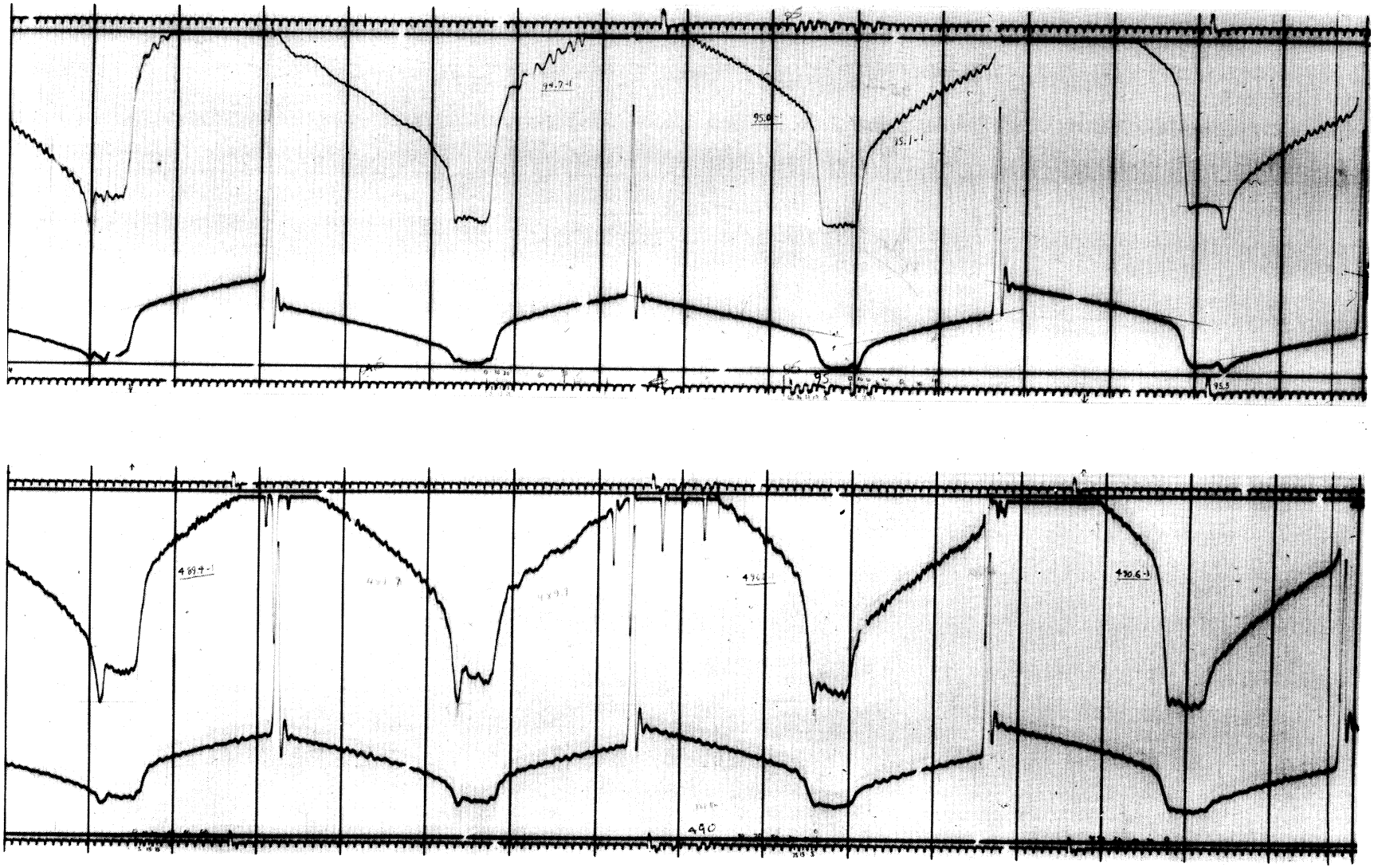

Figure 37. Segments of NASA 6.02 E-region telemetry record on the up-leg and down-leg, respectively.

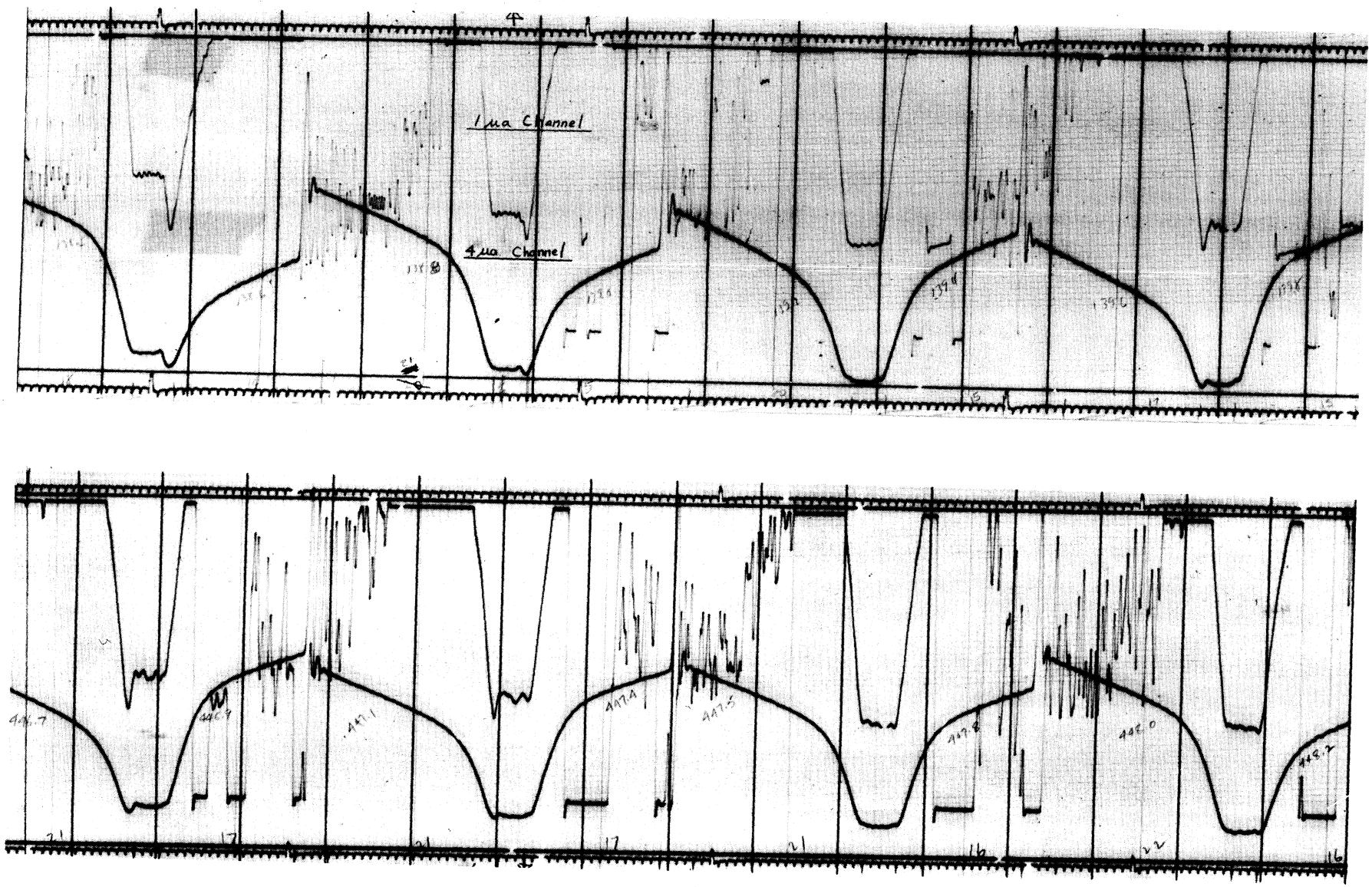

Figure 38. Segments of NASA 6.02 F_1-region telemetry record on the up-leg and down-leg, respectively.

continuously at a rate of six per second. The instrument reached a peak altitude of 420 kilometers and passed out of the ionosphere approximately 360 kilometers from the launcher at an azimuth of 128°, having a horizontal velocity of 600 meters per second. Also carried aboard the rocket was a two-frequency beacon experiment conducted by the Ballistic Research Laboratories.* The data from this experiment, which remained with the rocket (Figure 39 shows its location), was used to obtain an ionosphere electron density profile. An ionogram recorded during the flight at Wallops Station is shown in Figure 40.

8.6.1 The Ionosphere Profiles

Figure 41 shows the T_e and N_p profiles derived from the Dumbbell data and the N_e profiles from the two-frequency beacon experiment.

Ion Density.—This Dumbbell reached the highest apogee of the five measurements reported here (420 kilometers). It passed through the F_2 maximum near 320 kilometers on the up-leg and 280 kilometers on the down-leg. The N_e and N_p profiles show good correlation in general shape but, as in NASA 6.01, differ in magnitude, particularly at apogee. The "S" condition is evident in the ion density profile which shows an F_1 density nearly as great as the F_2 density.

Electron Temperature.—The electron temperature profile is quite similar to the Churchill profiles except for the lower temperature at the 100 kilometer level followed by a steep positive gradient and higher temperatures in the upper E-region. A slight negative gradient, not as pronounced in the auroral zone profiles, is evident between the E and F_1-regions. This may have some significance in establishing the mechanism for heating the auroral zone and the disturbed E-regions. In the F_1-region another positive gradient exists, and above this is a more or less isothermal region at a slightly lower temperature than was found at Ft. Churchill.

*Courtesy W. Berning, BRL.

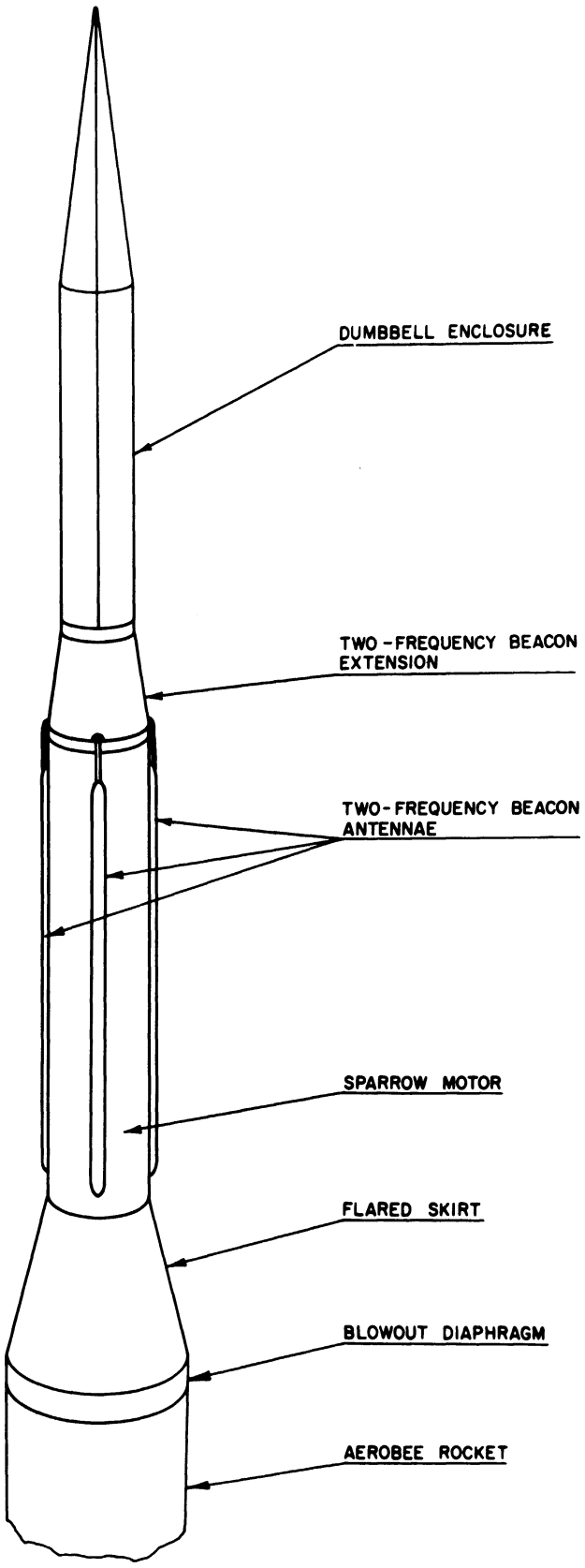

Figure 39. Sketch of third stage rocket showing location of two-frequency beacon.

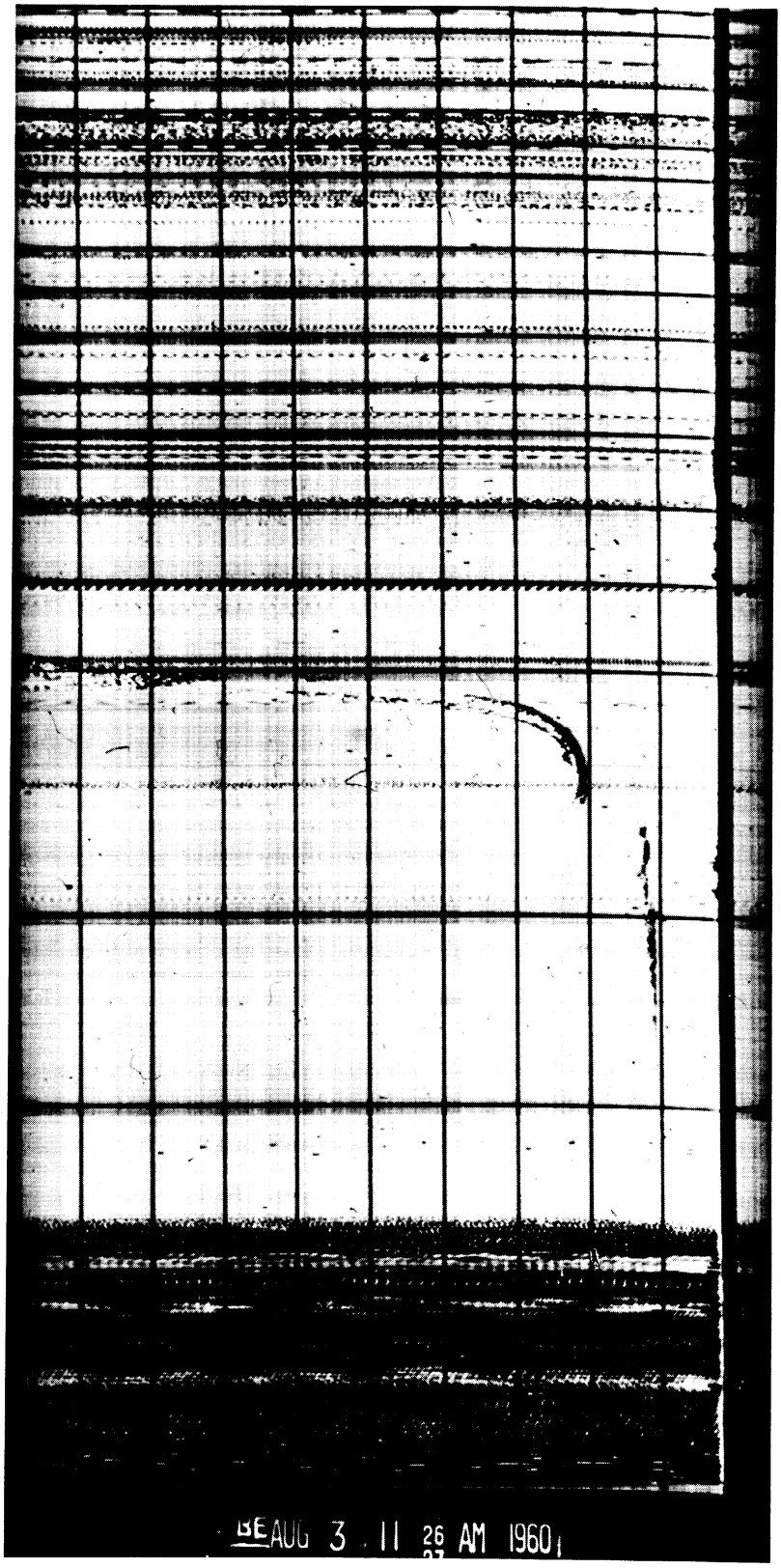

Figure 40. Ionogram recorded at Wallops Station during the NASA 6.03 flight.

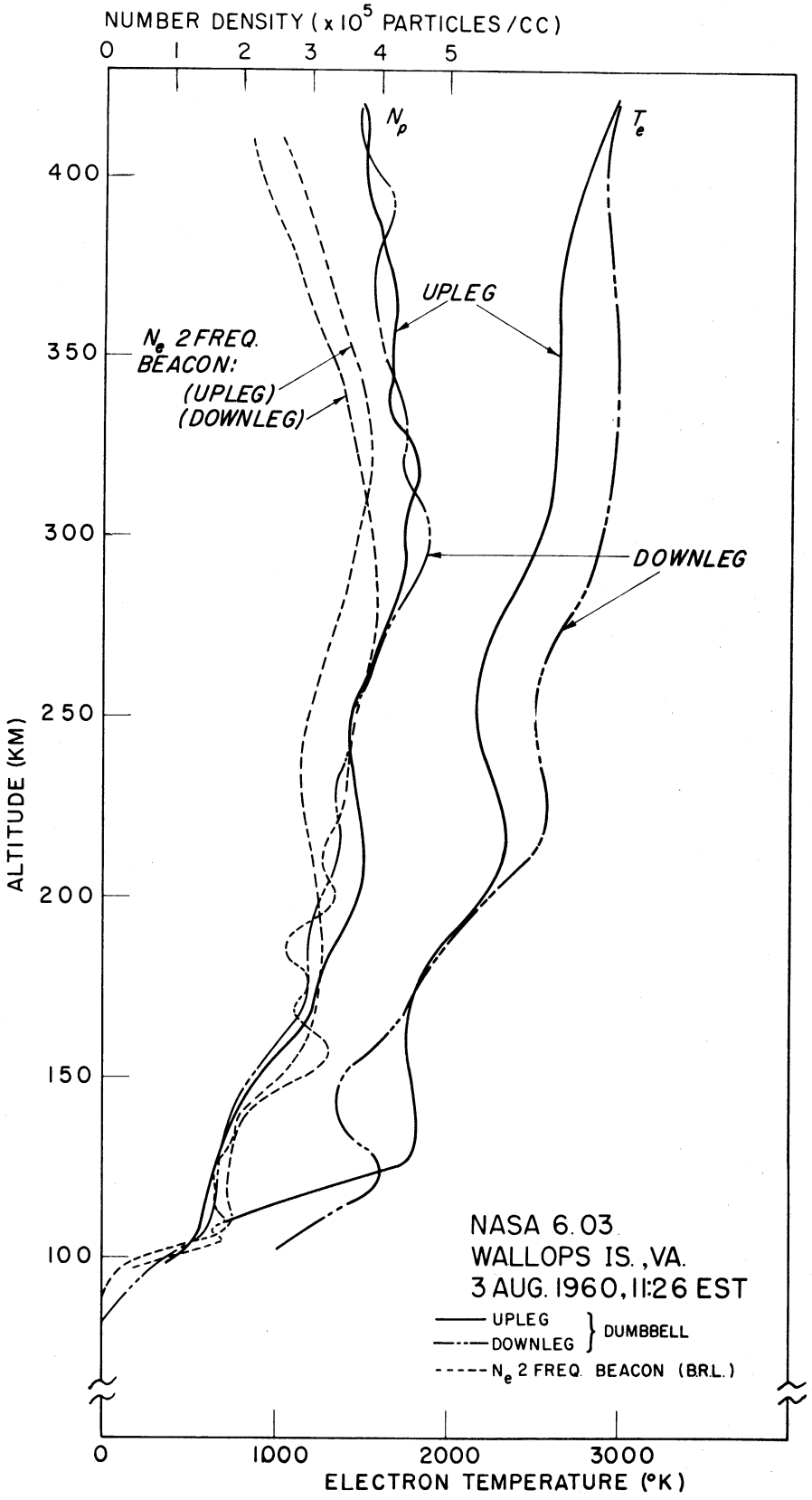

Figure 41. T_e and N_p profile from NASA 6.03. N_e from two-frequency beacon is also shown.

Later measurements at Wallops (NASA 6.04) lead us to believe that this is not a "normal" electron temperature profile for this latitude but is a distorted profile resulting from the effects of a magnetic storm which had not yet fully subsided. As before, further discussion and interpretation of this data will be reserved for Section 9.0. In the following section, we present some of the raw data in the form of photographs of the telemetry records.

8.6.2 The Raw Data

Telemetry Curves at Ejection and Apogee.—Figure 42 is a photograph of a two-second segment of the telemetry record at 110 kilometers, a few seconds after ejection. The helix AGC (signal strength) channel at the top shows that the rocket apparently passed between the ground station and the Dumbbell, occulting it in two stages; possibly with one of the clamshell halves and then with the entire third stage. After about 0.7 seconds, the Dumbbell comes into view again and the signal strength rises to its normal value. The upper record in Figure 43 shows the following second of flight on the same record. The radial magnetometer (which shares time on a channel with the axial magnetometer) shows the roll period of 1.7 seconds. The very slowly changing output of the axial magnetometer indicated a 19-second precession period. The 1 μa channel is already off-scale in the ion saturation regions, and the 4 μa channel shows half-scale deflection. The steepness of the curves and the sharp break at the ion saturation regions shows that the electron temperature is very low here as compared with the temperature near apogee (420 kilometers), as indicated by the segment of telemetry shown at the bottom of Figure 43.

E-Region Records.—The E-region curves recorded at 120 kilometers on both the up-leg and down-leg are shown in Figure 44. On the up-leg record (upper curves) the number 2 hemisphere is seen to be preceeding (sweeping out ions) and the number 1 hemisphere, trailing. On the down-leg record (lower curve) the

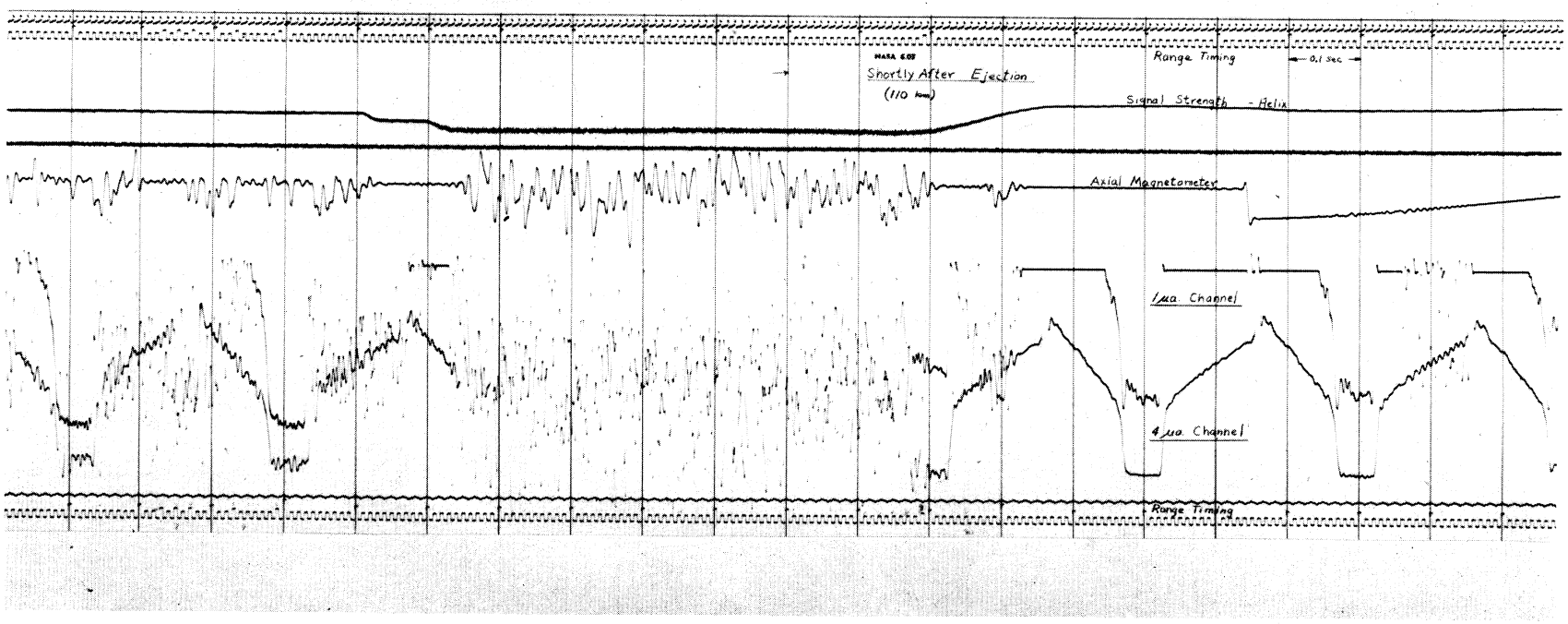

Figure 42. Photo of telemetry record at ejection of NASA 6.03.

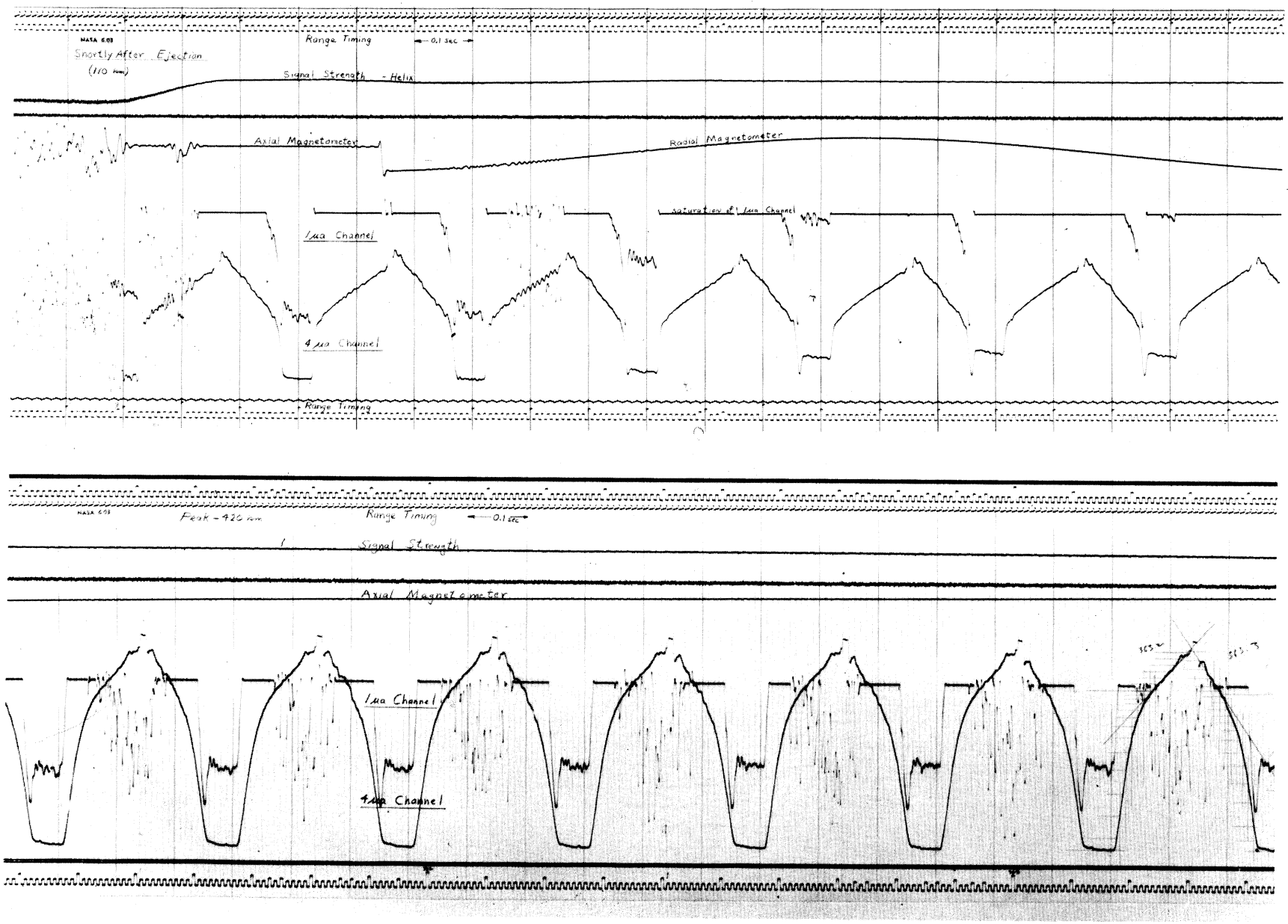

Figure 43. Segments of telemetry record just after ejection (upper record), and, for contrast, at apogee (lower record) of NASA 6.03.

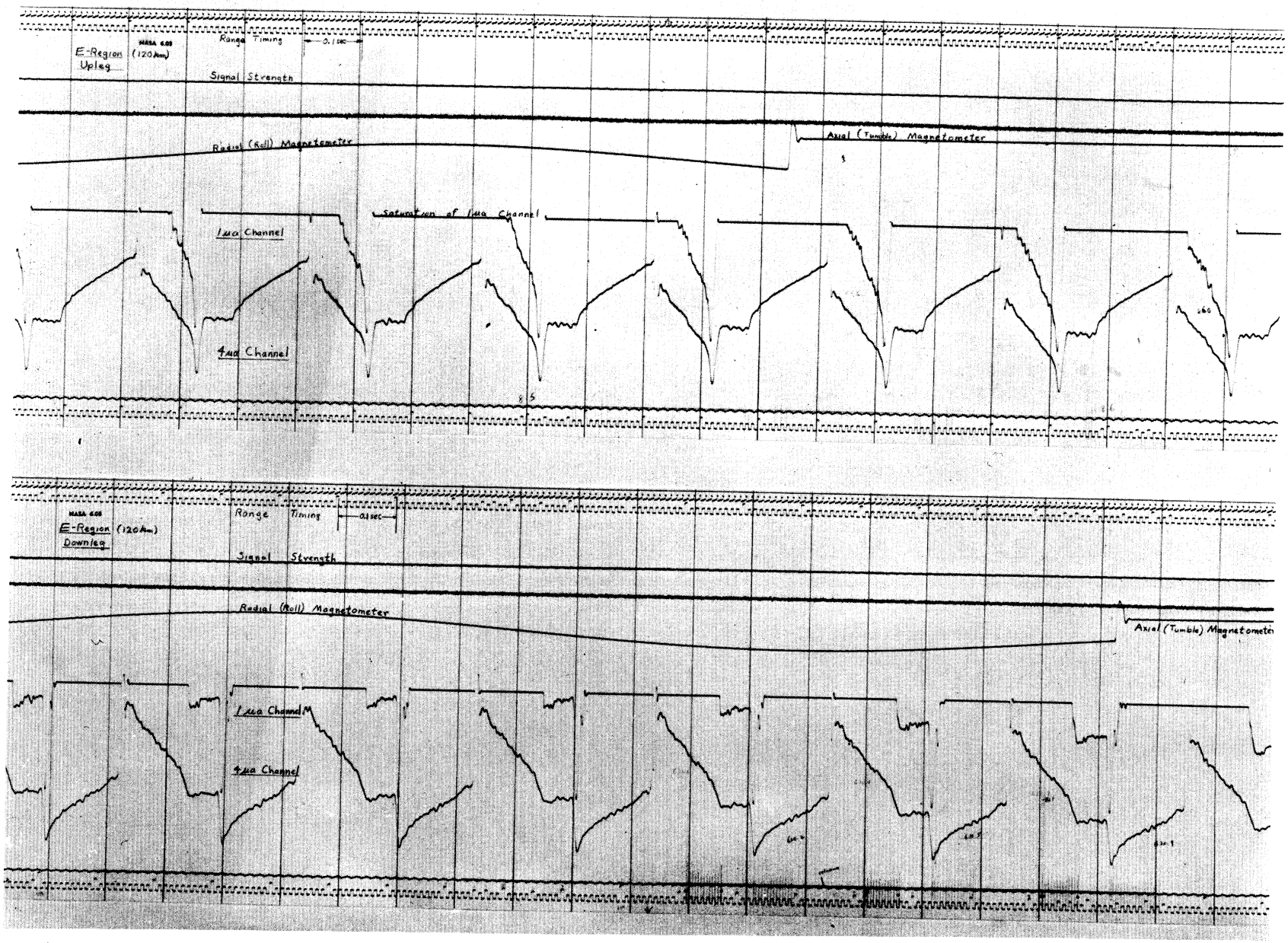

Figure 44. Segments of telemetry record in E-region of NASA 6.03 on the up-leg and down-leg, respectively.

reverse is true, since the Dumbbell remained generally vertical throughout this flight. The combination of low ionosphere temperature here and the highest rocket velocity yet obtained in any Dumbbell flight made the velocity-induced distortions the most extreme we have seen.

F1-Region Records.—F_1-region curves (190 kilometers) are shown in Figure 45. The symmetry of the up-leg curves in this segment, indicates a Dumbbell orientation of $\theta_1 = \theta_2 = 90°$ as shown in Figure 13, while the down-leg curves indicate a Dumbbell orientation of $\theta_1 = 0°$, $\theta_2 = 180°$ as shown in Figure 11.

The amplitude of the up-leg curves suggests an ion density which is at least as great as that at the apogee, Figure 43; however, some of this current is due to the velocity effect which is shown approximately by comparing the $\lambda = 1$ and $\lambda = 0$ characteristics of Figure 13.

The steepness of the electron current portion of the curves and the sharpness of the transition to ion saturation are indicative of the low F_1-region temperature compared with the temperature at apogee.

F2-Region Records.—The F_2-region flight records in Figure 46 show that the ion current was high enough to cause the 4 μA channel to limit. Unlike the Ft. Churchill records, the discriminator and recorder had been set up to limit precisely at 4 μa. Fortunately, the current detection and telemetry systems in the Dumbbell are linear to nearly twice full scale (8 μa in this case) so the curves were recovered from the flight magnetic tape. The playback records of the same curves (4 μa channel only) are shown in Figure 47.

8.7 NASA 6.04—EARLY SPRING, QUIET, MID-LATITUDE IONOSPHERE

Shortly before noon on March 26, 1961, a second Dumbbell was launched from Wallops Island to obtain quiet ionosphere data for comparison with the NASA 6.03 measurements in a magnetically disturbed ionosphere. Ionograms recorded continuously at Wallops Station, approximately 10 kilometers North of the launch

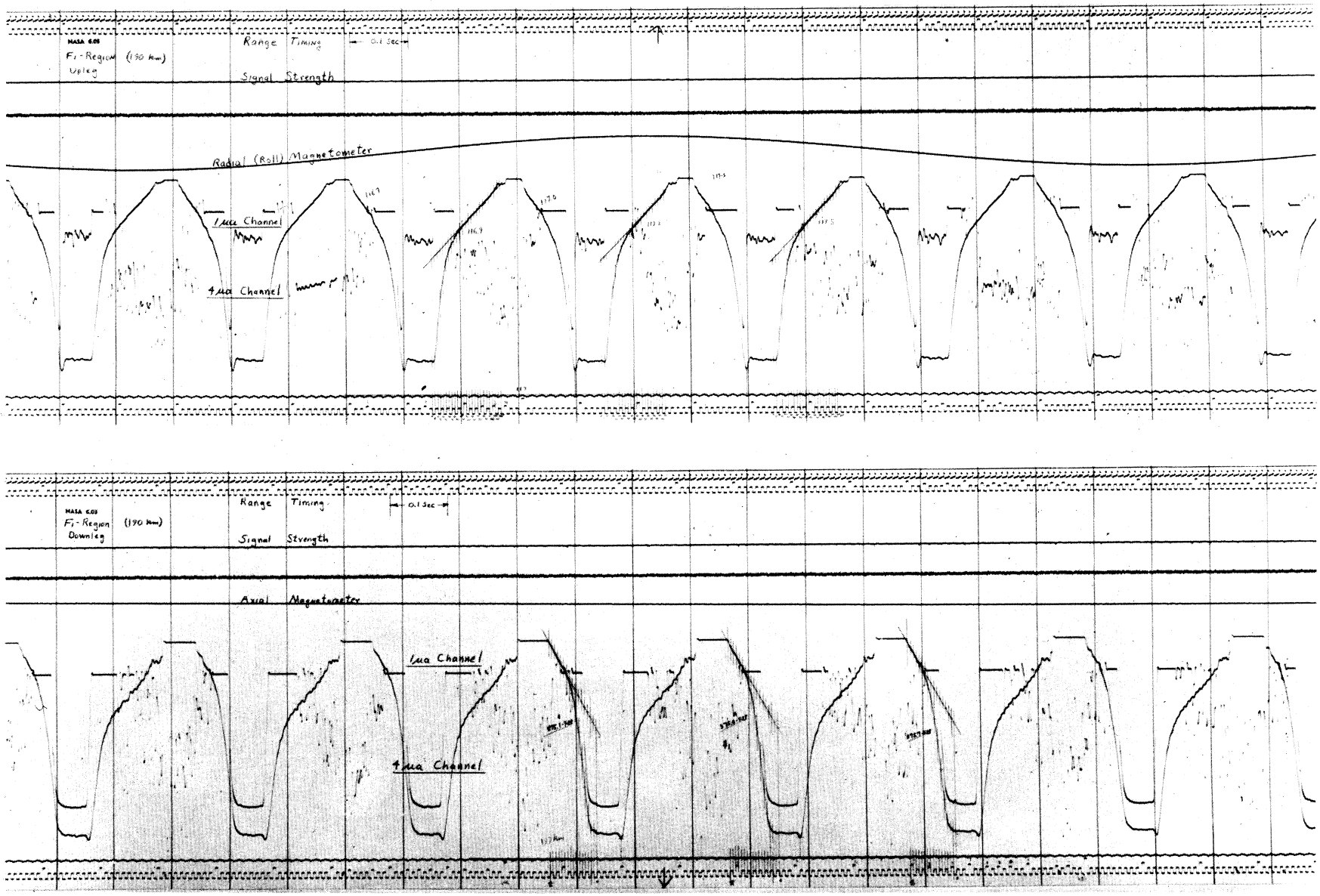

Figure 45. Segments of telemetry record in F_1-region of NASA 6.03 on the up-leg and down-leg, respectively.

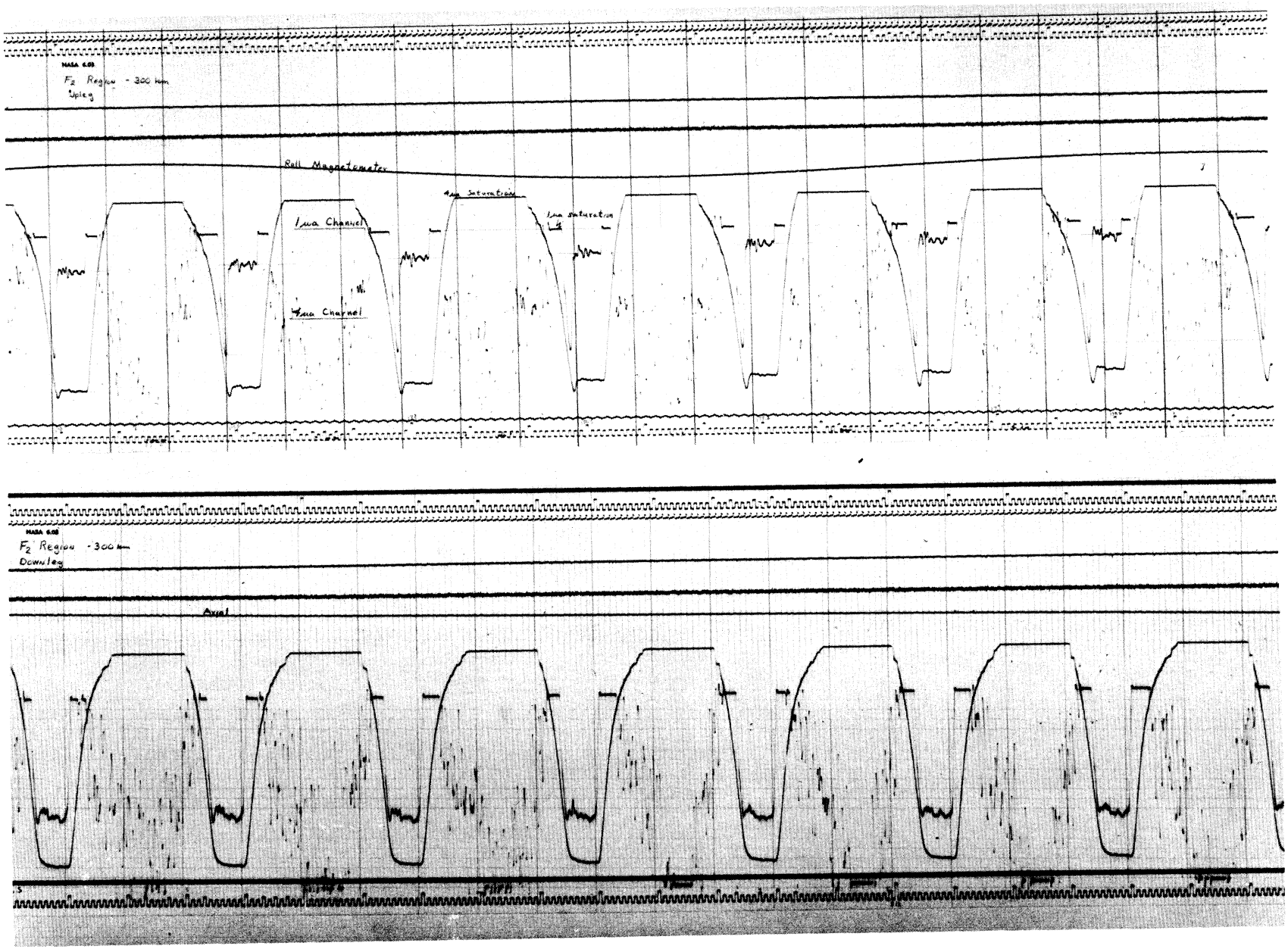

Figure 46. Segments of telemetry record in F_2-region of NASA 6.03 on the up-leg and down-leg, respectively.

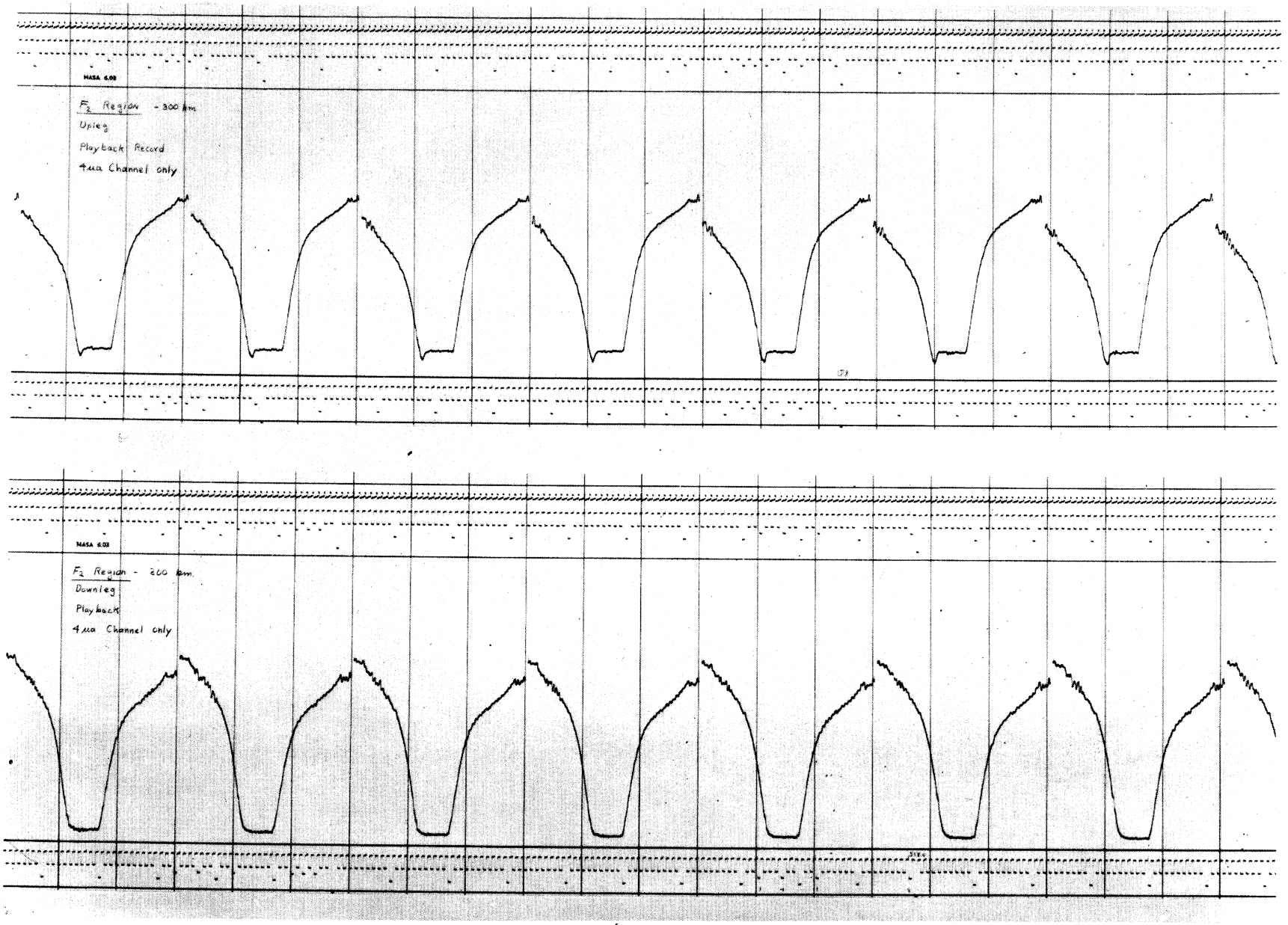

Figure 47. Playback record of F_2-region curves, NASA 6.03 (4 μa channel only).

site, showed no signs of ionosphere disturbance. Figure 48 shows one of these ionograms recorded during the boost phase of the launching, approximately one minute before the Dumbbell was ejected into the D-region at 86 kilometers. The instrument eventually reached an apogee of 359 kilometers and then passed out of the down-leg E-region approximately 350 kilometers from the launcher at an azimuth of 142°. The average horizontal velocity of the Dumbbell was 660 meters per second. As with NASA 6.03, a BRL two-frequency beacon was aboard to obtain an electron density profile.

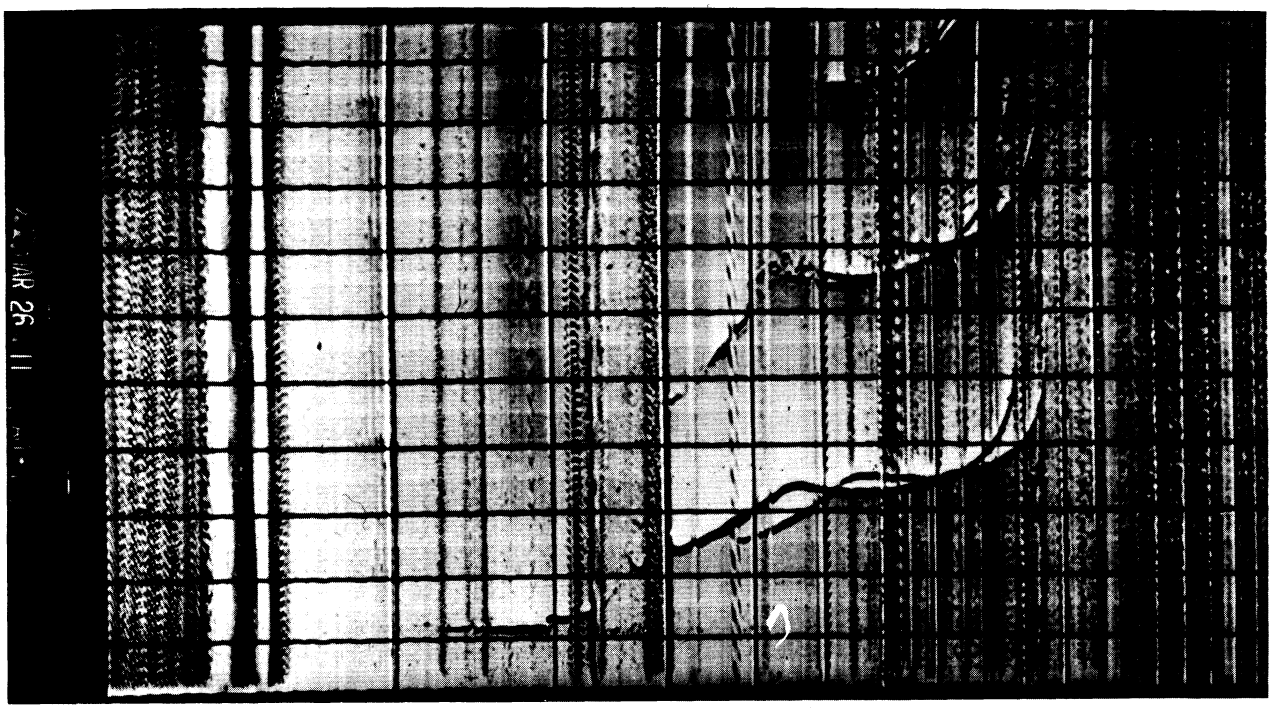

Figure 48. Ionogram recorded at Wallops Station during NASA 6.04 flight.

8.7.1 The Ionosphere Profiles

The Dumbbell-derived electron temperatures and positive ion densities, and the electron densities derived from the two-frequency beacon and the ionograms, are shown in Figure 49. The accuracy of the electron temperature values below approximately 140 kilometers was somewhat reduced in this flight because of the reduced sensitivity of the low current or E-region detector (2.25 μa, full scale).

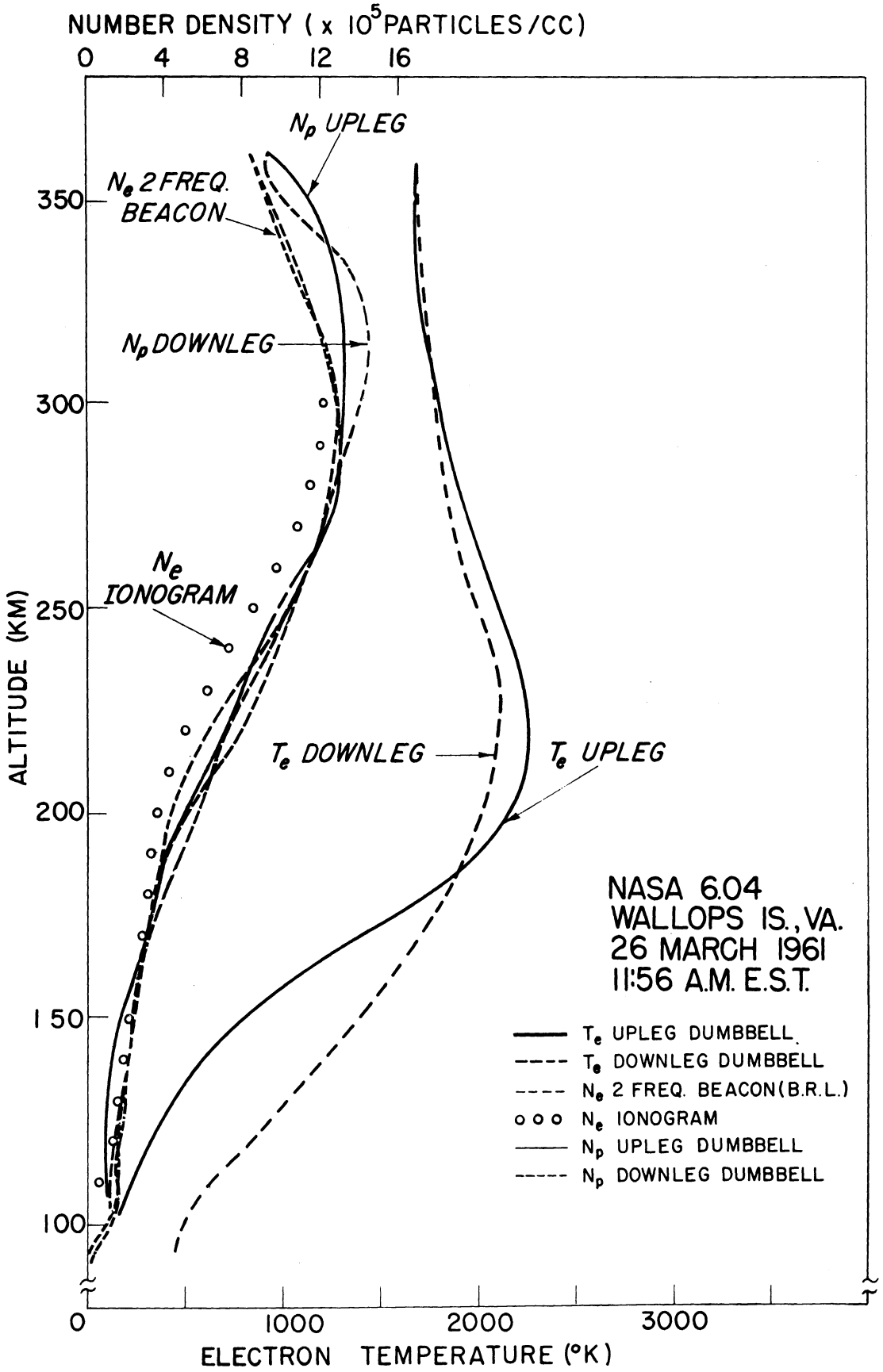

Figure 49. Quiet day-time T_e and N_p profiles, NASA 6.04. N_e from the two-frequency beacon and ionosonde are shown for comparison.

A third detector sensitivity (1.0 μa) had been planned for this flight, however, it was not available in time for the launching. Two factors in the measurement system introduce error into the electron temperature when the current is in the lower quarter of the detector current range: (1) reduced resolution of the curve introduces random error, (2) nonlinearity in the current detector characteristic (see Section 6.1) introduces a non-ionosphere curvature into the Dumbbell current characteristics. Since the shape of the volt-ampere characteristic is electron temperature dependent, care must be taken in the reduction process to avoid the nonlinear portions of the detector output (the lower 10% of its range) or to correct for this nonlinearity by use of the in-flight calibration. The correction process is sufficiently laborious, however, that a second means of reducing the electron temperature was sought; one not so dependent upon the linearity. Earlier, we had noted the approximately linear relation between the electron temperature and the electron cut-off voltage illustrated in Figure 15. Further correlation of these factors in the NASA 6.04 data above 150 kilometers, where the current resolution was excellent, provided an empirical relation which, when used on E-region data provided temperatures consistent with those obtained by the more laborious linearity correction process and the standard log-plot technique discussed in Section 4.0. It is difficult to assign an accuracy to the resulting E-region temperatures, but these data are thought to be accurate to within ±30% at 120 kilometers, as compared to the normal ± 10% above 150 kilometers.

Electron Temperature.—The electron temperature profile of the quiet, mid-latitude ionosphere differs markedly from that found earlier under disturbed conditions above the same site (Figure 40) as well as in the auroral zone ionosphere at Ft. Churchill (Figures 28 and 34). The most significant difference lies in the maximum of electron temperature which exists just above the F_1-region at approximately 230 km. The magnitude of the temperature here is actually slightly lower than was found at these altitudes in the earlier flights but

the strong negative gradient above 250 kilometers followed by the nearly isothermal region above 300 km is unique to this flight.

A second significant difference between this and earlier results is the lower E-region electron temperatures, which are in generally good agreement with the reference atmosphere gas temperatures up to about 170 km; the up-leg being lower and the down-leg higher than the reference. The possible significance of these data is discussed with the data of all flights in Section 9.0.

To demonstrate the sort of random variation in electron temperature which can be expected from the reduction of successive hemisphere characteristics, Figures 50 and 51 show the actual data points used in obtaining the temperature profiles of the ionosphere. Each data point represents a "hand reduction" of a particular characteristic. It will be noted that the "spread" in the points is somewhat less than found in the hand reductions of earlier flight data shown in Figure 35. This reduced spread is believed to be the result of the better guard action obtained in the NASA 6.04 instrument (see Section 8.7.2).

It should be noted that the temperature profiles given in Figure 49 are final data and represent an extension and modification of the preliminary data published earlier.[19]

The Ion Density.—Somewhat better agreement exists between the ion and electron densities (Figure 49) than occurred in earlier flights, although there remains a tendency for the ion density to be higher near apogee. On the other hand, the two frequency beacon N_e and the Dumbbell N_p are in good agreement at the F_2 maximum and are some 10% higher than the ionosonde N_e.

8.7.2 Modifications of NASA 6.04 and 6.05 Dumbbells

8.7.2.1—Single Reference Guard System.—The Dumbbells used in NASA 6.04 and 6.05 were electrically different from the previous Dumbbells as the result of two changes made in the system to make the instrument more versatile and re-

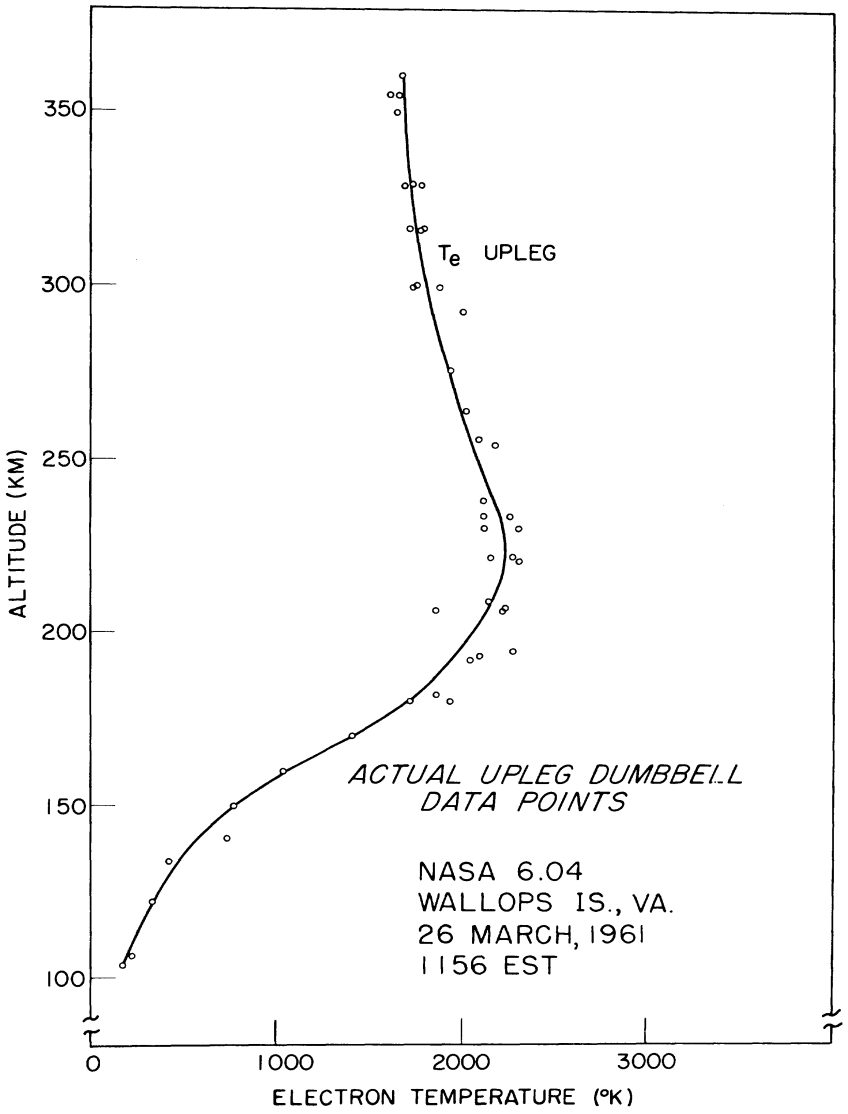

Figure 50. Actual up-leg temperature data points, NASA 6.04.

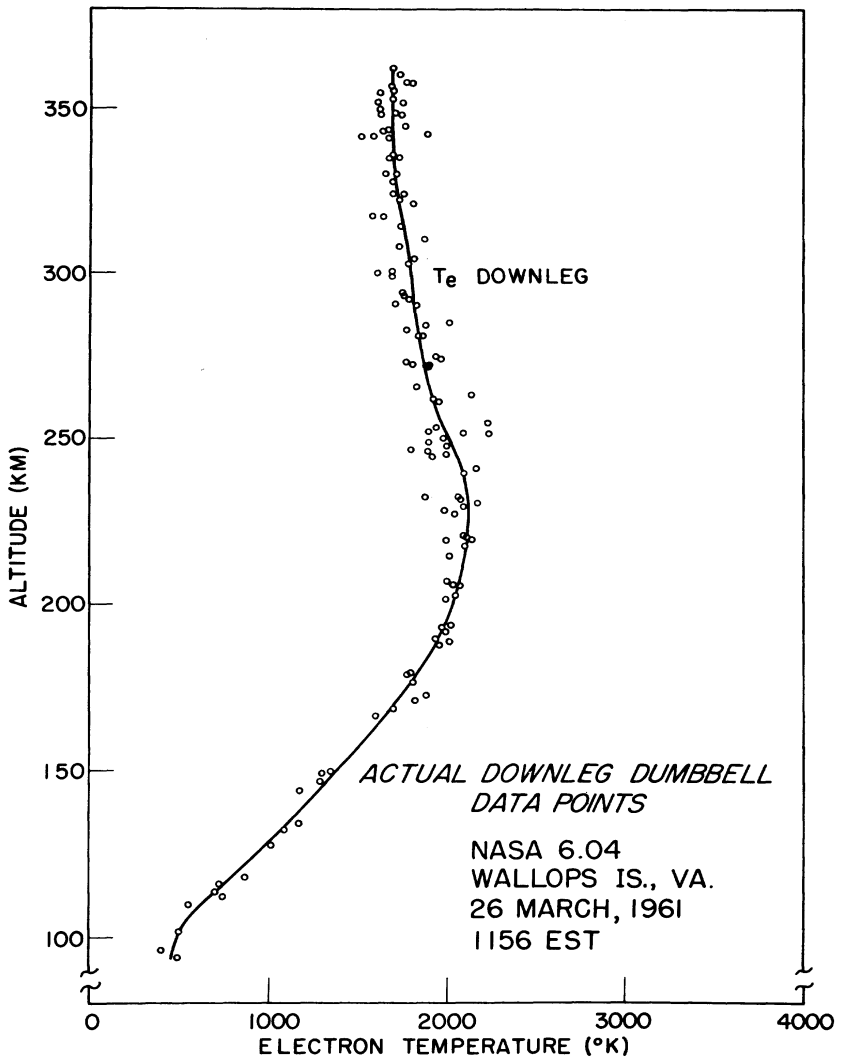

Figure 51. Actual down-leg temperature data points, NASA 6.04.

duce the random error in the measurements. The first modification was in the electrical connection of the funnel-shaped guard electrodes. All previous Dumbbells, although identical to 6.04 and 6.05 in external geometry and size, utilized a floating guard-electrode system, electrically isolated from the current measurement system as shown in Figure 3. Inflight measurements of the hemisphere-guard voltage on NASA 6.01 showed that the floating guard system did indeed maintain a reasonably small difference in voltage between each hemisphere and its associated guard, except at the lower altitudes where the effect of probe motion becomes extreme. However, it was felt that the guard action would be improved, particularly at low altitudes, by using a guard system in which only one hemisphere and its guard were insulated while the other hemisphere and guard were shorted together to act as a single reference, as shown in Figure 52. In this system, the single information electrode (hemisphere) is forced to maintain a potential identical to that of its associated guard electrode throughout the entire range of 8V.

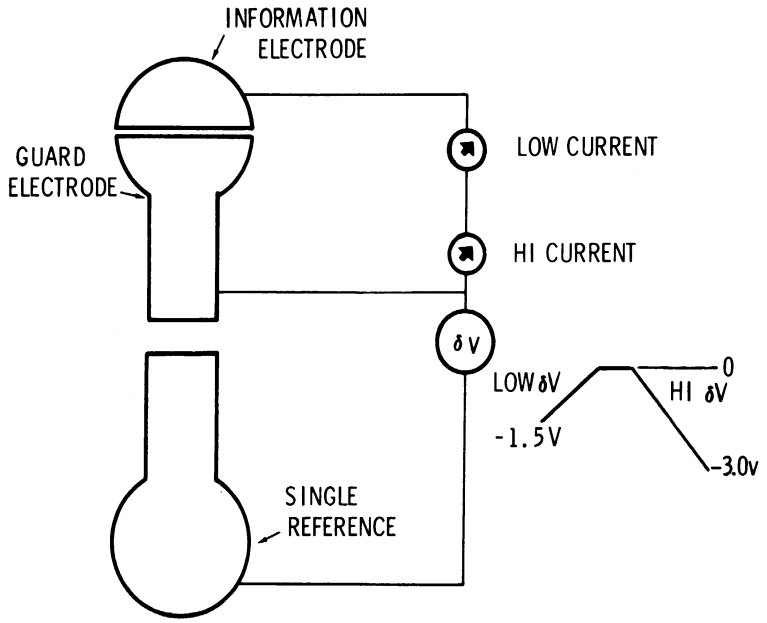

Figure 52. Single reference guard system used in NASA 6.04.

To test this mode of guard connection, NASA 6.02 was programmed to operate periodically in this shorted condition. The objective was eventually to use a single-reference guard system exclusively, if the test results confirmed its theoretical advantages. The resulting 6.02 data showed that the single-reference guard system, used alternately with the floating-guard system, gave electron temperatures which could not be distinguished from those measured with the original system. Although too few consecutive samples were taken, to show conclusively that the single-reference system actually reduced the data spread, the general experimental agreement and the obvious theoretical advantages led us to make this change in the Dumbbell used in NASA 6.04 which had not yet been constructed. NASA 6.03, identical to 6.01 and 6.02, was launched while these considerations were being evaluated.

The single-reference guard system made practical a refinement designed to increase the resolution of the 6.04 temperature measurements. Since only one polarity of δV was required, a simple wiring change provided two ranges of δV as shown in the waveform in Figure 52. The left slope (low δV) provides high resolution along the voltage axis for measurement of the lower E-region temperatures, while the right slope (high δV) is more suitable for the higher F-region temperatures.

8.7.2.2 A Small Cylindrical Langmuir Probe.—A second, totally unrelated, change in the recent Dumbbells was the addition of a small cylindrical Langmuir probe mounted on the central insulator as shown in Figure 53. A block diagram of the measurement circuit is shown in Figure 54. Using the entire instrument as a reference element, the small probe is swept through a wide range of potential and thus samples the entire population of thermal electrons, including the low energy part of the electron energy distribution, not available to a symmetrical probe like the Dumbbell. If the distribution is truly Maxwellian, (as our results indicate) no appreciably different temperature should be found in the

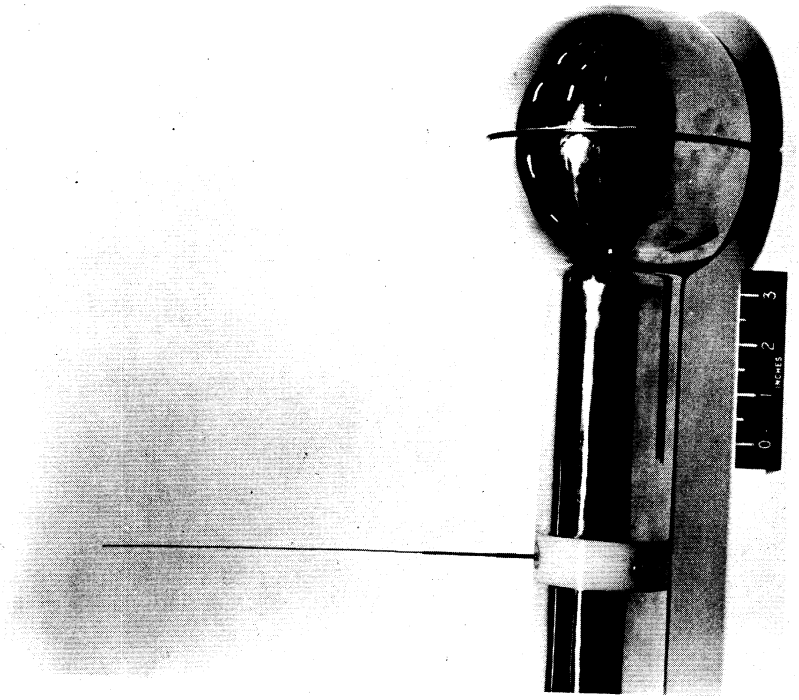

Figure 53. NASA 6.04 Dumbbell showing small cylindrical probe.

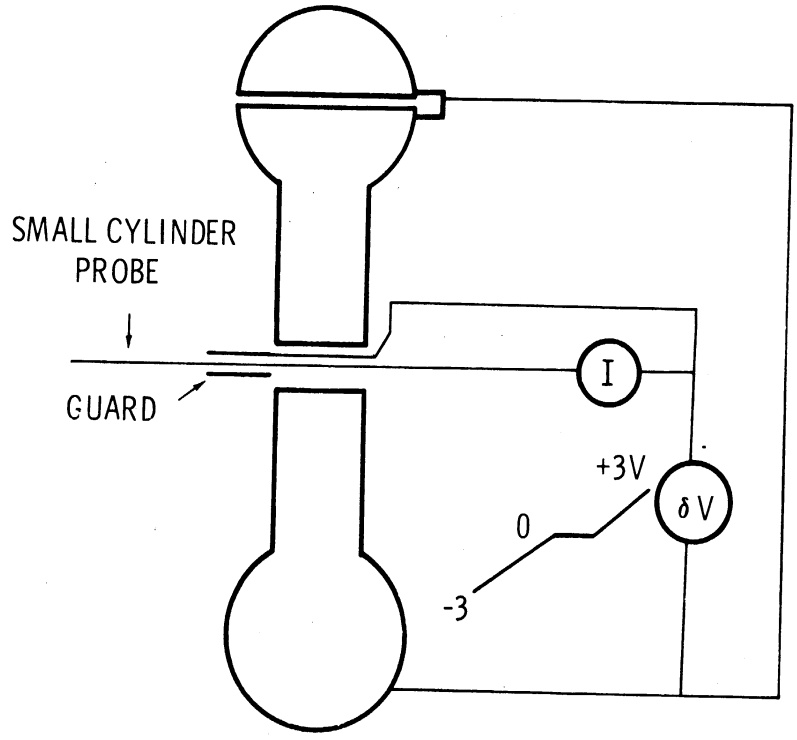

Figure 54. Block diagram of cylindrical probe system.

Dumbbell and cylinder measurements. If, on the other hand, the distribution is non-Maxwellian, the term temperature cannot be used to describe the distribution; and the difference between Dumbbell and cylinder-derived "temperatures" depends upon the actual nature of the distribution. It should be emphasized that the cylinder data has not been used extensively in arriving at the ionosphere profiles presented here for NASA 6.04 and 6.05, but has been sampled randomly as a consistency check with the Dumbbell's hemispherical collector data, both for electron temperature and ion density measurements. Although cylinder reductions are not completed, the density results are quite consistent with Dumbbell values and the temperature values appear to be some 10% high, for reasons which are suggested in the following sections.

The Dumbbell as a reference electrode.— It is recognized that the Dumbbell does not act as an ideal reference element for the cylindrical probe since its equilibrium potential varies with its orientation as it tumbles through the plasma; however, this effect has been minimized by selecting a sampling rate which is fast compared to the Dumbbell tumble rate.

The effect of the wake.— A second factor which is considered in the use of the cylinder experiment is the tendency for the cylinder to pass through the wake of the reference on which it is mounted, at which times the present probe theory is not adequate for interpretation of the resulting currents. This is particularly serious when the reference is an extended object like the Dumbbell or an entire rocket. Therefore, care is being taken in the reduction of data to interpret only those characteristics recorded while the cylinder generally preceeded the Dumbbell and thus measured the comparatively undisturbed plasma existing there.

Area ratio.— A third factor considered in the use of the cylindrical probe for measurement of electron temperature was the need to maintain an adequate ratio of probe area to reference area so that nearly all of the applied voltage appears as a change in the cylinder potential with respect to the plasma. To

achieve this requires an area ratio of many times the random electron to random ion current ratio (170:1 for 0^+ ions). An area ratio of greater than 1000:1 is considered adequate to make the change in reference potential negligible, but this is difficult to attain when working with a relatively small reference such as the Dumbbell (approximately 1000 cm^2). Part of the difficulty stems from the fact that the area of the guard electrode, which is also driven and collects current, must be considered part of the cylindrical probe area. Since its length must be great enough to reach outside the ion sheath which surrounds the Dumbbell to permit the collector to operate in an undisturbed plasma, and its diameter is greater than the concentric collector, the upper limit of attainable area ratios was fixed at somewhat less than 1000:1, using current detectors which would fit into the available instrumentation space.

It is possible to remove the guard electrode from the area ratio problem entirely by simply not applying a potential to it; but this destroys an important function of the guard, i.e., the task of maintaining the cylindrical electrostatic field about the collector where it joins the guard. The cylindrical probe used in NASA flights 6.04 and 6.05 was programmed in both the driven-guard and floating-guard modes having calculated area ratios of 350:1 and 700:1, respectively. Calculations from the theory indicated that the resulting voltage division between the cylindrical probe and the Dumbbell reference cause the uncorrected temperatures to be approximately 10% high for the driven-guard mode and 5% high for the floating-guard mode. However, exact calculation of this effect is difficult for the Dumbbell because of its complicated shape as a reference; and it was expected that comparison of the temperature results from the cylinder with and without the guard connected would permit evaluation of the voltage division problem. Though analysis of cylinder data is not well advanced, it appears from present indications that the voltage division between cylinder and reference is on the order of twice that which was predicted, thus (if not considered) causes the cylinder temperatures

(with guard connected) to appear some 20% higher than the true values. It is believed that this stems from a smaller than expected Dumbbell effective area resulting from the shielding effects which the various surfaces have upon each other. This earlier uncertainty in the voltage division factor was reflected in the preliminary cylinder-derived electron temperatures reported earlier[19] and caused them to be some 10% high. After further investigation of this voltage division factor, final cylinder-derived temperature profiles of NASA 6.04 and NASA 6.05 will be made.

8.7.3 The Raw Data

Figure 55 is a photograph or two segments or telemetry record showing in-flight calibrations of the NASA 6.04 current channels using two different ground recorders (a single recorder has insufficient paper capacity to record the entire flight in real time). The upper trace is a series of V-A characteristics of the small cylindrical probe as they appear on a 2.25 μa detector. Each Dumbbell calibration curve represents the detector outputs resulting from a -2 μa to +4.45 μa input current waveform.

Ejection and Apogee Telemetry Records.—Figure 56 shows a segment of the telemetry recorded during ejection of the Dumbbell at 86 kilometers (upper record) and, for contrast, near apogee at 359 kilometers (lower record). At the left of the upper record, the instrument is still within the nose cone and only receiver noise is recorded. At ejection, the 2.25 μa and the 5.0 μa channel (1 μa and 4 μa on previous flights) show a small trace of ionosphere current. The third (upper) channel in this portion of the record displays the radial or roll magnetometer output. At other times, it displays the axial magnetometer output (such as in the lower record) or the V-A characteristics of the small cylindrical probe.

The currents recorded at apogee (lower record) cause nearly full-scale de-

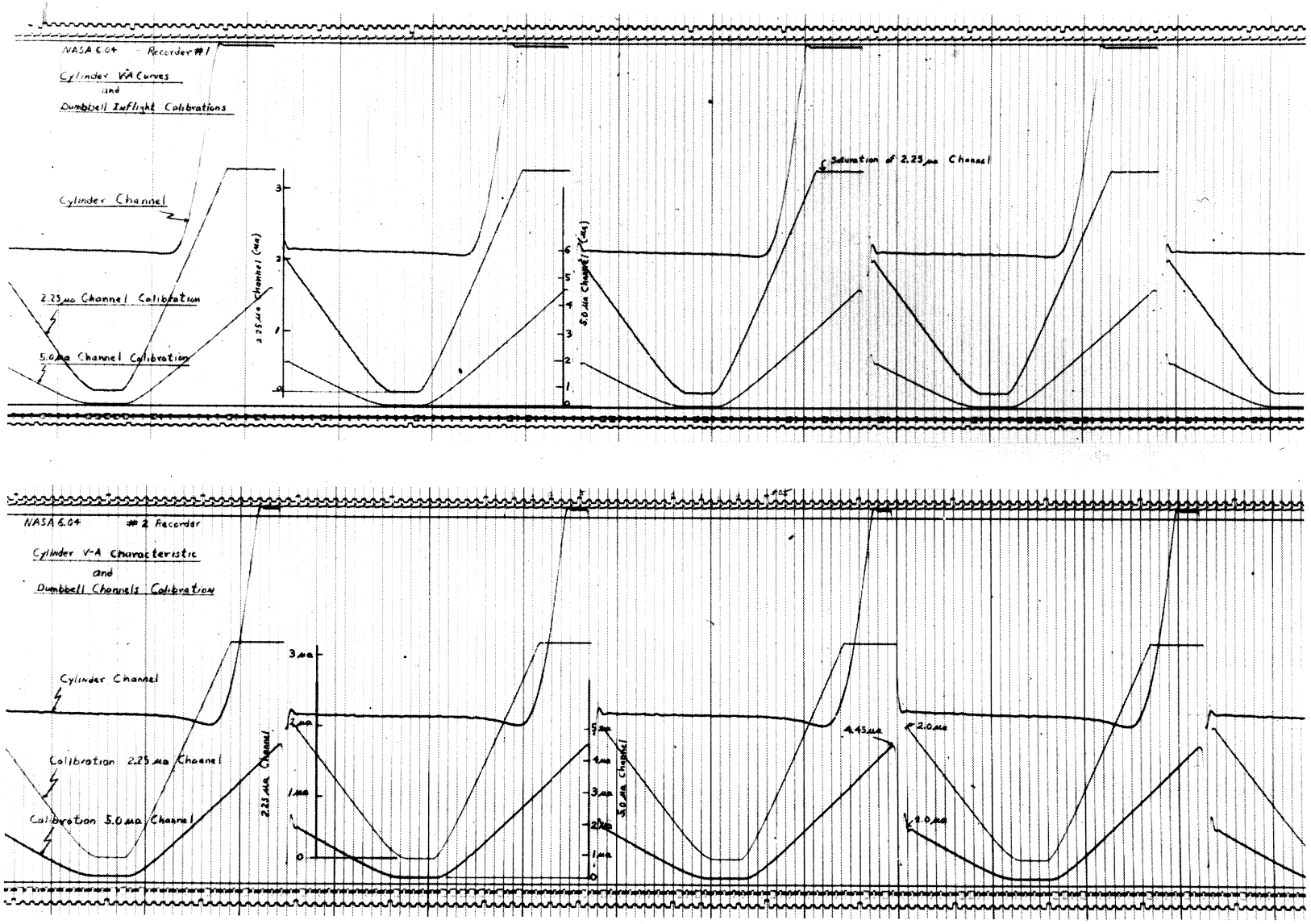

Figure 55. In-flight calibration of NASA 6.04 Dumbbell current channels on the two ground recorders used alternately through the flight to permit complete real time data recovery.

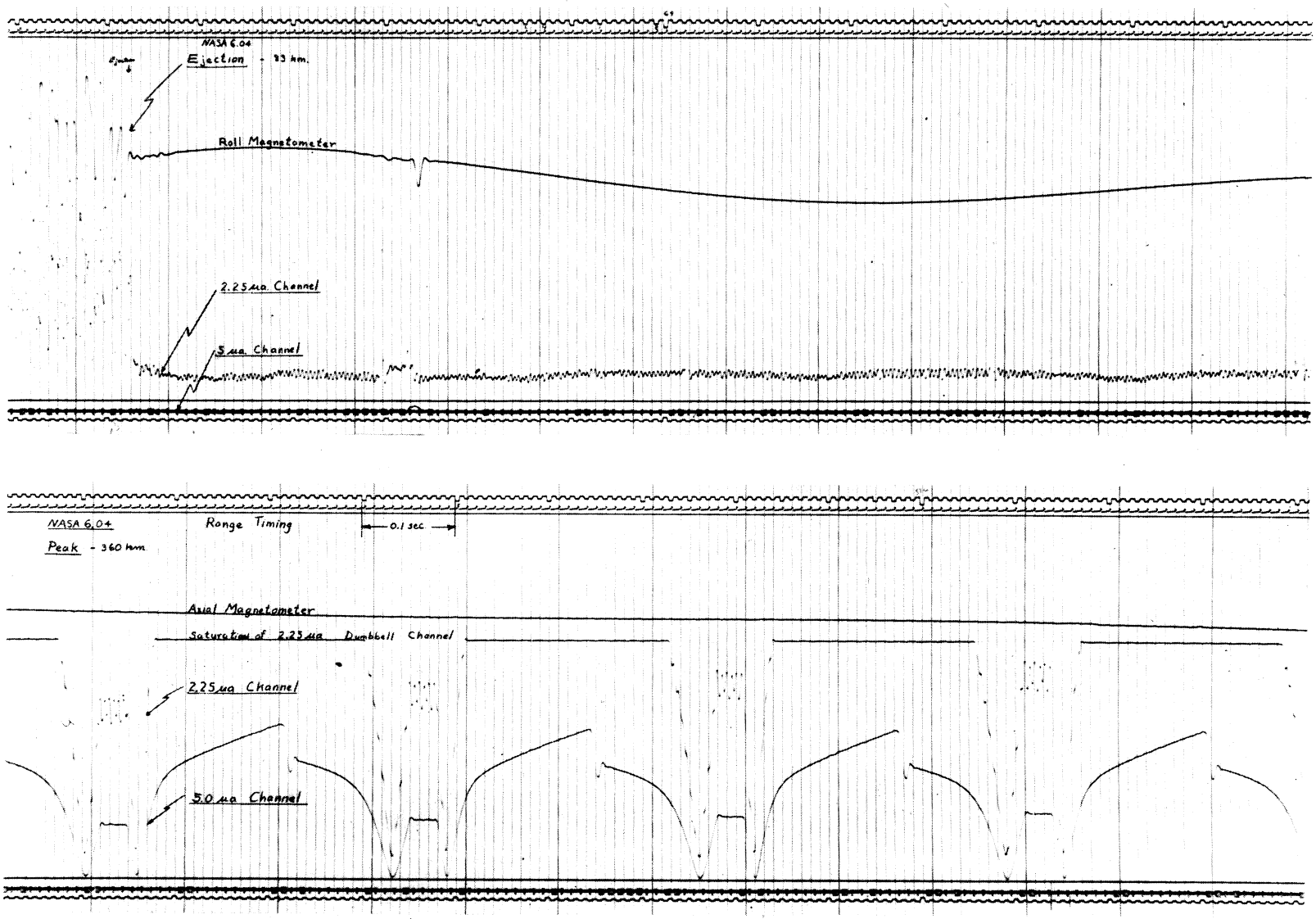

Figure 56. Segments of telemetry at ejection (upper) and near apogee (lower) of NASA 6.04.

flection of the oscillograph recorder. It will be noted that these characteristics appear somewhat modified as compared to the curves of the previous Dumbbells (which used the floating-guard system discussed in Section 8.7.2.1) in that a net electron current flows when zero δV is applied. This apparent unsymmetry results from the difference in the equilibrium potentials of the insulated hemisphere and the other elements. These potentials are such that, at zero δV, the hemisphere is held slightly more positive than its equilibrium potential, hence it draws a net electron current from the plasma. This was expected and observed in the tests of the single reference guard system carried out periodically during the NASA 6.02 flight, as discussed earlier. No change in interpretation of the characteristics is necessary since the probe system is still entirely symmetrical, as in earlier flights. The low δV curves lie to the left of each zero δV segment and the high δV curves lie to the right. During much of the flight the low δV was sufficient to permit the reduction of the relatively low electron temperature.

E-Region Telemetry Record.—Figure 57 shows segments of the telemetry record recorded on both up-leg and down-leg passage through the E-region. On its way up, the active hemisphere tended to trail the rest of the Dumbbell which preceeded in a cone of half angle 60°, while on the down-leg the hemisphere tended to precede the rest of the instrument. This was evident in the higher down-leg currents which were registered at any given altitude. The electron temperature interpretation is not significantly affected by the orientation except at very low densities which caused the current characteristics to fall into the nonlinear region of the current detector output, as it does here in the up-leg-E region.

To increase the accuracy of the electron temperature reduction, the interferring signal on the 2.25 μa channel was removed by means of a 35 cps filter in the ground station discriminator. Figure 58 is a photo of the resulting playback record showing the same E-region curves after filtering. A secondary effect of the filtering was the introduction of an overshoot in the steeper high δV

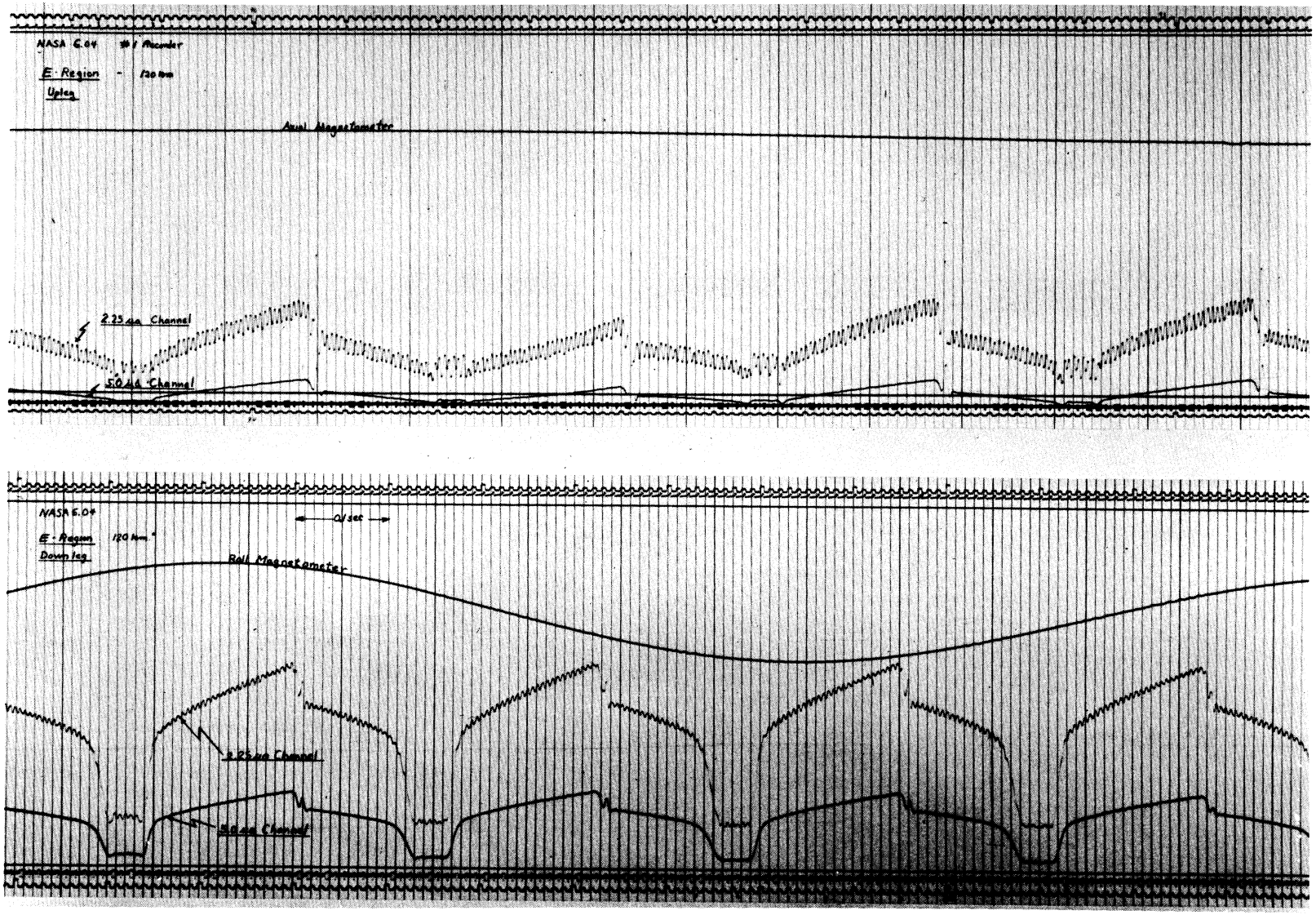

Figure 57. Segments of telemetry record in the E-region of NASA 6.05 on the up-leg and down-leg, respectively.

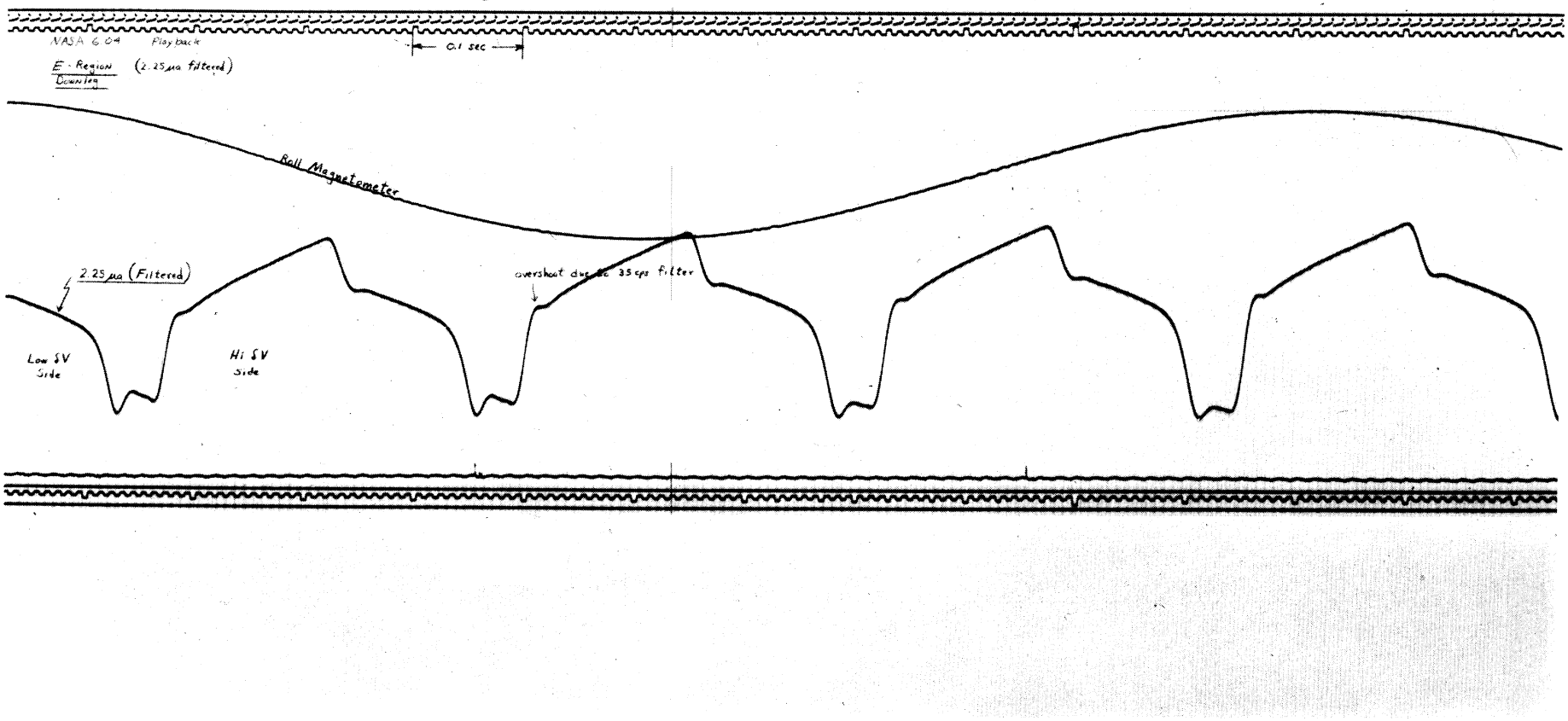

Figure 58. Filtered E-region curves on down-leg of NASA 6.04.

curves which are not used in the low temperature E-region.

F-Region Telemetry Records.—Typical F_1-region curves (180 kilometers) are shown in Figure 59. The axial magnetometer shows the Dumbbell precession period to be 8.6 seconds. Similarly, Figure 60 shows segments of the record made near the F_2 maximum (292 kilometers) on the up and down passages. The noise on the upper 5 μa channel was introduced by one of the two ground recorders and has been eliminated on recent playback records.

8.8 NASA 6.05—EARLY WINTER, NIGHTTIME, MID-LATITUDE IONOSPHERE

Since the completion of much of the foregoing report, a fifth Dumbbell of the present NASA series was launched into the nighttime ionosphere above Wallops Island. Several advantages were expected by such a measurement at this point in the program. The relatively high electron temperatures found in earlier flights had caused some concern regarding the interpretation of Dumbbell data in terms of electron temperature. Although a great deal of laboratory work had shown the double probe technique to be entirely valid[21,22], two attempts were made to provide additional evidence for the validity of the measurement technique as applied to the ionosphere.

The first attempt at substantiation of the Dumbbell measurements was to increase the versatility of the instrument by adding to it a small cylindrical Langmuir probe discussed in Section 8.7.2., where it was pointed out that small probes such as this have the advantage that the entire electron energy distribution may be sampled. Both NASA 6.04 and 6.05 carried this additional probe.

The second approach toward substantiation of the earlier results was to carry out the measurements in the nighttime ionosphere where the electron temperature can be estimated with a greater degree of confidence. Since temperature equilibrium ($T_e = T_p = T_g$) is to be expected at night, the nighttime ionosphere provides an excellent plasma in which to obtain a gross calibration of a temperature

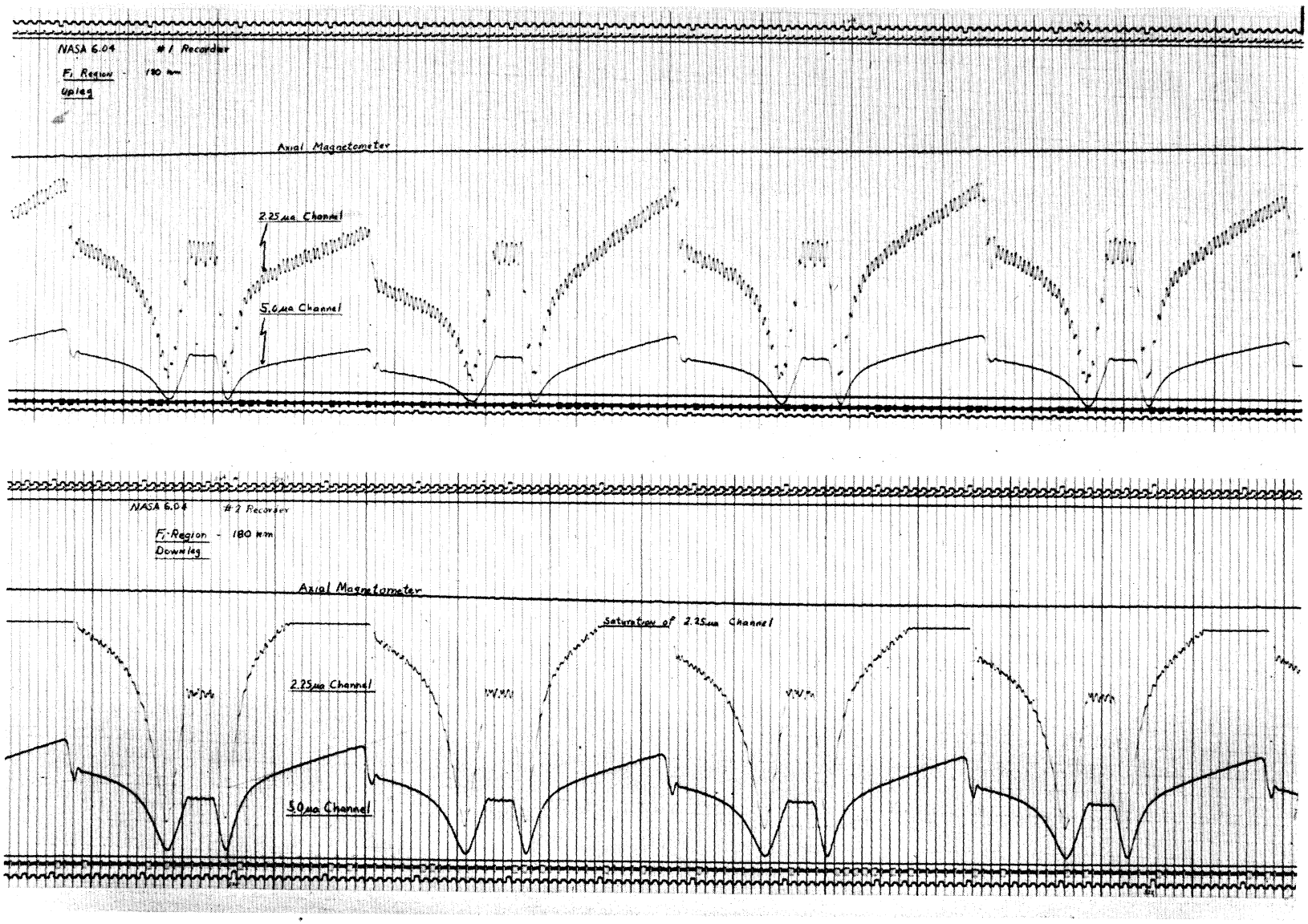

Figure 59. Segments of telemetry record in F_1-region of NASA 6.04 on the up-leg and down-leg, respectively.

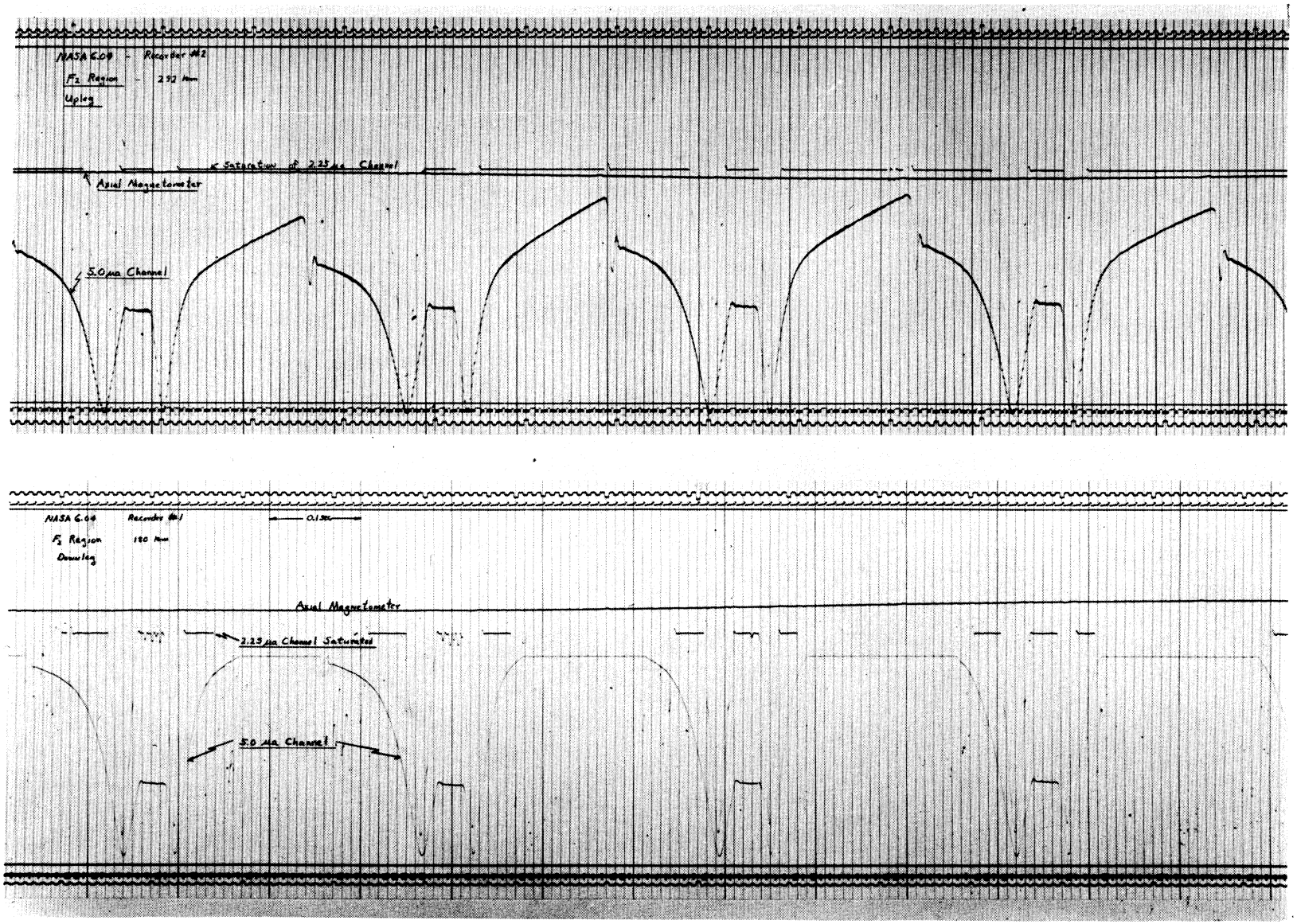

Figure 60. Segments of telemetry record in F_2-region of NASA 6.04 on the up-leg and down-leg, respectively.

measuring device of this kind. Satellite drag analyses as well as ion and electron scale height measurements suggest that an average minimum nighttime temperature of approximately 1100°K occurs some two to four hours after local midnight.[20, 23]

With these factors in mind, NASA 6.05 was launched at 11:25 p.m. on December 21, 1961. The Aerobee 300 vehicle carried an instrument, essentially identical to that on board NASA 6.04 in March, to an apogee of 365 kilometers. Approximately 2000 volt-ampere characteristics such as shown in Figures 61 and 62 were recorded. Figure 63 shows an ionogram recorded simultaneously at Wallops. The resulting temperature and density profiles, obtained entirely from the hemisphere data, are shown in Figure 64.

8.8.1 Electron Temperature

Diurnal Variation.—An interesting feature of this nighttime ionosphere is that the electron temperature measured in the F region on descent is from 5 to 15% lower than that found on ascent, although it is in good agreement with the nighttime minimum values given by the CIRA reference atmosphere. Some difference in up-leg and down-leg temperatures would normally be expected as the elapsed time and the eastward horizontal motion of the Dumbbell carried it toward the nighttime minimum. For example, the change in local time of the instrument as it passes from 100 km on ascent to the same altitude on descent is approximately 20 minutes. Since the rocket was launched generally eastward and toward the approaching nighttime minimum, this change in local time is in the correct direction to explain a lower down-leg temperature; however, the magnitude of the decrease is too great to ascribe entirely to diurnal variation unless the temperature was falling to a somewhat lower value than is given by the reference atmosphere. This 10% change is more consistent, however, with the large diurnal temperature variation found in the theoretical atmospheric models given by Harris and Priester,[23] shown in Figure 65, in which they considered the effects of ex-

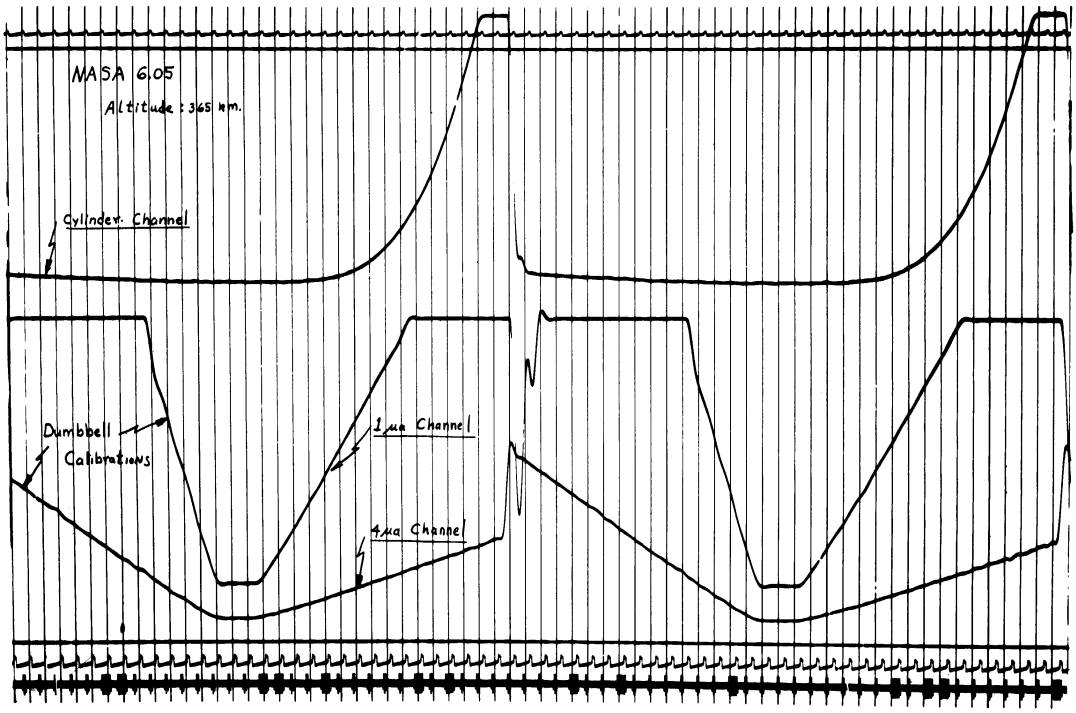

Figure 61. Typical cylinder current characteristics and Dumbbell in-flight calibration recorded near apogee (365 km) of NASA 6.05.

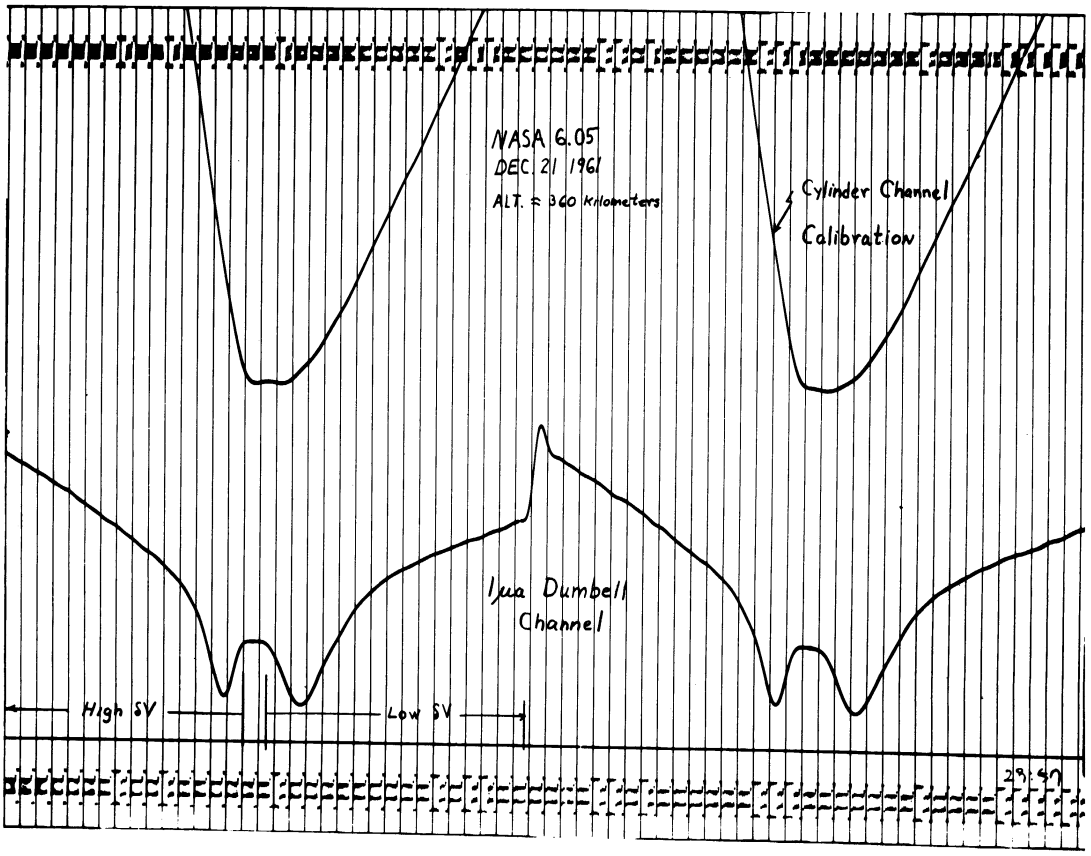

Figure 62. Typical hemisphere current characteristics and cylinder channel calibrations near apogee (360 km) of NASA 6.05.

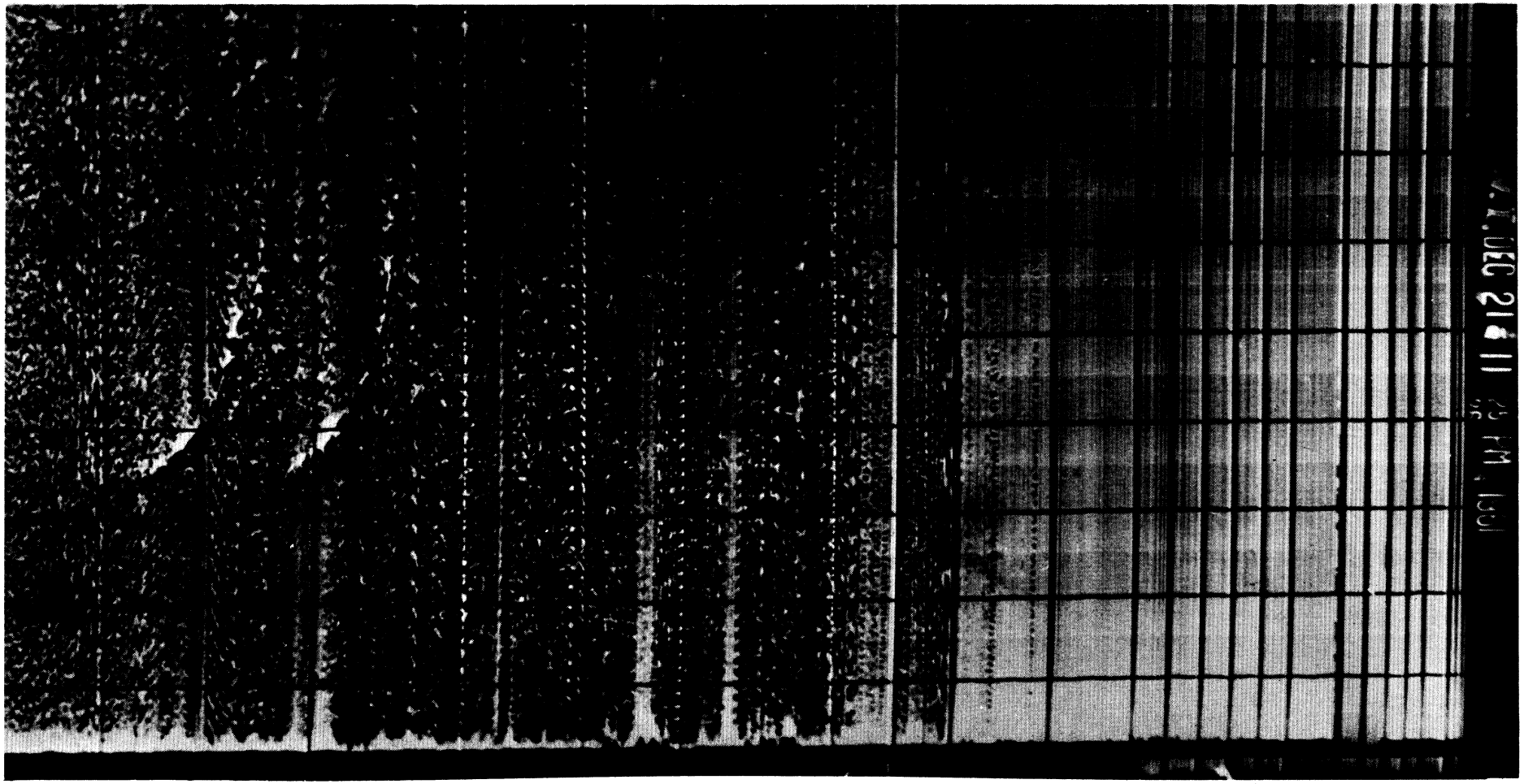

Figure 63. Ionogram recorded at Wallops Station during NASA 6.05 flight.

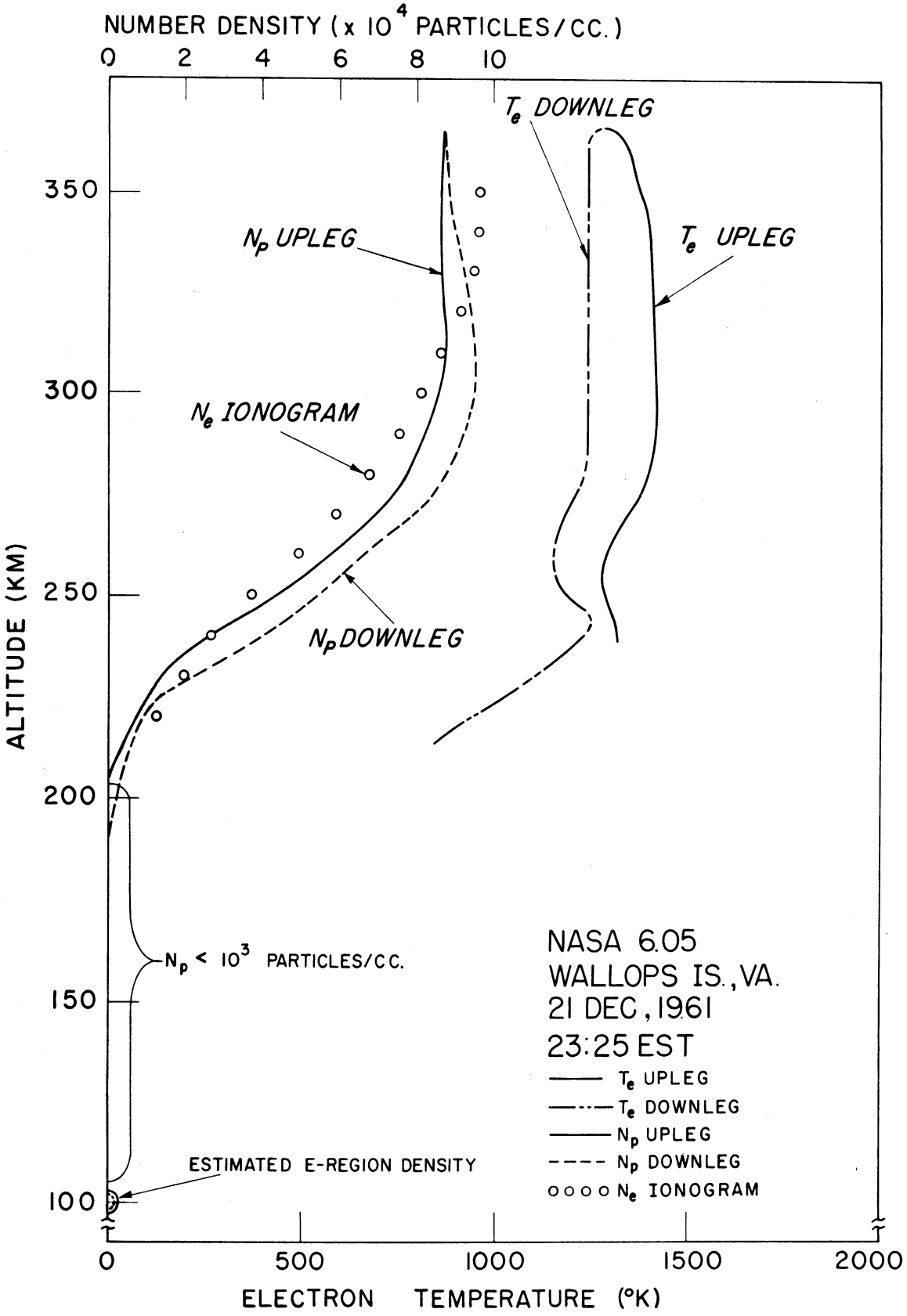

Figure 64. Nighttime T_e and N_p profiles, NASA 6.05. Ionogram-derived N_e profile is shown for comparison.

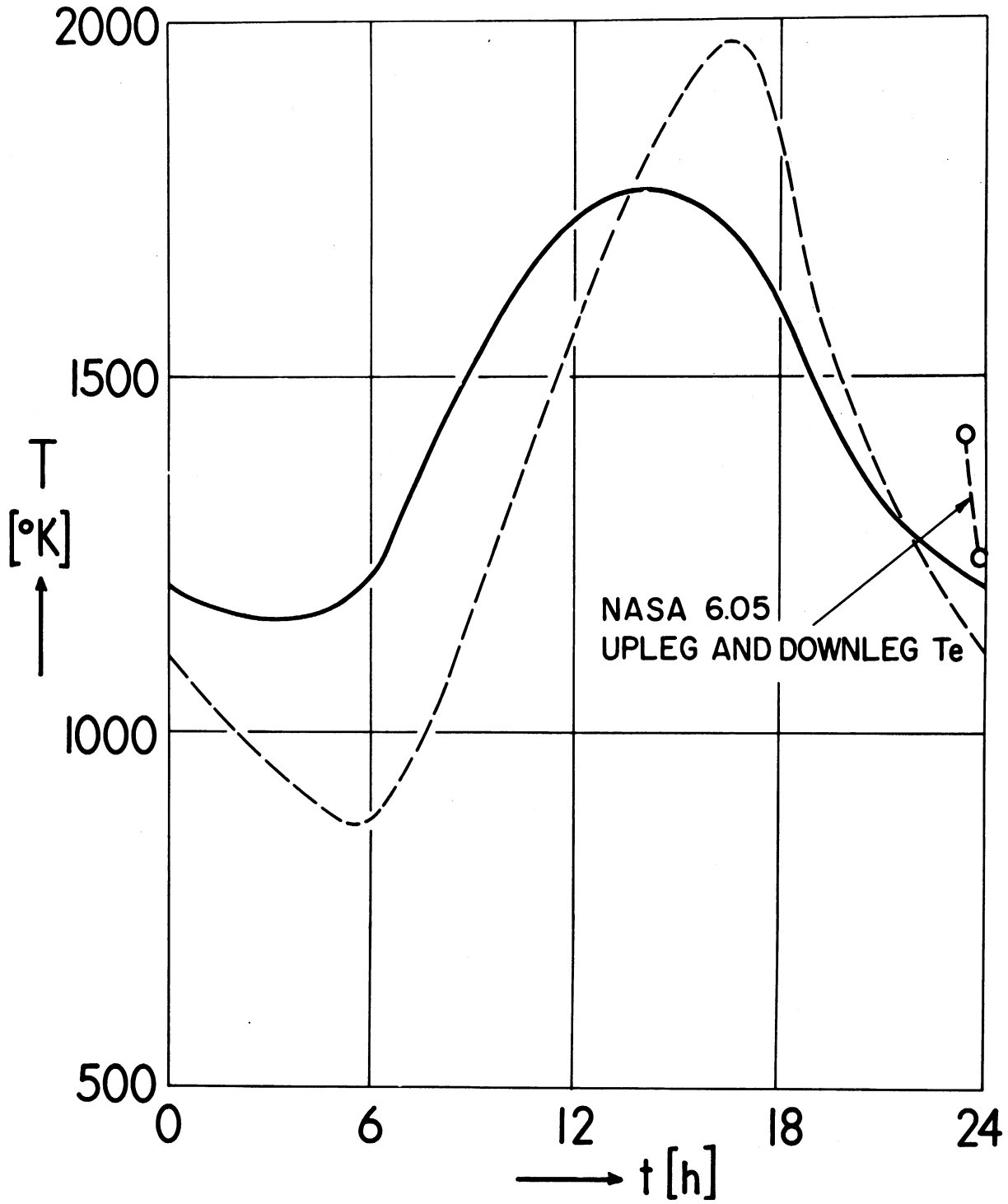

Figure 65. Harris and Priester theoretical atmospheric temperature models. NASA 6.05 up-leg and down-leg values are shown for comparison.

treme ultraviolet alone (shown dashed), as distinguished from the effects of both ultraviolet and corpuscular heating (shown solid). The up-leg and down-leg temperatures from NASA 6.05 are plotted on the same figure vs local time of the instrument.

Possible Latitude Effects.—A second, although less likely, source of the difference in up-leg and down-leg temperature is the change in latitude of the Dumbbell resulting from its northerly component of horizontal velocity which carried the rocket approximately 3° north during the flight. This might be considered an entirely negligible change in latitude except for the unique location of Wallops Island which places it near the horn of the inner Van Allen belt where high energy particles in the belt can penetrate to F-region altitudes. However, without more specific information than is available regarding the precise latitude of the horn at specified times, it is difficult to do more than speculate as to what degree this could be a factor in the higher up-leg temperatures.

Irregular Heating of the Nighttime F-Region.—Another possible explanation for the larger-than-expected difference in up-leg and down-leg temperature may be simply the irregular heating of the ionosphere by absorption of hydromagnetic wave energy. Johnson[24] points out that such irregularities in F-region behavior represent one of the greatest unsolved problems of the ionosphere. Such heating will certainly result in horizontal temperature gradients not necessarily related to the diurnal variations. The abrupt nature of the temperature change with horizontal range of the instrument, shown in Figure 66, tends to support this sort of mechanism. A smoother, more gradual horizontal gradient would be expected from the normal diurnal variation.

It is important to note that this sort of analysis in terms of ascent and descent data is made possible by the unique feature of an ejectable direct measuring probe such as the Dumbbell; namely, its equally valid results on both

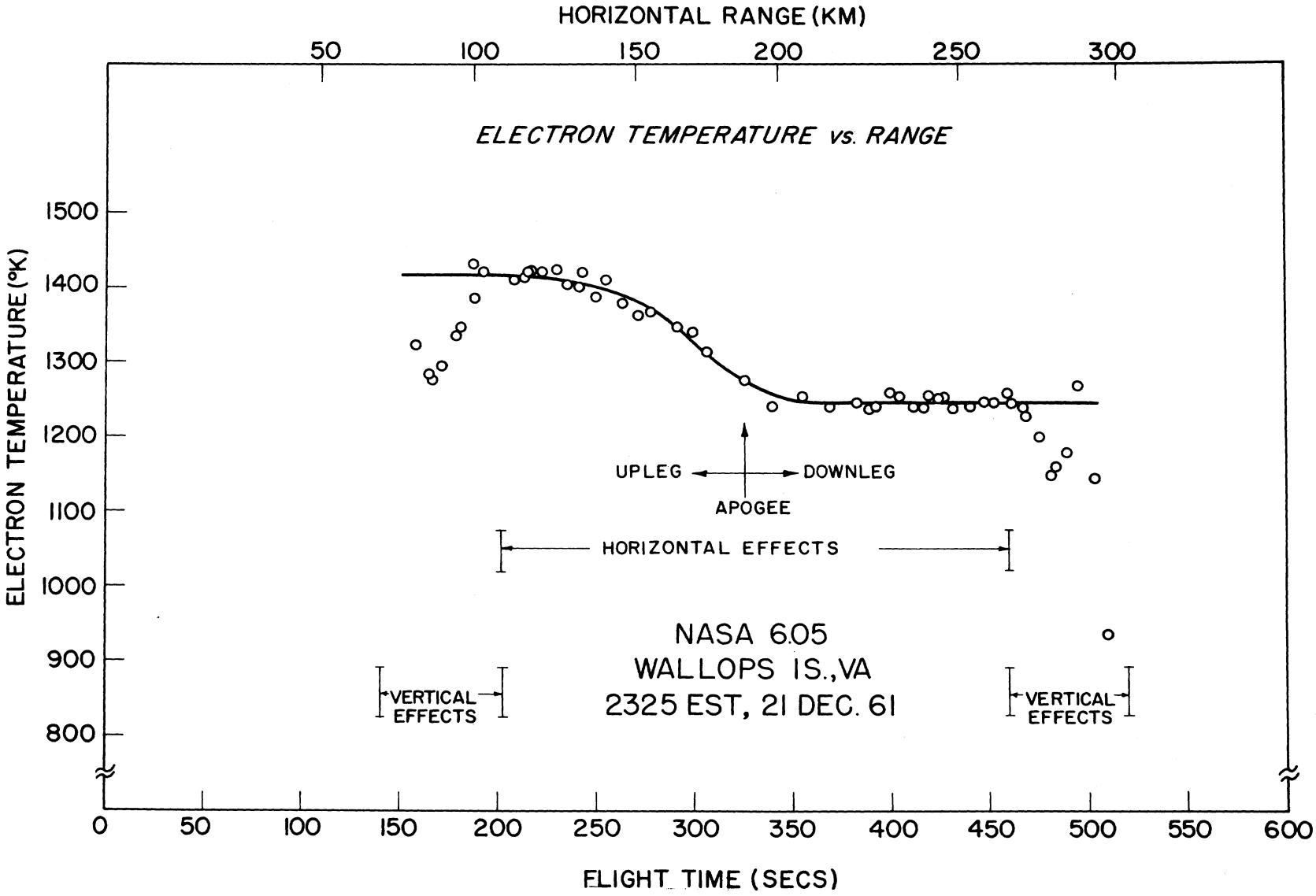

Figure 66. Temperature vs. horizontal range of Dumbbell showing a horizontal temperature gradient in the nighttime ionosphere.

ascent and descent. In general, a non-ejectable, rocket-mounted, direct measuring device operates quite differently on ascent when it proceeds the vehicle than on descent when it generally trails behind in the wake of exhaust gases and the usual rocket related contaminants.

Fine Structure in the Temperature Profile.—A second interesting feature of these temperature profiles is the "S" shaped variation near 240 kilometers, visible on both ascent and descent. A similar fine structure was found near 200 kilometers in the daytime flight at Ft. Churchill and shown previously in Figure 35; however, this is a particularly significant discovery for the nighttime ionosphere since the temperature profiles represent gas as well as electron temperatures. This "S" shaped structure was first noted in the analysis, by Kallman,[20] of density data by rockets and satellites, from which she derived average gas temperature profiles of both the daytime and nighttime atmosphere. To the knowledge of the author, the electron temperature data presented here represent the first direct temperature measurements which show this variation.

Low F_1-Region Temperatures.—A third result of the nighttime flight is the indication of lower than expected temperatures below 200 kilometers, as indicated by the steep temperature gradient occurring at about this altitude. This is in contrast to the CIRA reference atmosphere which shows the gradient occurring at about 150 kilometers, a region in which there is little daytime or nighttime temperature or density data since it is below the region in which satellite drag data are abundant and is above the altitude capabilities of present neutral particle experiments. Unfortunately, the charge density at these altitudes at this time of night is insufficient to permit temperature resolution within the design constraints of the Dumbbell probe, thus the temperature profile on this flight cannot be carried to lower altitudes than those shown.

Actual Data Points.—To illustrate the resolution obtained in the temperature reduction, Figure 67 shows the actual data points used in drawing the temperature

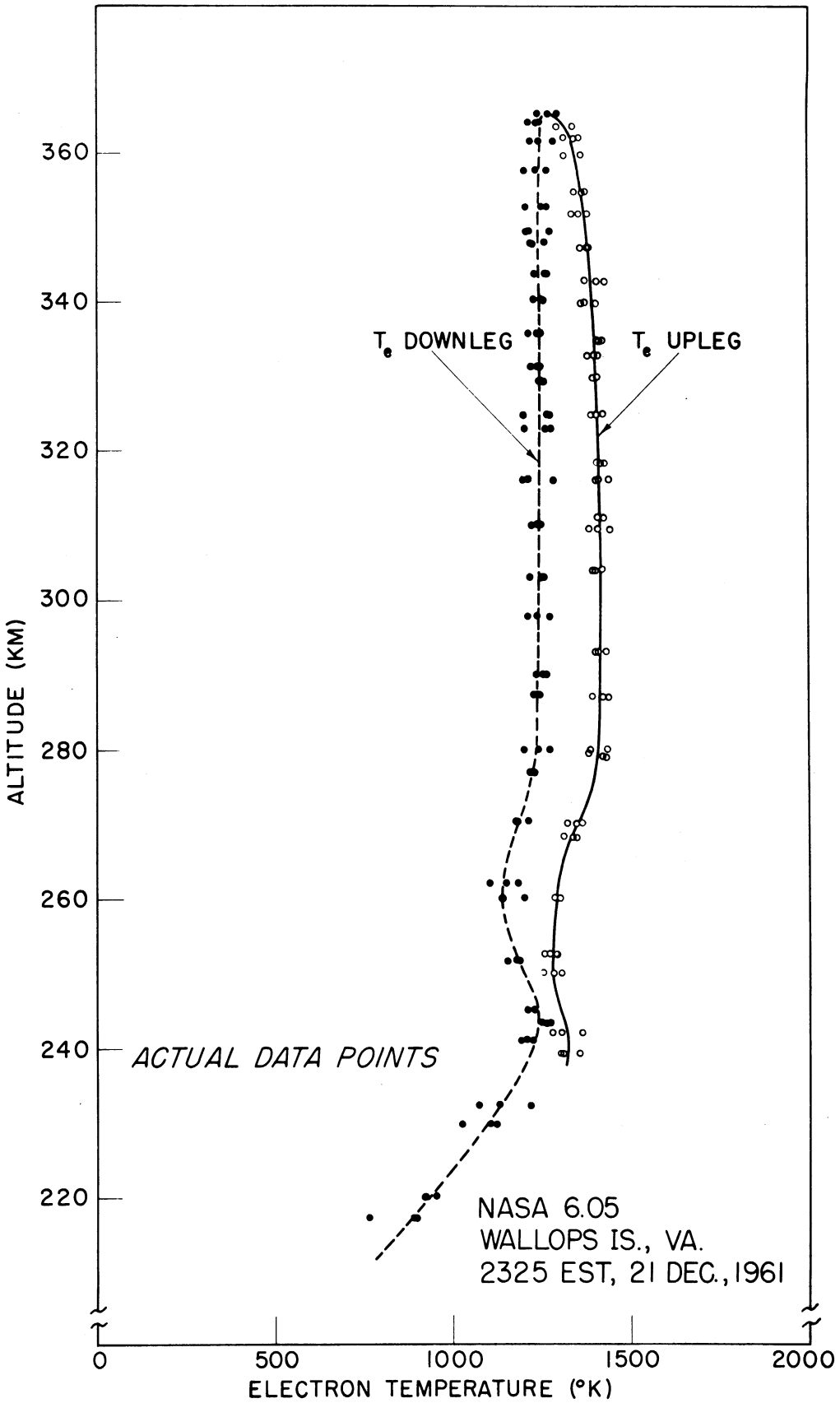

Figure 67. Actual temperature data points used for NASA 6.05 T_e profile.

profiles. As pointed out earlier, the random error in the temperatures is sufficiently small to permit resolution of relatively minor fine structure.

8.8.2 Positive Ion Density

Comparison of the Ion and Electron Density Profiles.—The ion density values in Figure 64 are in particularly good agreement with the ionosonde electron density values. Unlike the results of the previous flights in the daytime, N_p is generally slightly lower than N_e. Since volume neutrality ($N_p = N_e + N_-$) demands that N_e never exceed N_p, this difference must be attributed to (1) the horizontal density gradients in the region between the ascending Dumbbell and the area over Wallops Station which was being sounded, and/or (2) experimental errors in the N_p and N_e measurements, Lacking specific knowledge of the horizontal gradient, we assume that any difference is experimental error. In comparing these data, it is important to recognize that the direct measurement and ionosonde techniques are subject to distinctly different kinds of errors. As discussed in Section 5, the necessity of assuming m_p introduces some error into the process of converting collected ion current to ambient total positive ion density, N_p. Since m_p occurs as a factor to the 1/2 power, the error introduced is not as serious as one might expect but can be significant in establishing the absolute magnitude of N_p. The shape of this profile, however, is probably not seriously distorted, since the errors tend to be systematic.

Conversely, the magnitude of the ionosonde-derived N_e values at the various maxima (E, F_1, F_2) is most accurately known; but the assignment of altitude to these maxima is done with a great deal less assurance, particularly at night when the unresolved charge density at lower altitudes becomes more important. Thus the shape of the ionosonde N_e profile is often in question. This is illustrated in Figure 64 which shows an up-leg N_p maximum at 315 km and a corresponding N_e maximum at 350 km. If the N_e profile is appropriately com-

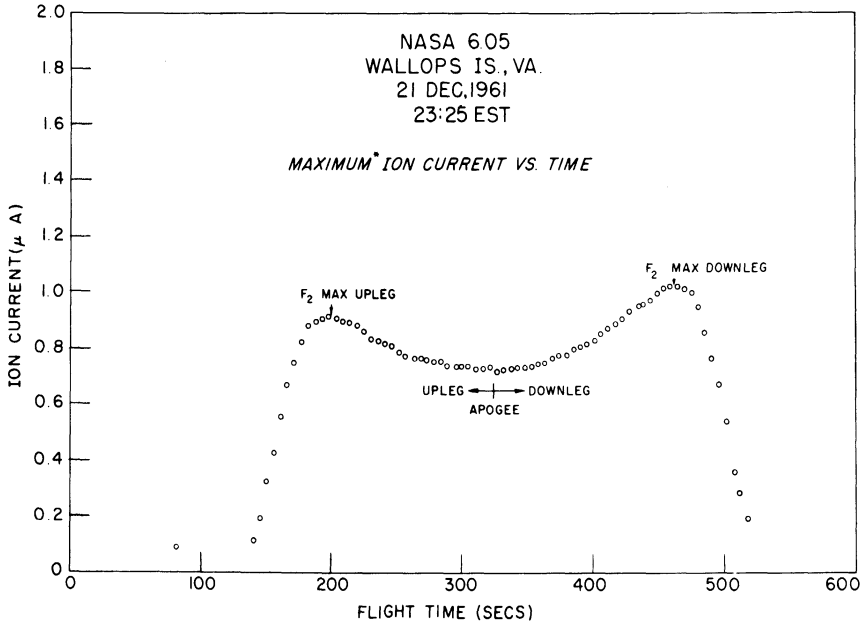

Figure 68. Positive ion current vs. time in the nighttime ionosphere (NASA 6.05).

pressed such that the N_e and N_p maxima agree in altitude, the two profiles are in much better overall agreement; however, the ion density at the maximum remains 7 to 8% lower than the more reliable electron density value here. Such an error in N_p can be produced by an increase in mean ion mass in the nighttime F region from the assumed value of 16 to about 18, possibly a mixture of O^+, O_2^+ and N_2

The Ion Current Profile.—Figure 69 shows the graph of ion current vs flight time which was used in the ion density reduction. Each point represents the magnitude of ion current, collected by the hemisphere, at full 8V with the hemisphere oriented normal to the velocity vector ($\theta = 0°$). It will be noted that the current profiles show stronger maxima in the F_2 region than do the resulting ion density profiles. This is caused by the higher velocity of the Dumbbell near the F maximum, as compared to the velocity at apogee, and the resulting increased ion current swept out by the hemisphere. Appropriate correction for probe velocity using the Dumbbell theory,[13] tends to flatten the maximum. Ionosphere theory and direct measurements have shown the F_2 region to be essentially parabolic in

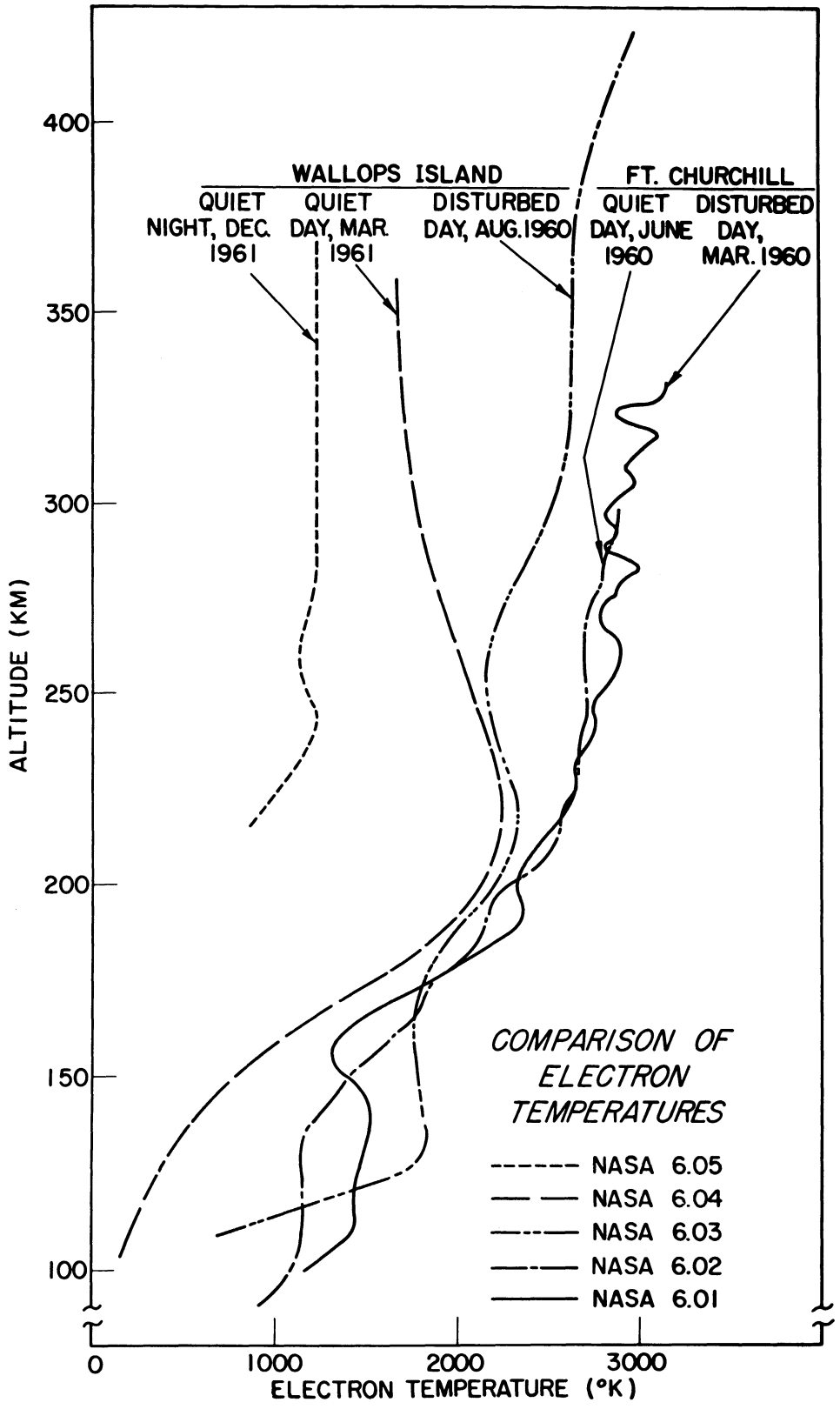

Figure 69. Composite of electron temperatures measured on all five flights between March 1960 and December 1961.

profile, thus the flattened N_p profile of Figure 64 seems to indicate that the probe theory introduces an overcorrection for the effects of velocity, at least near apogee. There was some evidence of this at apogee of the previous daytime flight, Figure 49, however, the good agreement between N_p and N_e profiles at lower altitudes in that and earlier measurements suggests that no such overcorrection exists at higher probe velocities. Further theoretical work is now in progress to attempt to account for this effect.

The Nighttime E-Region.—Another interesting feature of the nighttime ion density profile is the small, but resolvable, residual E-region visible near 100 kilometers in Figure 64. Although the ion currents here were too small to be resolved with the usual accuracy we estimate that the E-region density values are accurate to within a factor of two. It should be noted that heavy sporadic-E activity had been observed by the ionosonde throughout the evening preceeding the launch; however, none was visible at the time of launch. Furthermore, the vertical dimensions of the observed ion density maxima lead us to believe that we observed the normal residual E-region rather than sporadic E.

The persistence of the E-region at night has been a matter of some interest and was ascribed by Dubin[25] to micrometeorite ionization and by Nicolet[26] to the existence of meteoric debris which recombines very slowly.

In the valley which exists between the E and F-regions, the ion density fell below 1×10^3 ions/cc; the limit of resolution of the Dumbbell probe. Smith[27] and Ichimiya[28] have observed a similar valley in their nighttime E-region measurements. There is some question as to the relation between this valley and the E-region itself, and it has been suggested that the valley results from the draining of charge down into the nighttime E-region.

9.0 DISCUSSION OF THE DATA

9.1 INTRODUCTION

First, it should be emphasized that most of the data presented here are not representative of the quiet ionosphere which we like to envision as free from the anomalous effects of unusual solar activity which may produce magnetic storms and other forms of ionospheric disturbance. Actually, only the daytime ionosphere of NASA 6.04, and the nighttime ionosphere of NASA 6.05 could be described as quiet. As outlined in Table B, NASA 6.01 and 6.02 were launched in the auroral zone where leakage of high energy particles represents a continuous and variable source of heating and disturbance. In addition, NASA 6.01 was launched into a strongly "spread F" ionosphere. Similarly, NASA 6.03 at Wallops Island encountered an ionosphere which was still experiencing the effects of a magnetic storm which had begun three days earlier.

Among the five flights, NASA 6.04, launched at Wallops Island seems to best fit the criteria for a quiet daytime ionosphere. The 10.7 solar flux was 121×10^{-22} erg cm^{-2} sec^{-1}, the K index was 1.0, the relative sunspot number was 63, and no unusual cosmic ray activity was evident.[29] NASA 6.05, the only nighttime flight of this series, was also launched under essentially quiet ionosphere conditions; however, throughout the evening there had been intermittent sporadic E activity.

Clearly then, these measurements are too few in number and carried out under too widely varying ionospheric conditions to permit a detailed description of ionospheric behavior. However, certain general features of ionosphere behavior are apparent in these data as well as some clearly anomalous effects which have been touched on in previous sections where the individual flight profiles were discussed. In this section, the various flight profiles will be compared and

discussed further to permit evaluation of the general behavior of the ionosphere. We hope that others who may be more familiar with particular aspects of ionospheric behavior will find significant new relationships which have escaped our attention.

9.2 THE ELECTRON TEMPERATURE VARIATIONS IN THE IONOSPHERE

9.2.1 The Effects of Solar Activity and Latitude

Possibly the most significant result of the series of measurements reported here is the discovery of relatively high daytime electron temperature in certain regions of the ionosphere and its dependence upon latitude, solar activity and the degree of disturbance of the atmosphere. The combined effect of these three factors is demonstrated by the temperature profiles from all five flights, plotted together for comparison purposes in Figure 69. At Ft. Churchill in March 1960, the midday electron temperatures in the F-region reached 3000° K, while in June 1960 the temperature reached 2900° K. At Wallops Island, on August 1960, the electron temperature reached 2700° K, and in March 1961, it reached 2300° K. Clearly the measurements reveal a trend toward lower temperatures. The extent to which this reflects the decreased solar activity between March 1960 and March 1961 and latitude difference between Ft. Churchill and Wallops Island is not clear; however, earlier Dumbbell measurements in the E and F_1-regions at Ft. Churchill in 1958,[4] which showed even higher electron temperatures than were found there in the 1960 flights, indicate that solar activity is a primary factor.

With Figure 69 as a guide, one can reasonably postulate that lower values of electron temperature can be expected from subsequent flights at these launch sites as we approach the years of minimum solar activity. Furthermore, anticipating a latitude dependence, measurements at lower latitudes can be expected to show even lower daytime electron temperatures in the quiet ionosphere.

9.2.2 Magnetic Storm Effects

The high upper E-region temperatures found in the magnetically disturbed ionosphere of NASA 6.03, August 1960, represented an exception to the generally decreasing temperature trend. The absence of high E-region temperatures under quiet conditions at Wallops (NASA 6.04) suggests however that this was an anomalous effect related to the magnetic storm. The similarity of this profile to those found in the auroral zone suggests that the same mechanism which normally maintains the auroral zone E-region electron temperature at such high levels (order of 1000° K) is also at work at lower latitudes during the negative phase of a magnetic storm. This mechanism may be heating by X rays or secondary electrons generated in this region by the impact of high energy electrons which are known to accompany solar induced magnetic disturbances.

Figure 70 illustrates a second characteristic of the disturbed ionosphere; namely the absence of the strong negative temperature gradient which appears to be a feature of the quiet daytime F_2 region of NASA 6.04 (also shown). No mechanism for this high upper F-region electron temperature has been postulated.

9.2.3 The Question of Thermal Equilibrium

Mid-latitude Ionosphere.—If we accept the view that the daytime gas temperature (represented by the CIRA reference) cannot reach the high electron temperature values measured on NASA 6.03, the concept of thermal equilibrium must be discarded for that region of the ionosphere lying between 100 and 420 km, at least under disturbed conditions. On the other hand, the quiet ionosphere electron temperature (NASA 6.04) is in good agreement with the reference atmosphere gas temperature, except in the F_1-region where it exceeds the reference by a factor of 1.6. This is in qualitative agreement with the results of a theoretical study of Hanson and Johnson.[30] Using Hinterregger's values for $\mu\nu$ energy input to the ionosphere and considering the inefficient electron energy loss mechanisms,

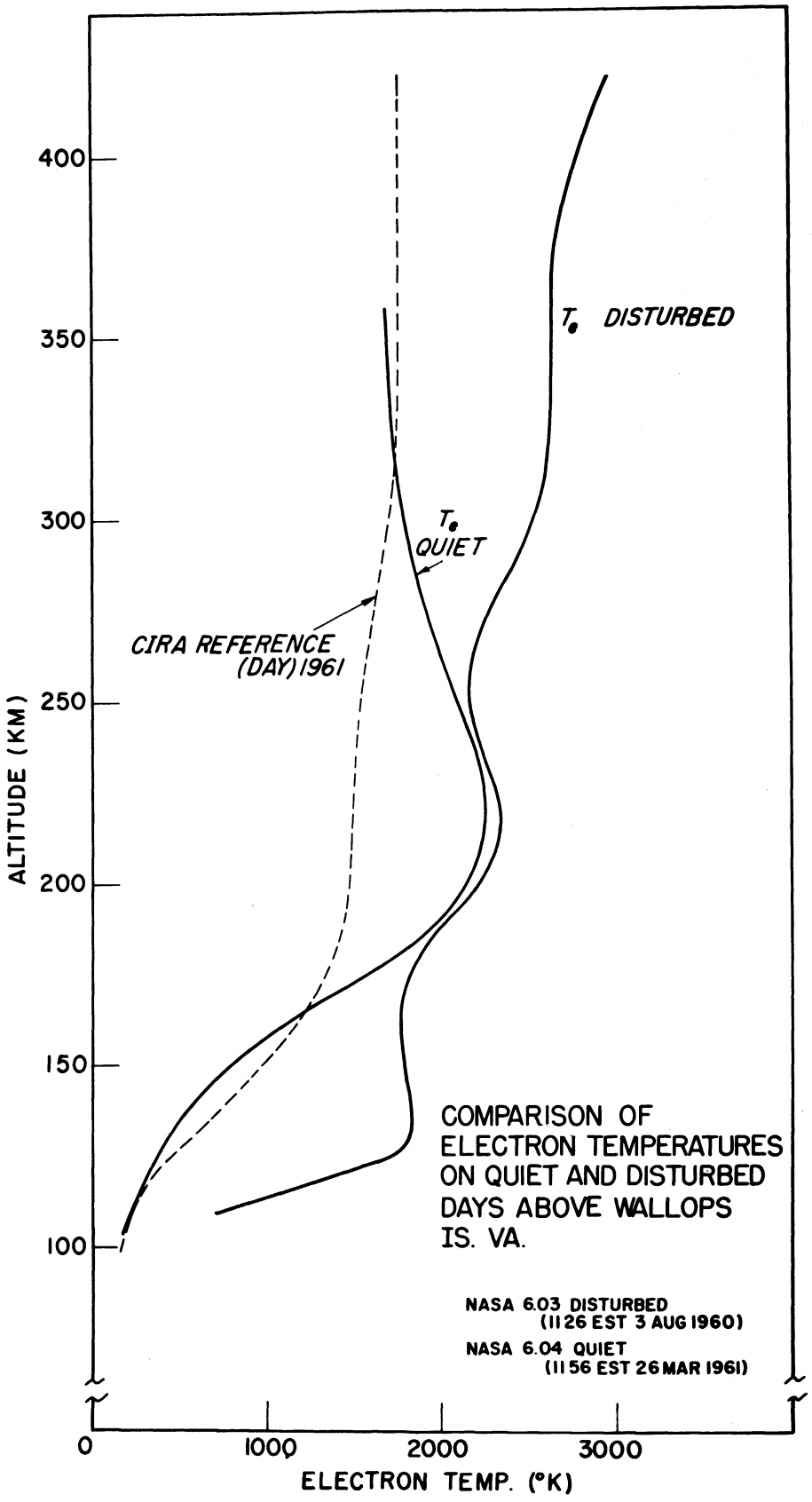

Figure 70. Comparison of quiet and disturbed mid-latitude ionosphere electron temperatures. The CIRA reference gas temperature is shown for comparison.

they calculated that the electron temperature can be expected to exceed the gas temperatures between 150 and 350 kilometers, as shown in Figure 71. A more recent calculation by Hanson using better cross-section data leads to still higher predicted electron temperatures (private communication).

The phenomenon of two species in equilibrium at different temperatures is not surprising since it is commonly observed in laboratory plasma experiments. The primary requirement is that there be a sufficiently large energy flux which affects the electrons selectively (such as extreme ultraviolet and x ray). The inefficient energy loss mechanisms available to the electron may then prevent temperature equilibrium from being established.

The Auroral Zone.—As pointed out earlier, the auroral zone electron temperature profiles are similar to those found in the disturbed mid-latitude ionosphere; however, the particle fluxes peculiar to this region make it easier to accept high gas temperature. Thus the question of thermal equilibrium in the auroral zone ionosphere cannot be decided on the basis of measurements of electron temperature alone.

The work of Horowitz and LaGow,[31,34] who derived gas temperature from rocket-borne measurements of neutral density at Ft. Churchill during the period of maximum solar activity, is particularly pertinent here. As shown in Figure 72, their gas temperature values, corrected for the changing mean molecular weight of the gas, are in reasonable agreement with the electron temperatures and are decidedly higher than the reference values above 140 kilometers. Below 140 km the electron temperature clearly exceeds the gas temperature by as much as a factor of two or three.

9.2.4 The Nighttime Measurements

Use of the Dumbbell probe in the nighttime ionosphere was considered particularly desirable since, in view of the expected thermal equilibrium, an electron temperature measurement constitutes a gas temperature measurement as

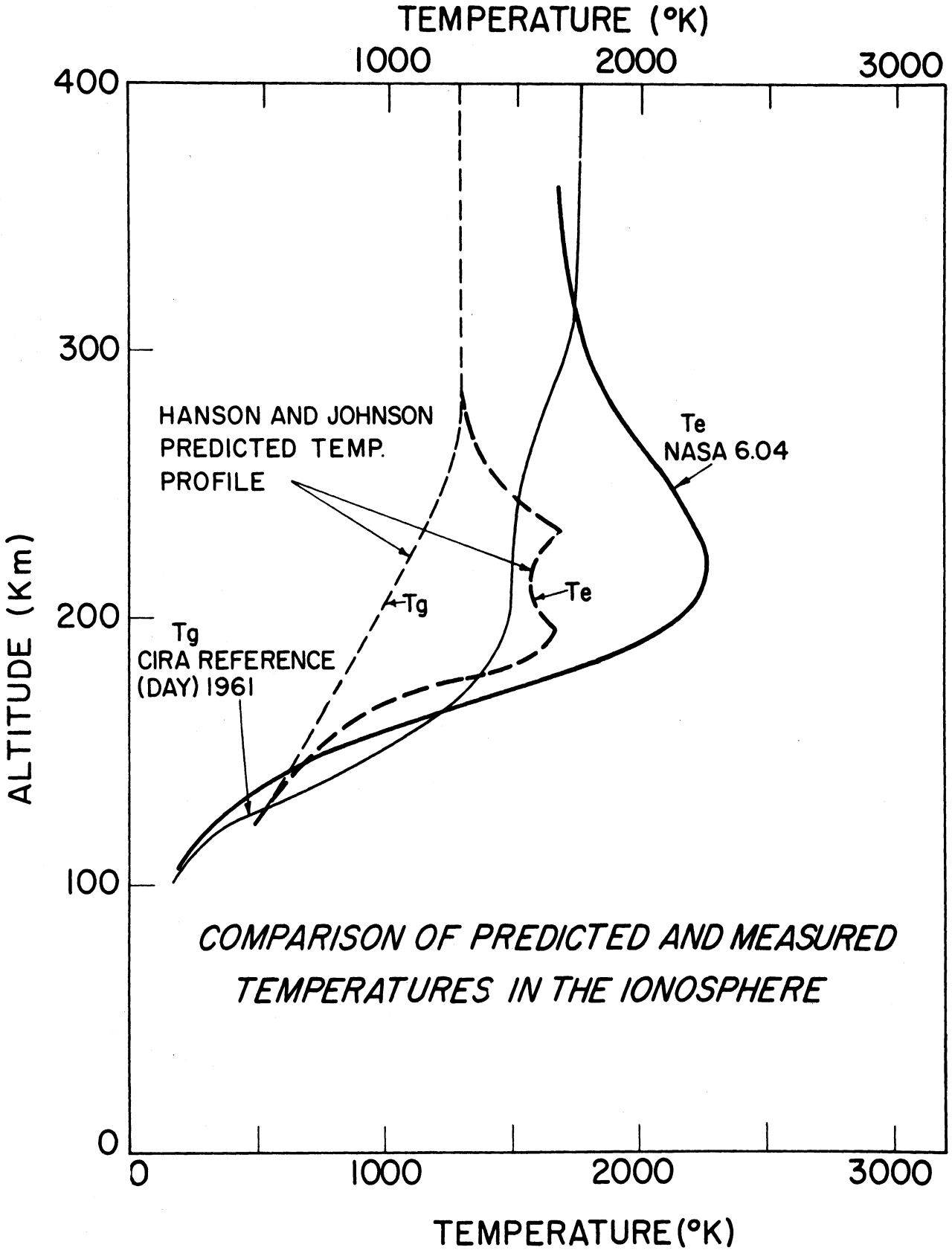

Figure 71. Comparison of predicted (Hanson and Johnson) and measured (Dumbbell) electron temperatures. The gas temperature assemed by Hanson and Johnson, and the reference gas temperature are also shown.

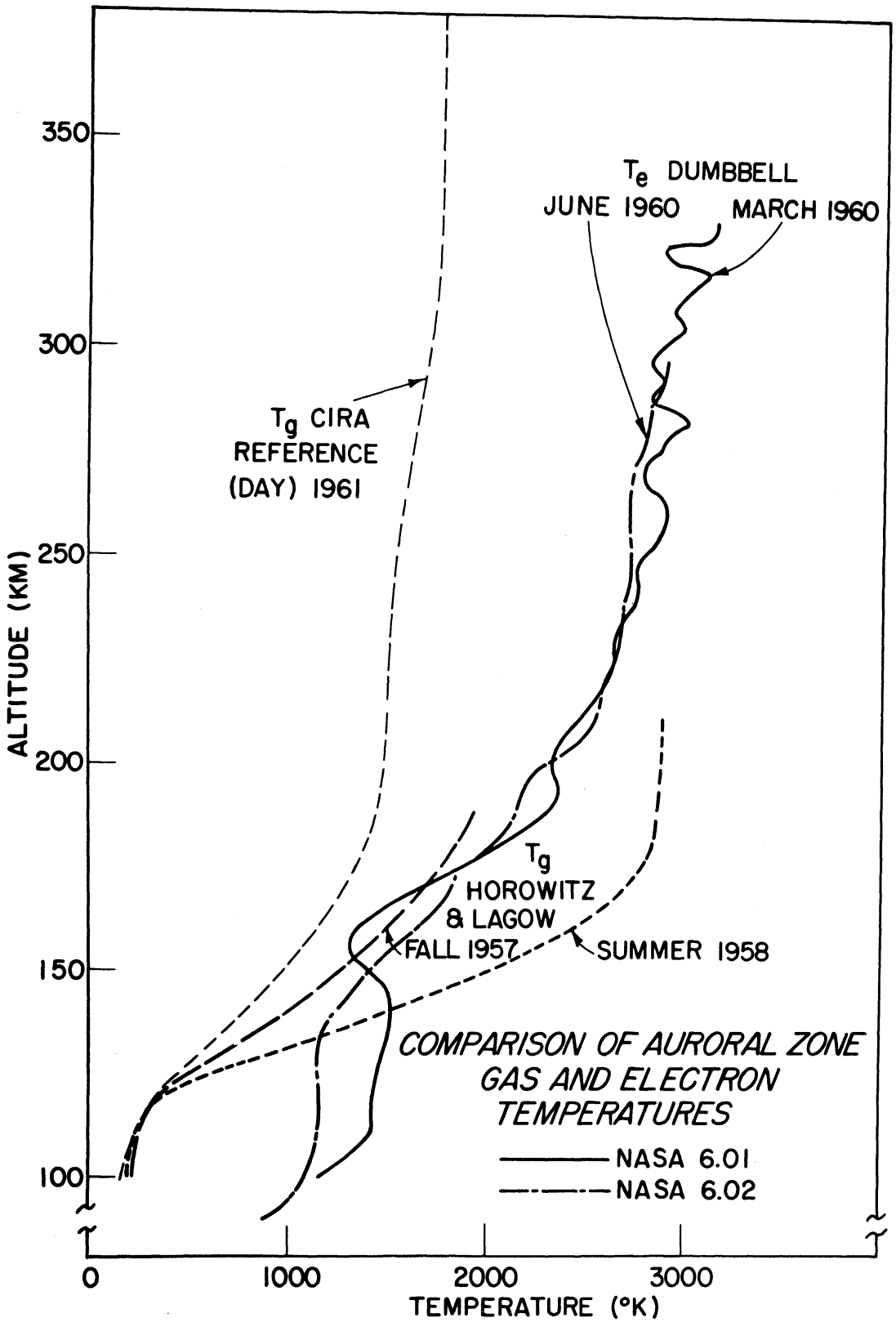

Figure 72. Comparison of measured auroral zone gas and electron temperatures.

well. The latter is a much more difficult parameter to determine directly and, until recently, could only be inferred from either direct or indirect measurements of neutral particle density or from the diffusion rate of vapor releases in the atmosphere.

A fallout of the nighttime Dumbbell measurements was a gross check of the validity of the technique itself. The validity of the double probe method has been amply demonstrated in laboratory plasma studies,[21,22] and it is believed that the general agreement between the measured nighttime temperatures and the reference atmosphere (see Figure 64) removes all reasonable doubt concerning the validity of the method as applied to measurements in the ionosphere.

9.2.5 Diurnal Temperature Variation

In addition to demonstrating the validity of the method, the nighttime temperature profile used with the earlier daytime profiles permits an evaluation of the diurnal temperature variation in the F-region, as shown in Figure 73. If one accepts the assertion that (1) thermal equilibrium existed at apogee of the quiet daytime ionosphere (NASA 6.04), and (2) the nighttime minimum had been reached on the down-leg of NASA 6.05, then the diurnal variation in gas temperature, expressed in terms of the ratio of day to night temperature, is found to be on the order 1.35. This may be observed in Figure 73 at apogee of the two flights. The former assertion is believed justified by the temperature curve's asymptotic approach at apogee to the theoretically expected isothermal profile. Assertion (2) is less certain since the measurement was carried out some three or four hours before the expected nighttime temperature minimum, therefore this profile must be considered an upper limit on the minimum nighttime electron (or gas) temperature. However, extrapolation of the nighttime results on the basis of the temperature models of Harris and Priester,[23] (Figure 65) leads to a nighttime minimum of approximately 1000°K, a value which suggests

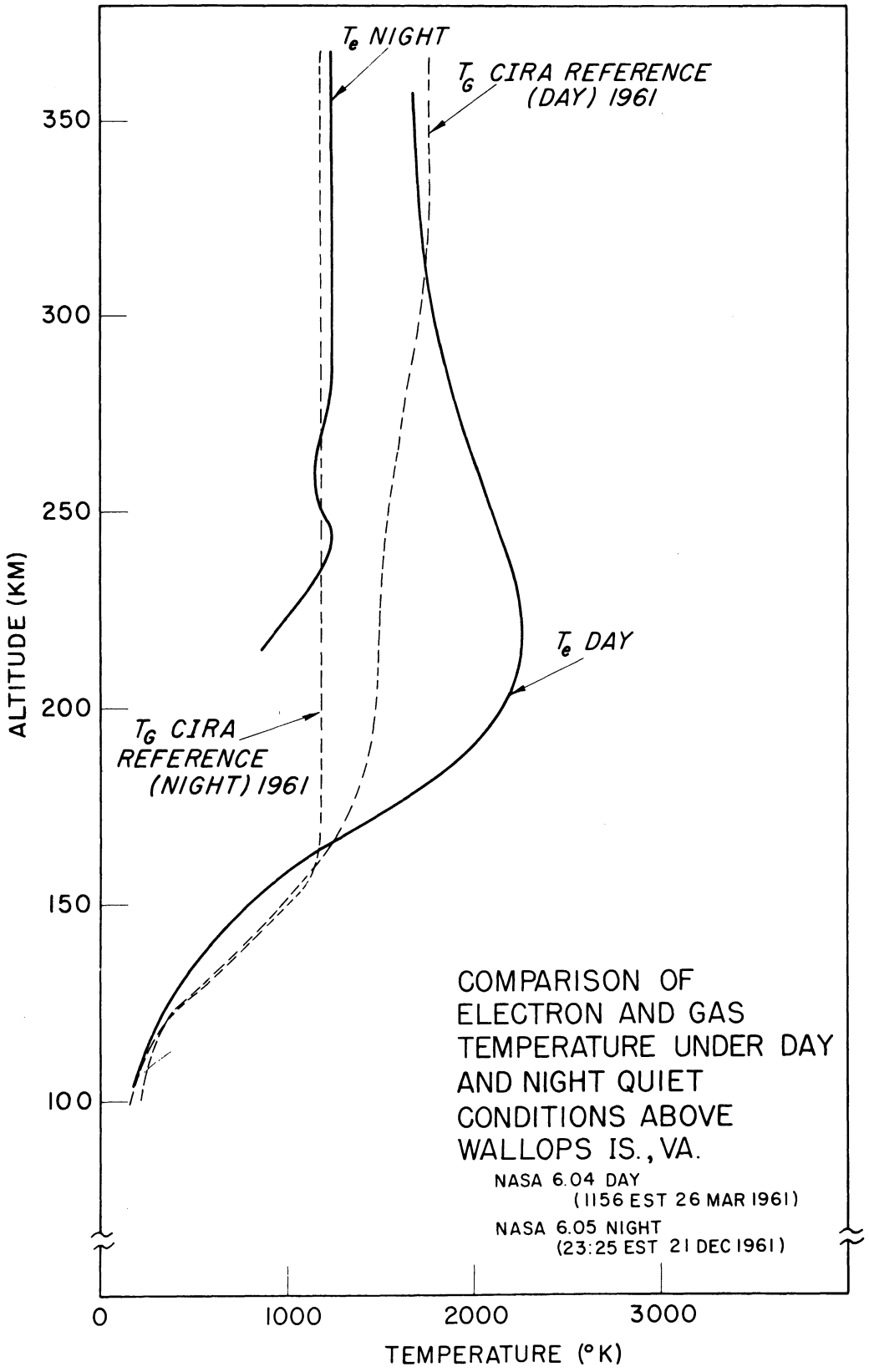

Figure 73. Comparison of quiet-day and quiet-night mid-latitude electron temperatures.

a diurnal temperature ratio of 1.7. Based on this range of nighttime minimum temperature, the total diurnal variation is between 35 and 70%.

9.3 ION AND ELECTRON DENSITY

9.3.1 Accuracy of the Density Measurements

Extensive laboratory work with Langmuir probes shows that the interpretation of probe characteristics is less straight-forward for ion and electron density than for electron temperature. Indeed, deviations in ion current from that predicted by the Langmuir probe theory may approach a factor of two according to some investigators,[18] One must be wary, however, of broad generalizations concerning the accuracy of the probe-derived densities, since this depends strongly on the size and geometry of the probe and the atmospheric region and the conditions in which it is used. For instance, the Dumbbell (hemisphere) probe is not suited to N_e measurement while the cylindrical probe characteristics provide measurements of both N_e and N_p. Other factors, such as the probe motion and orientation and the necessity of assuming a mean ion mass (see Section 5.0) also introduce varying degrees of error into the density reduction. Further, the electron and ion density are not interpreted from the cylindrical probe characteristics with equal ease. Although the Maxwell-Boltzmann relation on which the probe theory is based is believed to hold in the plasma surrounding an ion-saturated (highly negative) collector, this is not necessarily true as the probe approaches or exceeds the plasma potential when the surrounding plasma may be being depleted of electrons. Here, the electron-saturation currents may not accurately be interpreted in terms of electron density.

A sufficient number of experimental probe characteristics from rocketborne cylindrical, hemispherical and planar type probes are now on hand to begin to sort out and evaluate the aforementioned effects by comparison of probe results with known electron densities from simultaneous ionosonde data and/or two-

frequency beacon data. The results of this study, which is now underway, are expected to improve the interpretation of future probe results in terms of ion and electron density.

Though, it is difficult to assign error flags to the ion density measurements obtained from the Dumbbell data because of the approximations in the theory[13] and the necessity of assuming an ion mass, comparisons with simultaneous measurements of electron density indicates an accuracy of better than 20% can be expected when the present Dumbbell probe theory and the ion mass given by Figures 16 and 17 are used. When empirically derived corrections to the data (based on comparison of ion and electron density data from earlier flights) are applied, we expect to be able to significantly improve the accuracy of the ion density measurement, although this has not been attempted with the data presented here.

9.3.2 Evidence for the Existence of Negative Ions in the D and Lower E-Regions

Direct measurements on V-2 rockets immediately after World War II,[2] indicated that a significant negative ion population exists in the D-region of the ionosphere. These ions are difficult to measure directly, in the presence of even small numbers of electrons, because the negative currents they produce tend to be obscured by collection of the highly mobile electrons; and any attempt to separate the two components either electrically or magnetically is frought with theoretical problems in interpretation of the data.

The capability of simultaneous and independent measurement of both the positive ion density (Dumbbell) and electron density (two-frequency beacon) has permitted the negative ion density to be found on two of these flights through the assumption of volume neutrality,

$$N_p = N_- + N_e \qquad (9.1)$$

The two-frequency beacon, a version of the Seddon[35] propagation experiment,

which has been used extensively by the Ballistic Research Laboratories, was carried as a companion experiment aboard both NASA 6.03 and NASA 6.04. As shown in Figure 39, this experiment remained with the rocket after Dumbbell ejection and enabled measurements throughout the flights. The separation of the Dumbbell and the rocket is relatively small, on an ionospheric scale, thus a comparison of the electron and positive ion densities leads, through Equation (9.1), to the local negative ion density at any point along the flight path.

Since N_- is found by taking the difference between two relatively large numbers, N_p and N_e, its accuracy is dependent upon the relative rather than absolute accuracy of these parameters. Thus, to remove the effects of any experimental errors in the Dumbbell-derived N_p and the two-frequency beacon-derived N_e, it is valid to make the geophysical assumption that $N_e = N_p$ above the E-region in the daytime and then normalize one of the two density profiles to the other. In this case N_p was normalized to N_e. The original good agreement between N_e and N_p throughout the E and F_1-regions made the normalization factor very nearly unity. In the D-region and lower E-region of the disturbed Wallops Island ionosphere, shown in Figure 74, the N_e clearly fell far below N_p on both the up-leg and the down-leg, and the existence of negative ions was apparent. In the quite ionosphere shown in Figure 75, the negative ion region was smaller and existed at lower altitudes. The gap in N_p data between 90 and 98 km on the up-leg and 84 and 92 kilometers on the down-leg resulted from the operation of the time-shared cylinder experiment. The N_p in these regions was interpolated from measurements above and below.

It has been the practice, when considering negative ions in the ionosphere, to use the ratio $\lambda = N_-/N_e$. Figure 76 shows the four λ profiles from the two flights at Wallops Island as well as the λ derived from theoretical studies of the ionosphere.[32,33] Some of the pertinent facts which are apparent in these figures are:

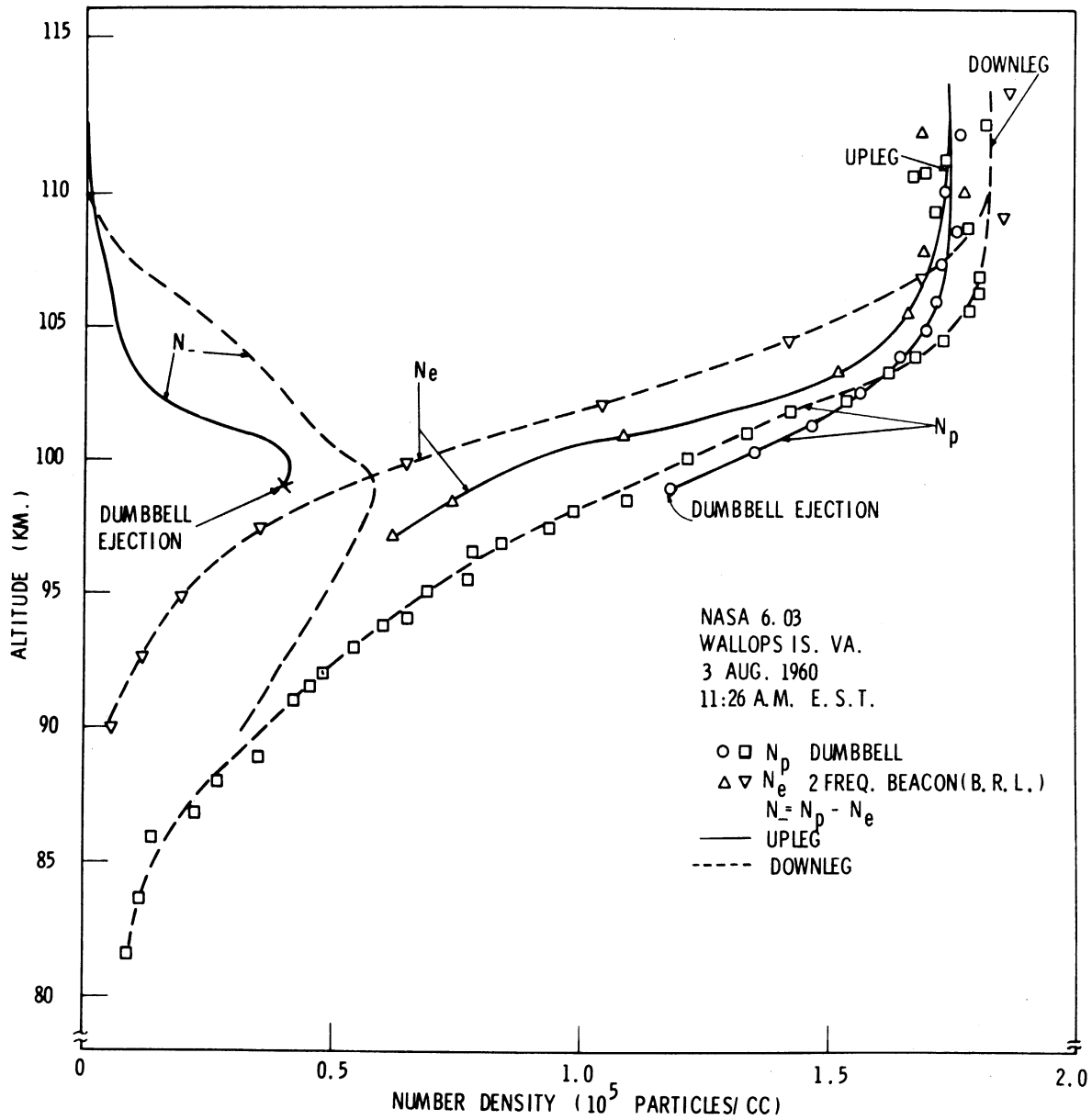

Figure 74. Disturbed ionosphere D-region electron and positive ion densities and the negative ion density resulting from assuming volume neutrality ($N_p = N_e + N_-$).

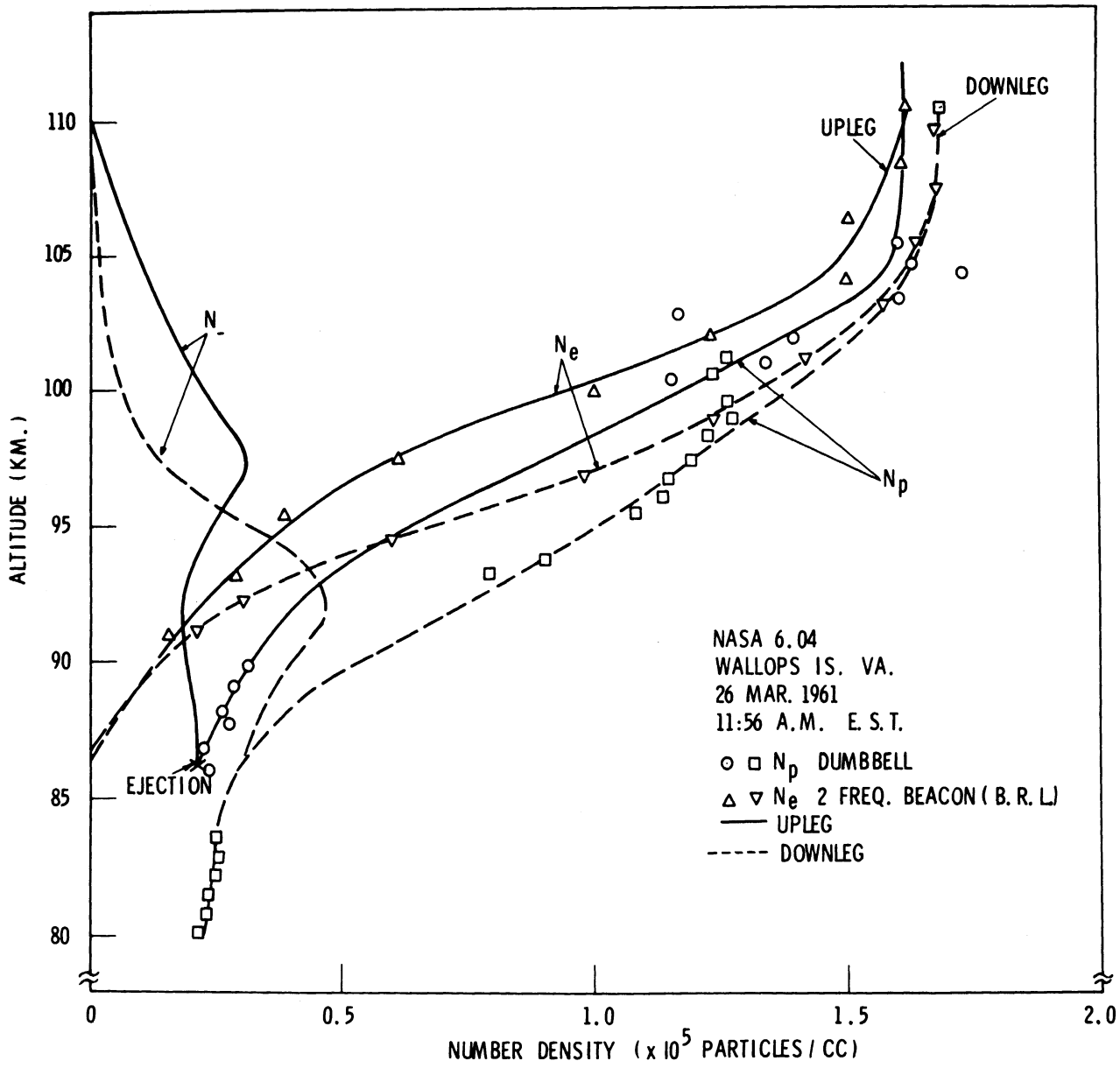

Figure 75. Quiet ionosphere D-region electron and positive ion densities and the negative ion density resulting from assuming volume neutrality ($N_p = N_e + N_-$).

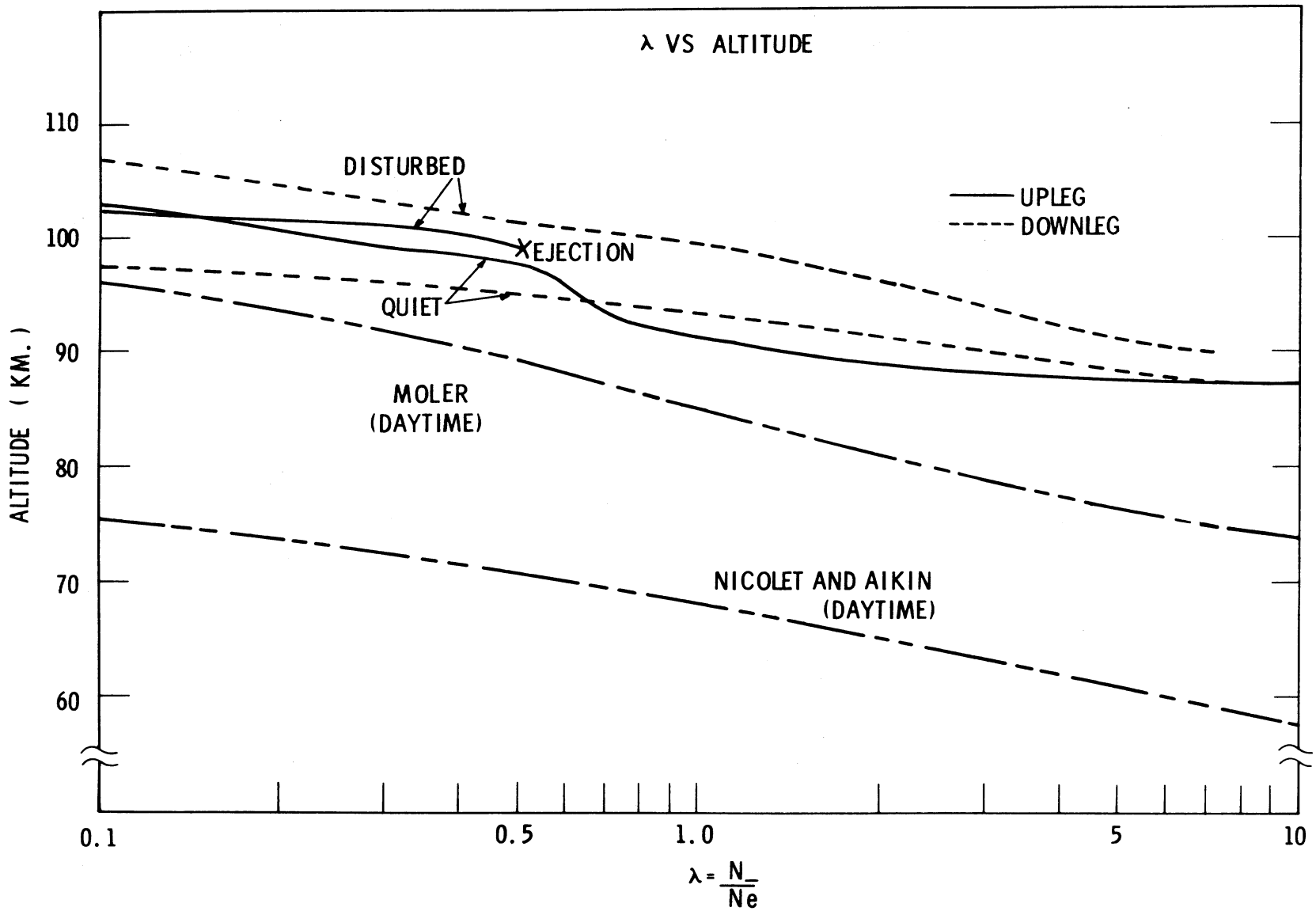

Figure 76. The theoretical and experimental values of the ratio $\lambda = N_-/N_e$ in the magnetically disturbed and quiet ionosphere.

(1) The negative ions exist at higher altitudes and in greater numbers under disturbed conditions.

(2) The experimentally-derived negative ion populations under both disturbed and quiet conditions exist at higher altitudes than the theoretical studies predict.

A great deal of time has been spent at BRL and Michigan to insure that the data points used in Figures 74 and 75 represent our best effort, and that the altitudes assigned to the given data points are as accurate as the trajectory. An error which is neglected is the increasing separation between the ejected Dumbbell and the two-frequency beacon on the rocket. Since the maximum separation velocity is approximately 4 feet per second, not more than a 2000-foot separation can exist in the down-leg E-region. This is assumed to be entirely negligible on an ionospheric scale.

Due to errors in trajectory, which tend to increase through the flight, one should not place too much significance upon the difference in altitude of the up-leg and down-leg negative ion peaks; particularly for NASA 6.03 for which the trajectory determination was not as certain. The uncertainty in the down-leg E-region trajectory is estimated to be as much as three kilometers, although comparison of ascent and descent density profiles does not suggest this much error actually existed.

Geophysical Significance of the Larger than Expected Negative Ion Population.—Clearly, the negative ion concentration is a function of the species and numbers of molecules present, their coefficients of attachment, the electron concentration, the energy flux available for detachment and the cross-sections for this phenomenon. Without simultaneous measurements of at least the most important of these factors, one can merely speculate as to which parameters in the theoretical treatments cited earlier are most likely to have been either in error or neglected entirely. We look upon the profiles of N_p, N_e and N_- as the end prod-

ucts of a rather complex problem in atmospheric chemistry and leave it to the specialists in this area to discover the exact nature and relative importance of the chemical process which caused these densities to exist.

10.0 CONCLUSION

The development of the Dumbbell theory and its implementation began in 1958 during the International Geophysical Year; and the technique, as applied in the flights reported here, is now believed to provide high resolution profiles of ionospheric electron temperature and positive ion density.

Because the flights were carried out over a period of nearly two years under varying ionosphere conditions and at two different latitudes, much can be deduced concerning the general behavior of the ionosphere and its response to solar cycle, diurnal and latitudinal variations. Some of these effects discussed in the previous sections are summarized below. Hopefully, other investigators will uncover relationships which have escaped us or will suggest other interpretations of the effects mentioned here.

1. The electron temperature decreases as we approach the solar cycle minimum (see Figure 69), although it is difficult to untangle the combined effects of solar activity and latitude.

2. The quiet ionosphere electron temperature in the lower F-region experiences a factor of two diurnal variation. (see Figure 73).

3. The quiet ionosphere electron and gas temperature in the upper F-region experiences a diurnal variation of 1.35 to 1.7 depending upon the estimated minimum nighttime temperature. (see Figure 73).

4. The daytime electron temperature in the quiet, mid-latitude ionosphere exceeds, at its maximum, the daytime reference gas temperature by approximately 60% in the lower F-region. (see Figure 70). This is considered strong evidence that temperature equilibrium does not exist in the daytime lower F-region.

5. The nighttime electron temperature is in good agreement with the nighttime reference gas temperature (see Figure 73). This tends to confirm the validity of the double probe technique for use in ionosphere temperature measurements.

6. The mid-latitude ionosphere, when disturbed by a magnetic storm, exhibits an electron temperature profile resembling that of the auroral zone ionosphere much more closely than the quiet mid-latitude ionosphere (see Figure 69). This suggests an additional energy source common to both the auroral and disturbed ionosphere; possibly a flux of solar charged particles coming either directly from the sun or by leakage from the Van Allen belts.

7. Negative ions found to exist in the D and lower E-regions occur at higher altitudes and in greater numbers than theoretical models suggest (see Figure 76). This points up the primitive state of our present knowledge concerning the kinds of negative ions present and their production and detachment rates as a function of altitude.

8. The auroral zone temperatures are higher than the mid-latitude values but, except in the E-region, are in generally good agreement with neutral temperatures deduced from the neutral density profiles of Horowitz and LaGow (see Figure 72). Thus thermal equilibrium does not exist in the auroral zone E region but may exist at higher altitudes.

To facilitate the use of the data, Table C presents the mean electron temperature and ion density from all five flights tabulated at 2-kilometer intervals.

Plans for Future Atmosphere Studies.—The series of measurements described above have provided much needed data which we hope will prove valuable in understanding the upper atmosphere. However it is becoming clear, as is usually the case in a new and rapidly developing area of physical interest, that a single measurement, or series of measurements, of one or two parameters is no longer as profitable as it was during the exploratory stage of study. As our knowledge of the important physical factors increases, a rocketborne experiment becomes worth the required effort only if a sufficient number of the key parameters are measured simultaneously, and preferably in the same region of the atmosphere.

Therefore, future plans include the implementation of a more comprehensive multiple-experiment package, based upon the ejection technique developed for the Dumbbell series, but directed toward a wider range of aeronomy experiments including various combinations of neutral and ion mass spectrometers, neutral density gages as well as the hemispherical and cylindrical probes used on the recent Dumbbells. Ejection from the vehicle and vacuum pumping prior to and through the launch phase will permit the use of neutral particle experiments up to several hundred kilometers without significant disturbance due to outgassing in the sensor chambers or from the vehicle, itself. The instrument, called the Thermosphere Probe, was named for the region of intended use which exists between approximately 100 and 400 kilometers. This is a particularly interesting region since most of the important aeronomic phenomenon occur or begin here; namely, the dissociation of O_2 and N_2, the ionization of atomic and molecular species to form the ionosphere, gravitational separation of the neutral species, and others. The need for this type of rocketborne experiment is further increased by the short life of satellites in orbits below 200 kilometers and the increased risk of failure which accompanies such orbits.

The Thermosphere Probe work is under the direction of the author* and is one of the flight programs of the Aeronomy and Meteorology Division of Goddard Space Flight Center, NASA.

*Now with Goddard Space Flight Center, Greenbelt, Maryland.

TABLE C

TABULATED DUMBBELL PROBE DATA

Altitude	NASA 6.01				NASA 6.02				NASA 6.03				NASA 6.04				NASA 6.05			
	Up-Leg		Down-Leg		Up-Leg		Down-Leg		Up-Leg		Down-Leg		Up-Leg		Down-Leg		Up-Leg		Down-Leg	
	T_e (°K)	N_p (10^5/cc)	T_e (°K)	N_p (10^5/cc)	T_e (°K)	N_p (10^5/cc)	T_e (°K)	N_p (10^5/cc)	T_e (°K)	N_p (10^5/cc)	T_e (°K)	N_p (10^5/cc)	T_e (°K)	N_p (10^5/cc)	T_e (°K)	N_p (10^5/cc)	T_e (°K)	N_p (10^5/cc)	T_e (°K)	N_p (10^5/cc)
80								0.10												
82								0.10				0.02								
84								0.15				0.10								
86								0.18				0.17		0.21		0.29				
88								0.25				0.26		0.26		0.38				
90					910	0.15	920	0.35				0.35		0.31		0.55				
92					950	0.21	1020	0.50				0.45		0.40		0.75				
94					995	0.31	1080	0.63				0.55		0.55	460	0.94				
96			1150		1030	0.40	1115	0.73				0.65		0.75	465	1.09				
98			1220	0.40	1070	0.50	1135	0.76		0.93		0.78		0.97	475	1.24				
100	1160	0.26	1280	0.60	1100	0.61	1140	0.80		1.05		0.93		1.19	485	1.38				
102	1220	0.38	1320	0.75	1110	0.72	1145	0.81		1.15	1000	1.15		1.39	505	1.52				
104	1280	0.50	1355	0.87	1120	0.82	1140	0.82		1.27	1060	1.30	190	1.56	520	1.61				
106	1330	0.60	1375	0.95	1130	0.90	1130	0.82		1.36	1120	1.43	210	1.61	550	1.66				
108	1385	0.65	1375	0.98	1140	1.02	1105	0.85		1.41	1190	1.52	230	1.61	580	1.67				
110	1415	0.70	1365	1.00	1150	1.15	1100	0.85	730	1.45	1260	1.56	245	1.62	615	1.70				
112	1430	0.78	1340	1.02	1155	1.21	1100	0.90	840	1.48	1320	1.60	265	1.45	660	1.65				
114	1430	0.84	1250	1.12	1160	1.25	1110	0.94	980	1.51	1390	1.64	280	1.30	710	1.60				
116	1430	0.83	1130	1.28	1160	1.30	1115	0.96	1110	1.53	1460	1.67	295	1.10	750	1.55				
118	1430	0.80	1090	1.40	1160	1.35	1120	1.00	1230	1.55	1540	1.70	310	1.00	800	1.50				
120	1430	0.83	1075	1.42	1160	1.39	1140	1.00	1360	1.57	1590	1.70	330	0.94	840	1.55				
122	1435	0.86	1075	1.38	1155	1.39	1155	1.02	1490	1.60	1610	1.70	350	0.93	880	1.60				
124	1450	0.88	1090	1.40	1150	1.38	1190	1.07	1610	1.63	1620	1.70	370	0.95	915	1.70				
126	1460	0.88	1105	1.45	1150	1.38	1205	1.10	1730	1.65	1610	1.70	390	0.96	950	1.75				
128	1470	0.87	1125	1.50	1160	1.36	1225	1.17	1790	1.67	1590	1.70	420	0.96	990	1.80				
130	1480	0.80	1150	1.50	1155	1.37	1240	1.23	1810	1.72	1560	1.73	445	1.00	1025	1.85				
132	1490	0.80	1175	1.50	1160	1.41	1240	1.29	1825	1.75	1500	1.75	475	1.05	1065	1.90				
134	1500	0.81	1190	1.51	1165	1.50	1240	1.35	1835	1.80	1440	1.77	510	1.10	1100	2.00				
136	1510	0.82	1200	1.50	1185	1.60	1240	1.44	1840	1.85	1410	1.80	540	1.20	1140	2.05				
138	1520	0.85	1210	1.49	1210	1.72	1245	1.52	1830	1.90	1390	1.85	580	1.20	1170	2.10				
140	1525	0.87	1225	1.55	1250	1.84	1250	1.60	1825	1.95	1370	1.88	610	1.30	1210	2.10				
142	1525	0.92	1245	1.59	1280	1.94	1260	1.70	1820	2.02	1360	1.93	645	1.40	1245	2.20				
144	1510	0.97	1270	1.62	1315	2.02	1275	1.80	1810	2.07	1360	2.00	680	1.45	1280	2.20				
146	1485	1.06	1295	1.65	1345	2.10	1290	1.85	1800	2.13	1370	2.05	720	1.50	1320	2.25				
148	1484	1.15	1330	1.66	1380	2.14	1320	1.90	1800	2.21	1380	2.10	760	1.60	1345	2.30				
150	1405	1.26	1360	1.68	1410	2.20	1360	2.00	1795	2.28	1400	2.17	800	1.70	1380	2.40				
152	1360	1.37	1390	1.70	1460	2.20	1420	2.07	1790	2.37	1430	2.25	850	1.85	1415	2.40				
154	1330	1.42	1410	1.70	1510	2.15	1470	2.12	1785	2.45	1480	2.35	900	2.00	1445	2.40				
156	1320	1.46	1420	1.75	1560	2.15	1530	2.19	1780	2.55	1530	2.40	950	2.20	1475	2.45				
158	1330	1.49	1430	1.87	1610	2.15	1590	2.21	1780	2.64	1580	2.46	1010	2.30	1510	2.55				
160	1360	1.49	1435	1.95	1650	2.20	1670	2.30	1770	2.75	1620	2.57	1070	2.45	1545	2.60				
162	1400	1.48	1430	2.05	1690	2.23	1725	2.35	1770	2.83	1660	2.67	1135	2.60	1570	2.70				
164	1450	1.50	1400	2.15	1730	2.30	1770	2.46	1770	2.92	1700	2.76	1200	2.75	1605	2.85				
166	1510	1.55	1350	2.27	1780	2.40	1800	2.56	1775	2.98	1730	2.82	1270	2.90	1635	2.95				

TABLE C (Continued)

Altitude	NASA 6.01				NASA 6.02				NASA 6.03				NASA 6.04				NASA 6.05			
	Up-Leg		Down-Leg		Up-Leg		Down-Leg		Up-Leg		Down-Leg		Up-Leg		Down-Leg		Up-Leg		Down-Leg	
	T_e (°K)	N_p (10^5/cc)	T_e (°K)	N_p (10^5/cc)	T_e (°K)	N_p (10^5/cc)	T_e (°K)	N_p (10^5/cc)	T_e (°K)	N_p (10^5/cc)	T_e (°K)	N_p (10^5/cc)	T_e (°K)	N_p (10^5/cc)	T_e (°K)	N_p (10^5/cc)	T_e (°K)	N_p (10^5/cc	T_e (°K)	N_p (10^5/cc)
168	1600	1.54	1360	2.35	1810	2.50	1820	2.65	1780	3.03	1760	2.88	1350	2.95	1665	3.05				
170	1670	1.53	1415	2.35	1820	2.58	1840	2.70	1790	3.08	1780	2.93	1410	3.00	1695	3.25				
172	1760	1.58	1480	2.35	1840	2.66	1880	2.76	1800	3.12	1810	2.97	1480	3.10	1725	3.40				
174	1840	1.72	1580	2.30	1865	2.73	1910	2.82	1815	3.13	1830	2.99	1550	3.20	1750	3.60				
176	1910	1.86	1670	2.22	1910	2.80	1960	2.90	1835	3.16	1860	3.00	1610	3.30	1780	3.70				
178	1980	1.84	1810	2.17	1960	2.85	2000	2.95	1855	3.18	1880	3.00	1670	3.45	1810	3.85				
180	2050	1.75	1910	2.16	2010	2.90	2040	3.00	1880	3.22	1910	3.00	1730	3.60	1840	4.00				
182	2110	1.67	1990	2.30	2065	2.95	2090	3.06	1905	3.27	1940	3.00	1790	3.65	1870	4.10				
184	2180	1.60	2000	2.48	2100	3.04	3140	3.15	1940	3.32	1960	3.00	1850	3.70	1890	4.30				
186	2445	1.57	1950	2.72	3130	3.16	2200	3.22	1970	3.37	1990	3.00	1910	3.85	1910	4.45				
188	2305	1.60	1855	3.00	3145	3.28	2260	3.30	2005	3.43	2030	3.02	1960	3.95	1930	4.65				
190	2345	1.72	1805	3.07	3160	3.42	2305	3.40	2040	3.50	2060	3.02	2000	4.05	1950	4.80				0.02
192	2360	1.90	1820	3.05	2175	3.50	2345	3.40	2070	3.55	2090	3.05	2040	4.20	1970	4.95				0.04
194	2360	2.12	1860	3.01	2190	3.50	2370	3.41	2110	3.60	2125	3.07	2080	4.40	1985	5.20				0.07
196	2355	2.25	1920	3.00	2220	3.52	2390	3.41	2145	3.65	2160	3.10	2110	4.60	2000	5.40				0.10
198	2350	2.25	2000	2.99	2250	3.55	2410	3.40	2185	3.68	2200	3.15	2140	4.75	2010	5.55				0.15
200	2340	2.21	2050	2.99	2300	3.56	2430	3.39	2220	3.72	2250	3.20	2160	4.95	2020	5.65				0.18
202	2345	2.20	2080	3.12	2370	3.57	2460	3.37	2245	3.75	2280	3.25	2180	5.20	2035	5.85				0.23
204	2365	2.22	2070	3.20	2430	3.60	2490	3.37	2270	3.77	2330	3.30	2190	5.45	2045	6.00		0.01		0.27
206	2390	2.24	2080	3.20	2490	3.60	2520	3.35	2285	3.80	2370	3.35	2210	5.60	2055	6.20		0.08		0.32
208	2425	2.21	2180	3.19	2510	3.61	2560	3.35	2300	3.81	2420	3.38	2230	5.85	2065	6.30		0.15		0.40
210	2455	3.17	2310	3.17	2535	3.64	2600	3.40	2320	3.81	2470	3.41	2240	6.00	2075	6.40		0.25		0.47
212	2490	2.18	2350	3.17	2560	3.67	2645	3.50	2335	3.80	2510	3.44	2250	6.25	2080	6.50		0.40	795	0.55
214	2520	2.32	2360	3.23	2575	3.70	2685	3.60	2345	3.79	2530	3.45	2260	6.45	2085	6.65		0.50	830	0.64
216	2550	2.53	2360	3.35	2585	3.72	2710	3.72	2350	3.78	2550	3.46	2265	6.70	2095	6.80		0.70	865	0.72
218	2590	2.64	2355	3.47	2590	3.79	2735	3.79	2345	3.77	2570	3.45	2265	6.90	2105	6.90		0.85	900	0.85
220	2620	2.50	2330	3.46	2600	3.81	2745	3.81	2340	3.75	2580	3.45	2270	7.15	2110	7.15		0.98	935	0.98
222	2640	2.35	2320	3.40	2620	3.89	2760	3.89	2335	3.75	2585	3.42	2270	7.35	2115	7.40		1.05	970	1.13
224	2650	2.31	2325	3.40	2645	3.95	2765	3.90	2325	3.74	2590	3.42	2265	7.50	2115	7.65		1.13	1000	1.35
226	2660	2.32	2385	3.46	2665	4.05	2765	3.91	2320	3.73	2590	3.40	2260	7.70	2115	7.90		1.20	1040	1.60
228	2660	2.34	2465	3.50	2670	4.12	2770	3.95	2305	3.72	2590	3.40	2260	7.85	2115	8.10		1.30	1070	1.93
230	2660	2.37	2510	3.52	2680	4.18	2770	4.00	2295	3.71	2580	3.40	2250	8.00	2115	8.30		1.43	1100	2.30
232	2660	2.40	2530	3.60	2680	4.31	2765	4.10	2275	3.68	2580	3.42	2240	8.20	2115	8.55		1.61	1130	2.70
234	2685	2.43	2535	3.75	2680	4.44	2760	4.15	2260	3.67	2570	3.45	2230	8.35	2110	8.75		1.85	1160	3.12
236	2720	2.45	2520	4.00	2685	4.55	2755	4.25	2250	3.65	2550	3.50	2220	8.50	2100	8.95		2.10	1185	3.45
238	2750	2.45	2500	4.02	2690	4.66	2750	4.30	2230	3.63	2545	3.54	2200	8.65	2090	9.15	1320	2.40	1210	3.75
240	2770	2.48	2480	4.00	2700	4.80	2750	4.39	2215	3.62	2540	3.57	2190	8.80	2080	9.35	1320	2.70	1225	4.05
242	2770	2.57	2480	3.93	2720	4.90	2750	4.50	2210	3.60	2530	3.58	2175	9.00	2070	9.55	1320	3.05	1240	4.35
244	2760	2.65	2510	3.75	2725	4.98	2755	4.61	2195	3.60	2525	3.59	2160	9.20	2055	9.75	1310	3.40	1240	4.65
246	2755	2.80	2615	3.33	2730	5.07	2760	4.73	2185	3.60	2520	3.59	2150	9.40	2035	10.00	1295	3.75	1236	4.93
248	2760	2.93	2705	3.17	2735	5.16	2760	4.85	2180	3.61	2520	3.60	2135	9.60	2020	10.15	1287	4.10	1220	5.20
250	2785	2.94	2760	3.17	2730	5.24	2760	5.00	2180	3.62	2520	3.62	2120	9.80	2000	10.30	1280	4.40	1200	5.45
252	2830	3.00	2785	3.22	2725	5.35	2760	5.10	2180	3.65	2520	3.66	2100	10.05	1990	10.55	1280	4.70	1180	5.70
254	2865	3.10	2800	3.32	2720	5.55	2760	5.20	2180	3.68	2520	3.72	2090	10.30	1970	10.75	1282	5.00	1166	5.93
256	2890	3.17	2770	3.35	2710	5.80	2765	5.30	2180	3.73	2530	3.77	2070	10.60	1960	10.90	1285	4.25	1153	6.15
258	2895	3.18	2745	3.33	2710	6.01	2765	5.42	2180	3.78	2540	3.82	2060	10.80	1945	11.10	1290	5.53	1145	6.40

TABLE C (Continued)

Altitude	NASA 6.01				NASA 6.02				NASA 6.03				NASA 6.04				NASA 6.05			
	Up-Leg		Down-Leg		Up-Leg		Down-Leg		Up-Leg		Down Leg		Up-Leg		Down-Leg		Up-Leg		Down-Leg	
	T_e (°K)	N_p (10^5/cc)	T_e (°K)	N_p (10^5/cc)	T_e (°K)	N_p (10^5/cc)	T_e (°K)	N_p (10^5/cc)	T_e (°K)	N_p (10^5/cc)	T_e (°K)	N_p (10^5/cc)	T_e (°K)	N_p (10^5/cc)	T_e (°K)	N_p (10^5/cc)	T_e (°K	N_p (10^5/cc)	T_e (°K)	N_p (10^5/cc)
260	2900	3.15	2850	3.27	2710	6.20	2760	5.58	2185	3.82	2550	3.87	2045	11.00	1930	11.35	1290	5.80	1140	6.60
262	2905	3.33	2940	3.22	2715	6.33	2760	5.72	2190	3.87	2555	3.92	2030	11.30	1920	11.50	1297	6.03	1143	6.90
264	2890	3.48	2975	3.22	2720	6.47	2760	5.93	2200	3.91	2560	3.95	2015	11.60	1905	11.65	1305	6.30	1150	7.16
266	2840	3.55	2910	3.26	2725	6.60	2760	6.10	2210	3.95	2570	3.98	2000	11.85	1895	1180	1315	6.50	1160	7.42
268	2805	3.72	2740	3.40	2730	6.72	2760	6.30	2225	3.98	2590	4.01	1985	12.05	1885	12.00	1330	6.75	1170	7.70
270	2800	3.92	2665	3.46	2740	6.82	2765	6.50	2240	4.02	2610	4.05	1970	12.25	1875	12.20	1355	6.95	1185	7.91
272	2810	3.88	2740	3.47	2750	6.97	2780	6.65	2260	4.05	2630	4.08	1955	12.40	1870	12.30	1370	7.14	1200	8.20
274	2850	3.92	3060	2.46	2765	7.13	2805	6.78	2280	4.09	2660	4.13	1940	12.60	1860	12.40	1385	7.30	1213	8.35
276	2890	3.99	3155	3.50	2785	7.30	2830	6.90	2300	4.13	2690	4.18	1930	12.70	1850	12.50	1396	7.50	1224	8.50
278	2905	3.98	3020	3.70	2800	7.50	2850	7.00	2325	4.17	2720	4.24	1910	12.80	1845	12.60	1404	7.62	1230	8.63
280	2950	3.97	2755	3.90	2810	7.68	2875	7.10	2340	4.21	2745	4.30	1900	12.90	1840	12.70	1410	7.75	1237	8.75
282	3010	4.01	2675	4.08	2820	7.85	2890	7.20	2365	4.25	2760	4.37	1890	12.95	1830	12.80	1410	7.86	1238	8.86
284	3000	4.10	2700	4.22	2820	8.00	2900	7.35	2390	4.30	2780	4.42	1875	13.00	1825	12.85	1411	7.95	1240	8.95
286	2910	4.30	2805	4.30	2830	8.10	2910	7.50	2415	4.33	2810	4.49	1865	13.00	1820	12.95	1413	8.03	1240	9.04
288	2825	4.40	2865	4.32	2840	8.20	2920	7.67	2440	4.36	2820	4.55	1855	13.00	1815	13.15	1415	8.11	1240	9.12
290	2870	4.46	2875	4.29	2870	8.30	2920	7.86	2460	4.38	2840	4.61	1845	13.00	1810	13.30	1416	8.20	1240	9.20
292	2895	4.57	2845	4.27	2885	8.38	2920	8.02	2480	4.40	2850	4.66	1835	13.00	1805	13.40	1418	8.27	1241	9.25
294	2875	4.80	2825	4.29	2890	8.45	2910	8.24	2495	4.40	2860	4.70	1830	13.00	1800	13.60	1419	8.35	1242	9.32
296	2825	4.96	2880	4.33	2900	8.57	2900	8.44	2515	4.40	2870	4.72	1820	13.00	1795	13.80	1419	8.41	1242	9.38
298	2840	5.00	2980	4.40	2900	8.65	2900	8.65	2530	4.40	2880	4.73	1815	13.05	1790	14.00	1419	8.48	1243	9.42
300	2885	5.00	2960	4.60		← Apogee			2545	4.40	2890	4.74	1810	13.10	1785	14.20	1419	8.55	1243	9.44
302	2930	5.05	2880	4.76					2560	4.40	2900	4.73	1800	13.20	1785	14.30	1420	8.60	1245	9.47
304	2990	5.10	2850	4.80					2570	4.42	2910	4.72	1795	13.20	1780	14.50	1420	8.65	1245	9.49
306	3000	5.03	2860	4.82					2585	4.43	2920	4.68	1790	13.20	1780	14.60	1420	8.70	1245	9.50
308	2945	4.86	2875	4.90					2590	4.46	2930	4.65	1785	13.20	1770	14.70	1420	8.73	1245	9.50
310	2960	4.82	2890	5.02					2600	4.48	2940	4.60	1780	13.25	1765	14.80	1420	8.75	1245	9.49
312	2995	4.82	2900	5.07					2605	4.52	2950	4.54	1775	13.25	1760	14.90	1418	8.77	1246	9.47
314	3040	4.88	2915	5.00					2615	4.55	2955	4.48	1765	13.20	1750	15.00	1416	8.77	1247	9.45
316	3100	4.90	2955	4.87					2620	4.57	2960	4.42	1760	13.20	1740	15.00	1415	8.76	1247	9.44
318	3125	4.91	2990	4.82					2620	4.58	2960	4.38	1755	13.20	1735	15.00	1414	8.74	1248	9.41
320	3030	5.01	3030	4.87					2625	4.58	2965	4.36	1750	13.20	1725	14.95	1412	8.70	1249	9.40
322	2930	5.18	3065	4.92					2630	4.56	2970	4.37	1745	13.15	1720	14.90	1411	8.64	1249	9.35
324	2890	5.35	3030	5.00					2635	4.52	2975	4.38	1740	13.10	1715	14.80	1410	8.54	1249	9.32
326	3120	5.55	3005	5.25					2640	4.48	2980	4.40	1735	13.05	1710	14.60	1410	8.53	1248	9.29
328	3155	5.57	3015	5.23					2640	4.42	2980	4.40	1730	12.95	1705	14.45	1410	8.51	1248	9.24
330	3160	5.53	3080	5.21					2640	4.33	2985	4.40	1725	12.85	1700	14.20	1409	8.50	1249	9.20
332	3170	5.65	3170	5.60					2640	4.25	2990	4.40	1725	12.75	1700	14.00	1405	8.50	1250	9.16
334		← Apogee							2640	4.19	2990	4.38	1720	12.65	1695	13.60	1404	8.50	1250	9.12
336									2640	4.16	2995	4.37	1720	12.50	1690	13.25	1402	8.49	1250	9.06
338									2640	4.15	2995	4.33	1715	12.40	1690	12.70	1400	8.49	1250	9.02
340									2640	4.16	2995	4.28	1710	12.30	1690	12.10	1400	8.49	1248	8.97
342									2640	4.18	3000	4.24	1705	12.15	1690	11.80	1396	8.49	1248	8.94
344									2640	4.20	3000	4.20	1705	12.00	1690	11.40	1392	8.50	1246	8.90
346									2640	4.20	3000	4.15	1700	11.90	1690	11.00	1388	8.52	1246	8.88
348									2640	4.20	3000	4.12	1700	11.70	1690	10.60	1381	8.56	1245	8.84
350									2640	4.20	2995	4.08	1700	11.50	1690	10.20	1377	8.63	1244	8.82

TABLE C (Concluded)

Altitude	NASA 6.01				NASA 6.02				NASA 6.03				NASA 6.04				NASA 6.05			
	Up-Leg		Down-Leg		Up-Leg		Down-Leg		Up-Leg		Down-Leg		Up-Leg		Down-Leg		Up-Leg		Down-Leg	
	T_e (°K)	N_p (10^5/cc)	T_e (°K)	N_p (10^5/cc)	T_e (°K)	N_p (10^5/cc)	T_e (°K)	N_p (10^5/cc)	T_e (°K)	N_p (10^5/cc)	T_e (°K)	N_p (10^5/cc)	T_e (°K)	N_p (10^5/cc)	T_e (°K)	N_p (10^5/cc)	T_e (°K)	N_p (10^5/cc)	T_e (°K)	N_p (10^5/cc)
352									2640	4.20	2995	4.06	1695	11.20	1690	9.85	1370	8.69	1243	8.82
354									2640	4.21	2990	4.03	1695	10.90	1690	9.50	1365	8.72	1243	8.80
356									2645	4.22	2990	4.01	1690	10.60	1690	9.30	1360	8.76	1245	8.80
358									2645	4.22	2985	3.99	1690	10.20	1690	9.20	1350	8.80	1245	8.80
360									2650	4.24	2980	3.98	1685	9.80	1685	9.25	1345	8.85	1249	8.85
362									2650	4.24	2980	3.96	1685	9.50	1685	9.50	1340	8.90	1250	8.90
364									2650	4.24	2980	3.95		Apogee			1320	8.96	1253	8.96
366									2650	4.23	2980	3.93					1275	9.00	1275	9.00
368									2650	4.22	2970	3.92						Apogee		
370									2655	4.22	2965	3.92								
372									2660	4.20	2960	3.93								
374									2665	4.17	2955	3.95								
376									2670	4.14	2950	3.95								
378									2680	4.10	2960	3.98								
380									2685	4.07	2950	4.00								
382									2690	4.06	2945	4.04								
384									2700	4.03	2940	4.08								
386									2710	4.02	2935	4.12								
388									2730	3.98	2930	4.16								
390									2740	3.94	2925	4.18								
392									2755	3.90	2920	4.20								
394									2770	3.87	2920	4.19								
396									2780	3.84	2910	4.17								
398									2800	3.82	2910	4.11								
400									2810	3.80	2915	4.02								
402									2820	3.80	2920	3.93								
404									2840	3.80	2920	3.87								
406									2850	3.80	2925	3.82								
408									2865	3.80	2930	3.77								
410									2880	3.82	2940	3.74								
412									2900	3.82	2945	3.72								
414									2910	3.82	2950	3.71								
416									2925	3.82	2965	3.71								
418									2940	3.80	2980	3.72								
420									2965	3.77	2990	3.73								
422									2990	3.75	2990	3.75								

11.0 ACKNOWLEDGMENTS

Clearly, the conception, theory and implementation of a major research effort such as the one reported here is the result of the combined skills and efforts of many individuals whose work can never be adequately acknowledged; however, I will attempt to credit the major contributors for their various roles in this work.

Theory.—The experiment configuration was conceived by N. W. Spencer* and R. L. Boggess. The early theoretical development was part of the doctoral thesis of Boggess. Later theoretical work which extended the theory to include the effects of velocity was by W. Hoegy, M. Kanal and the author.

Implementation.—Early circuit design and instrumentation development work was by the author, while the earlier experiments were directed by N. W. Spencer. Construction, testing, and launching of the later Dumbbells was directed by G. R. Carignan.

Among the engineers who were responsible for the preparation of the various Dumbbell instruments and nose cones were Gary Rupert, Jack Horvath, James Findlay and Duane Beechler while the leading technicians were Lyle Slider, Plymouth Freed, William Kartlick, and Merlyn Street.

Bud Campbell and John Check were responsible for the drafting and much of the design of the nose cone and Dumbbell structures.

John Maurer had wide responsibility in preparation of the rockets for launching as well as in the design of the rocket and Dumbbell electronic circuitry. Without the dedicated efforts of Messers Carignan and Maurer in the field operations, this series of five rocket launchings could not have been nearly so successful.

Data Reduction.—The data reduction of all flights was directed by the author

*Now with NASA Goddard Space Flight Center, Greenbelt, Md.

with strong assistance from Hugo DiGiulio, who carried major responsibility in this area.

Direction.—Overall direction of the research effort from its inception through the launching of NASA 6.03 in August of 1960 rested with N. W. Spencer, while the author directed the effort from August 1960 to August 1962, during which period NASA 6.04 and NASA 6.05 were launched.

Correlative Data.—We are greatly indebted to W. Berning (Ballistics Research Laboratory, Aberdeen, Md.) for the electron density data from his two-frequency beacon experiment carried aboard NASA 6.03 and 6.04, and to J. W. Wright, National Bureau of Standards, Boulder, Colorado) for providing the ionograms for these launchings and for their reduction to electron density profiles. This correlative charge density data has been invaluable in evaluating the accuracy of the Dumbbell theory and indicating in which areas the theory has needed refinement.

12.0 REFERENCES

1. Hok, G., Spencer, N. W., and Dow, W. G., "Dynamic Probe Measurements in the Ionosphere," J. Geo. Res., 58, No. 2 (1953).

2. Hok, G., Spencer, N. W., Dow, W. G., and Reifman, A., Dynamic Probe Measurements in the Ionosphere, Univ of Mich. Eng. Res. Inst. Report, Ann Arbor, August, 1951.

3. Reifman, A., and Dow, W. G., "Theory and Application of the Variable Voltage Probe for Exploration of the Ionosphere," Phys. Rev., 75, 1311 A (1949).

4. Boggess, R. L., Brace, L. H., and Spencer, N. W., "Langmuir Probe Measurements in the Ionosphere," J. Geo. Res. 64, 1627 (1959).

5. Carignan, G. R., and Brace, L. H., The Dumbbell Electrostatic Ionosphere Probe: Engineering Aspects, Univ. of Michigan ORA Report No. 03599-6-S, Ann Arbor.

6. Boggess, R. L., Theoretical Considerations in Design of an Ionospheric Probe, Univ. of Mich. Res. Inst. Report FS-2, Ann Arbor, Feb., 1959.

7. Boggess, R. L., Electrostatic Probe Measurements of the Ionosphere, Univ. of Mich. Res. Inst. Report GS-1, Ann Arbor, Nov., 1959.

8. Langmuir, I., and Compton, K. T., "Electrical Discharges in Gases," Rev. Mod. Phy., 3, 191 (1931).

9. Mott-Smith, H. H., and Langmuir, I., "The Theory of Collectors in Gaseous Discharges," Phys. Rev., 28, 727 (1926).

10. Johnson, E. O., and Malter, L., "A Floating Double Probe Method for Measurements in Gas Discharges," Phys. Rev., 80, 58 (1950).

11. Koyiuna, S., and Takayana, K., J. Phys. Soc. Japan, 4, 349 (1949).

12. Brace, L. H., Transistorized Circuits for Use in Space-Research Instrumentation, Univ. of Mich. Res. Inst. Report, Ann Arbor, Oct. 1959.

13. Hoegy, W., and Brace, L. H., The Dumbbell Electrostatic Ionosphere Probe: Theoretical Aspects, Univ. of Mich. ORA Report No. JS-1 (03599-5-S), Ann Arbor, Sept. 1961.

14. Johnson, C. Y., Meadows, E. B., and Holmes, J. C., "Ion Composition of the Artic Ionosphere," J. Geo. Res., 63, 443-444 (1958).

15. Taylor, H. A., and Brinton, H. C., "Atmospheric Ion Composition Measured Above Wallops Island, Va.," J. Geo. Res., 66, 2587-88 (1961).

16. Bohm, D., Burhop, E.H.S., and Massey, H.S.W., The Characteristics of Electrical Discharges in Magnetic Fields, Chap. 2 (Eds. A. Guthrie and R. K. Wakerling) (McGraw-Hill: New York, 1949).

17. Whipple, E. C., "The Ion Trap Results from the Third Soviet Sputnik," Proc. of IRE, Nov. 1960, pp. 2023.

18. Schultz, G. C., and Brown, S.C., "Microwave Study of Positive Ion Collection by Probes," Phys. Rev., 98, 6 pp. 1642-1649 (1955).

19. Spencer, N. W., Brace, L. H., and Carignan, G. R., "Electron Temperature Evidence for Non-Thermal Equilibrium in the Ionosphere," J. Geo. Res., 62, 157-175 (1962).

20. Kallman-Bijl, H. K., "Daytime and Nighttime Atmospheric Properties Derived from Rocket and Satellite Observations," J. Geo. Res., 66, 787-796 (1961).

21. Wada, J. Y., and Knechtli, R. C., "Generation and Application of Highly Ionized Quiescent Plasma in Steady State," Proc. of IRE, 49, 12, 1926-31, Dec. 1961.

22. Johnson, E. O., and Malther, L., "A Floating Double Probe Method for Measurements in Gas Discharges," Phys. Rev., 80, 58-69, Oct. 1950.

23. Harris, I., and Priester, W., "Time-Dependent Structure of the Upper Atmosphere," paper given at Third Int. Annual Space Science Symposium (COSPAR), Wash., D.C., May 1962.

24. Johnson, F. S., Progress in Astrophysical Science, Chap. 2, North Holland Pub. Co., Amsterdam (1962).

25. Dubin, M., "Meteor Ionization in the E Region," Meteors, pp. 111-118 (Ed. T. R. Kaiser), Pergamon Press, London (1955).

26. Nicolet, M., "Meteor Ionization and the Nighttime E Layer," Meteors, pp. 99-110 (Ed. T. R. Kaiser), Pergamon Press, London (1955).

27. Smith, L. G., "Rocket Measurements of Electron Density and Temperature in the Nighttime Ionosphere," paper presented at First Western National Meeting of the AGU, Los Angeles, Dec. 1961.

28. Ichimiya, T. I., et al., "Measurements of the Positive Ion Density in the Ionosphere by Sounding Rocket," Nature, 190, 156-158 (1961).

29. U. S. Department of Commerce, National Bureau of Standards CRRL-F, Part B, Solar Geophysical Data.

30. Hanson, W. G., and Johnson, F. S., "Electron Temperatures in the Ionosphere," Tenth International Astrophysical Colloquium, Liege, Belgium, 1961.

31. Horowitz, R., and Lagow, H. E., "Summer Day Auroral Zone Atmospheric Structure Measurements from 100 to 210 Kilometers," J. Geo. Res., 66, 757-773 (1958).

32. Nicolet, M., and A. C. Aikin, "The Formation of the D Region of the Ionosphere," J. Geo. Res., 65, 1469-1483 (1960).

33. Moler, W. F. "VLF Propagation Effects of a D-Region Layer Produced by Cosmic Rays," J. Geo. Res., 65, 1459-1467 (1960).

34. Horowitz, R., Lagow, H. E., and Giuliani, J. F., "Fall Day Auroral Zone Atmospheric Structure Measurements from 100 to 188 Kilometers," J. Geo. Res., 64, 2287-2295 (1959).

35. Seddon, J. C., "Propagation Measurements in the Ionosphere with the Aid of Rockets," J. Geo. Res., 58, 323-335 (1953).